Daniela Gier Della Rocca

Synthesis, characterization and catalytic activity of silver molybdate to pantoprazole removal from water under visible or UV light

Master thesis submitted to the Program of Graduate in Chemical Engineering of the Federal University of Santa Catarina to obtain the Degree of master in Chemical Engineering
Advisor: Profª. Drª. Regina de Fátima Peralta Muniz Moreira
Co-advisors: Prof. Dr. Agenor de Noni Júnior and Prof. Dr. Humberto Jorge José

Florianópolis
2019

Ficha de identificação da obra elaborada pelo autor através do Programa de Geração Automática da Biblioteca Universitária da UFSC.

Della Rocca, Daniela Gier

Synthesis, characterization and catalytic activity of silver molybdate to pantoprazole removal from water under visible or UV light / Daniela Gier Della Rocca ; orientadora, Regina de Fátima Peralta Muniz Moreira ; coorientador, Agenor de Noni Júnior, coorientador, Humberto Jorge José. Florianópolis, SC, 2018.

129 p.

Dissertação (mestrado) - Universidade Federal de Santa Catarina, Centro Tecnológico. Programa de Pós-Graduação em Engenharia Química.

Inclui referências.

1. Engenharia Química. 2. Ag_2MoO_4. 3. Processos Avançados de Oxidação. 4. Fotocatálise. 5. Reações tipo Fenton. Pantoprazol. I. Moreira, Regina de Fátima Peralta Muniz. II. De Noni Junior, Agenor. III. José, Humberto Jorge. IV. Universidade Federal de Santa Catarina. Programa de Pós-Graduação em Engenharia Química. V. Título.

Daniela Gier Della Rocca

Synthesis, characterization and catalytic activity of silver molybdate to pantoprazole removal from water under visible or UV light

This master thesis was deemed appropriate to obtain the title of master in Chemical Engineering and approved in its final form by the Program of Graduate in Chemical Engineering of the Federal University of Santa Catarina
Florianópolis, March, 12, 2019.

_____
Profª. Cíntia Soares, Drª.
Course Coordinator

Examination Board:

_____
Prof.ª Regina, de Fátima Peralta Muniz Moreira, Dr. ª
Advisor
Federal University of Santa Catarina

_____
Prof. Agenor de Noni Júnior, Dr.
Co-Advisor
Federal University of Santa Catarina

_____
Prof. Humberto Jorge José, Dr.
Co-Advisor
Federal University of Santa Catarina

_____
Profª. Marla Azário Lansarin, Drª
Federal University of Rio Grande do Sul

_____
Jaqueline Oliveira de Moraes, Drª.
Federal University of Santa Catarina

This work is dedicated to all my dear colleges, friends, and family who supported me in this entire trajectory.

ACKNOWLEDGMENTS

I would like to start thanking God, for having taking good care of me during this entire journey and giving me all the courage I needed for surpassing it.

I am very grateful to my advisor, Profª. Drª. Regina de Fátima Peralta Muniz Moreira, for all help and teaching dedicated to me during this dissertation construction. I've learned a lot.

To my co-advisors, Prof. Dr. Agenor de Noni Júnior and Prof. Dr. Humberto Jorge José, for all the support and help.

To the examining bank professors, for its dedication and time availability to contribute to the enhancement of this dissertation.

To UFSC and to the Postgraduate Program in Chemical Engineering (PósEnq) for the structure.

To CNPq (National Council for Scientific and Technological Development) and CAPES (Coordination for the Improvement of Higher Education Personnel), for the scholarships and financial investments.

To Central Laboratory of Electronic Microscopy (LCME), for the FEG-SEM analysis.

To Analysis Central of Chemical Engineering of Federal University of Santa Catarina, for the BET and FTIR analyses.

To André Roos and Prof. Philippe Gleize, for the XRD analysis.

To Thiago Boimer Correia and Aline Maria de Borba from LINDEN laboratory, for the zeta potential measurements.

To all my colleges of Energy and Environment Laboratory (LEMA), for their friendship, contributions and encouragement during my mastering period.

To all my friends, who believed and cheered me up all this time.

To my father, Mauro, my mother, Beth, my sister, Cris, and my grandmother, Cida, for the love, affection, support, prays, and believe in my potential.

To my love, João, for helping me create some of my figures, but mainly, for the strength, patience, confidence, affection, love, support,... given to me. In short, everything I needed to conclude this challenge.

To everyone else, that contributed, somehow, for the development of this study.

“I am among those who think that science has great beauty.”
(Marie Curie, 1937)

RESUMO

Neste trabalho, o molibdato de prata (Ag_2MoO_4) foi utilizado como catalisador em processos avançados de oxidação (AOP) para degradar o fármaco pantoprazol (PAN) em suspensão aquosa, o qual é tóxico e cancerígeno. O catalisador foi sintetizado por um método controlado de precipitação e caracterizado por TGA/DTA, XRD, FTIR, FEG-SEM/EDS, BET, DRS e potencial zeta. α-Ag_2MoO_4 e β-Ag_2MoO_4 foram identificados em estruturas cristalinas das partículas semelhantes a borboletas, e a fase α-Ag_2MoO_4 metaestável foi completamente convertida em β-Ag_2MoO_4 por tratamento térmico em temperatura superior a 280 ºC . A energia de band gap do Ag_2MoO_4 calcinado ($Ag_2MoO_4^{Calc}$) (E_g = 3,25 eV) é ligeiramente superior à do catalisador preparado (α-Ag_2MoO_4 + β-Ag_2MoO_4) (E_g = 3,09 eV), possuindo maior atividade responsiva à luz visível. Ag_2MoO_4 e $Ag_2MoO_4^{Calc.}$ mostraram atividades fotocatalíticas superiores ao TiO_2-P25 sob luz visível. Sob luz UV, o catalisador calcinado e o não-calcinado exibiram atividade catalítica semelhante na degradação do PAN. Entretanto, como esperado, sob luz visível Ag_2MoO_4 teve melhores resultados (12% maior remoção de TOC), devido ao seu menor band gap. Além disso, durante as reações de fotólise, observou-se que o PAN é sensível à irradiação de luz, especialmente a UV (72-99%). A adição de H_2O_2 (como aceptor de elétrons) aumentou a taxa de mineralização na presença de luz UV, mas nenhuma mudança significativa foi observada, quando foi combinado com a luz VIS. Os resultados mostraram que os tratamentos mais eficientes para a mineralização do PAN foram a peroxidação catalítica e foto-peroxidação sob luz VIS, onde o composto foi quase completamente mineralizado (> 95%). O estudo de avaliação de espécies reativas de oxigênio mostrou que o ânion superóxido ($O_2^{\bullet -}$) é o principal radical responsável pela reação de degradação do PAN nos processos oxidativos avançados.

Palavras-chave: Ag_2MoO_4. Processos Avançados de Oxidação. Fotocatálise. Reações tipo Fenton. Pantoprazol.

RESUMO EXPANDIDO

Introdução

O pantoprazol (PAN) é um medicamento consumido em grande quantidade para o tratamento de problemas gástricos. Sua presença em águas naturais tem sido detectada em concentrações crescentes ao longo dos anos (NÖDLER et al., 2010; BOIX et al., 2015). Além disso, os métodos convencionais de tratamento não são completamente eficientes para sua remoção da água (NÖDLER et al., 2010). Embora seja instável, especialmente em pH ácido e sob luz UV (JUNGNICKEL, 2000; RAFFIN et al., 2008), sua completa remoção e mineralização em estações de tratamento de efluente é pouco estudada. Ainda que este poluente se decomponha no meio ambiente, formando compostos intermediários de degradação, os estudos utilizando óxidos de ferro como adsorvente (ALI; AL-OTHMAN; ALHARBI, 2016) ou como catalisador em processos avançados de oxidação (GAN et al., 2017) têm demonstrado que a completa remoção da água e mineralização é difícil de ser alcançada. Uma alternativa de tratamento de fármacos que tem se mostrado eficaz é a aplicação de processos avançados de oxidação (AOP), em especial fotocálise e reações tipo Fenton (SHARMA; AHMAD; FLORA, 2018). Entretanto, esses processos possuem limitações para serem aplicados em larga escala, sendo a foto-ativação apenas sob luz UV e a produção de lama residuária, respectivamente, os maiores desafios a serem superados para implementação desses processos (DI PAOLA et al., 2012; MA et al., 2015). Um catalisador que tem mostrado excelente atividade tanto sob luz UV quanto sob luz VIS é o molibdato de prata (Ag_2MoO_4), que possui propriedades únicas, tais como: fotoluminescência, ambientalmente amigável, alta condutividade elétrica, atividade antimicrobiana, atividade oxidante, entre outros (BHATTACHARY; GHOSH, 2007; DE SANTANA et al., 2014; KUMAR et al., 2016; WANG et al., 2017). Além disso, Ag_2MoO_4 foi capaz de promover a formação de radicais hidroxilas em suas reações, mostrando potencial aplicação em outros AOP, como em reações de peroxidação heterogênea. Assim, o objetivo deste trabalho é avaliar a remoção do PAN em solução aquosa através dos processos de fotocatálise (sob luz UV ou VIS), bem como pelos métodos de peroxidação e foto-peroxidação.

Objetivos

Os objetivos principais deste trabalho são: sintetizar, caracterizar e avaliar a atividade catalítica de Ag_2MoO_4 como catalisador heterogêneo em reações de fotocatálise, peroxidação e foto-peroxidação catalíticas,

utilizando o PAN como poluente de interesse. Além disso, pretende-se investigar mais a fundo o comportamento do PAN quando exposto a AOP.

Metodologia

PAN (99,5% de pureza) foi fornecido pela empresa Pharmanostra, Índia, e utilizado sem purificação adicional. O TiO_2-P25 (fornecido pela Evonik-Degussa, Alemanha) foi utilizado para comparar a performance fotocatalítica do Ag_2MoO_4 sintetizado. O Ag_2MoO_4 foi sintetizado pelo método de precipitação controlada (WANG et al., 2017), utilizando acetato de prata (pureza de 98%, Neon), polivinilpirrolidona (PVP, massa molecular média de 40000 $g \cdot mol^{-1}$, Sigma-Aldrich,) e molibdato de amônio (pureza P.A., Vetec). A síntese do Ag_2MoO_4 foi iniciada dissolvendo-se 0,1669 g de acetato de prata e 0,8325 g de PVP em 50 mL de água deionizada. Em seguida, foram gotejados 2,5 mL da solução de molibdato de amônio (0,0285 M). O sólido foi removido por filtração em papel de filtro, e seco em estufa a 60 ºC por 12 h. O catalisador preparado (Ag_2MoO_4) foi tratado termicamente em uma mufla por 3 h a 300 ºC, e o catalisador calcinado foi denominado $Ag_2MoO_4^{Calc.}$. Os catalisadores foram caracterizados por difração de raios-X (XRD), análises termogravimétrica e térmica diferencial (TGA e DTA), área superficial (S_{BET}), espectroscopia de infravermelho com transformada de Fourier (FTIR), espectroscopia de refletância diferencial (DRS) e potencial zeta. Os testes de degradação do fármaco foram realizados em reator anular de 1 L de volume útil. Inicialmente, foram adicionados ao reator 750 mL de solução aquosa de pantoprazol (0,2 $g \cdot L^{-1}$) e 0,5 $g \cdot L^{-1}$ de fotocatalisador sólido. Para as reações fotocatalíticas, o sistema foi protegido de fontes luminosas e mantido sob agitação até atingir o equilíbrio de adsorção (1 h para TiO_2-P25 e overnight para os molibdatos de prata). Para iniciar as reações com condições similares àquelas que não foram submetidas à adsorção – de forma que a diferença na concentração de moléculas no meio não afetaria as condições da reação - a concentração inicial do PAN nessas reações era maior (0,25 $g \cdot L^{-1}$ para TiO_2-P25, 0,3 $g \cdot L^{-1}$ para $Ag_2MoO_4^{Calc.}$ e 0,4 $g \cdot L^{-1}$ para Ag_2MoO_4). Após a adsorção, para as reações de fotocatálise, iniciou-se a injeção de ar (a uma taxa de 0,22 vvm) e a lâmpada UV (UVA e visível, 70W, Osram) ou VIS (Visível, 2W, Brilia) foi acesa. Nos experimentos de peroxidação, apenas Ag_2MoO_4 foi utilizado e nenhuma adsorção prévia foi realizada. A concentração de H_2O_2 foi de 0,5 $g \cdot L^{-1}$. E as reações de foto-peroxidação foram realizadas de forma semelhante às peroxidações, apenas com o adicional acendimento da lâmpada ao iniciar a reação. As alíquotas

coletadas foram analisadas em relação à concentração de PAN em espectrofotômetro UV-Vis e TOC, pH e concentração de peróxido de hidrogênio (quando aplicável). Ademais, também foram realizados experimentos com sequestrantes de radicais para avaliar quais as espécies oxidantes reativas (ROS) formadas.

Resultados e Discussão

Ag_2MoO_4 não apresentou perda de peso apreciável no TGA, mas a transformação da estrutura α para β foi detectada no DTA (pico exotérmico a 272 ºC). Os principais picos XRD do Ag_2MoO_4 coincidiram com α-Ag_2MoO_4 (JCPDS 21-1340) e β-Ag_2MoO_4 (JCPDS 08-0473), enquanto $Ag_2MoO_4^{Calc.}$ apresentou apenas a fase β (JCPDS 08-0473), como esperado. A S_{BET} do Ag_2MoO_4 foi 1.9 $m^2 \cdot g^{-1}$, valor semelhante ao retratado na literatura. A morfologia do catalisador Ag_2MoO_4 mostrou aglomerados de partículas de tamanhos irregulares (variando de 1 a 5 µm) com formatos do tipo borboletas ou pétalas. Os espectros de FTIR de ambos os molibdatos de prata apresentaram os picos correspondentes às vibrações de estiramento anti-simétricas de O-Mo-O. Os intervalos de bandas do Ag_2MoO_4 e $Ag_2MoO_4^{Calc.}$ são, respectivamente, 3,09 eV e 3,25 eV. A formação do complexo $[Ag(PVP)]^+$ foi essencial para a formação de α-Ag_2MoO_4. Os dados de potenciais zeta do Ag_2MoO_4 apresentaram apenas valores negativos para todos os pH medidos. A capacidade de adsorção do catalisador Ag_2MoO_4 (280 $mg \cdot g^{-1}$) foi aproximadamente o dobro do $Ag_2MoO_4^{Calc.}$ (138 $mg \cdot g^{-1}$). Além disso, ambos os catalisadores sintetizados mostraram-se mais eficientes nas reações fotocatalíticas sob luz VIS do que TiO_2-P25. Ademais, observou-se que o PAN é sensível à irradiação luminosa. Como esperado, pelo seu menor valor de *band gap*, o Ag_2MoO_4 mostrou-se mais foto-reativo sob luz visível do que o $Ag_2MoO_4^{Calc.}$, embora sob luz UV ambos tenham apresentado comportamentos semelhantes. O uso de H_2O_2 como aceptor de elétrons aumentou a remoção de TOC do PAN ao longo da reação. Para reações catalíticas que empregaram UV, grandes degradações (acima de 85%) foram obtidas, mas essas reações não mostraram mineralização proporcional, chegando apenas a 32%, em alguns casos. Esse fato pode ser explicado pela rápida acidificação do meio proporcionada pelas reações UV, à qual o PAN é sensível. Os melhores tratamentos aplicados foram: peroxidação catalítica e foto-peroxidação sob luz VIS, nas quais altas taxas de mineralização foram obtidas (> 95%), destacando-se que, no escuro, 90% do PAN foi removido em 15 min. Por fim, foi avaliada a formação de radicais e, para os dois casos

analisados (fotocatálise UV e peroxidação catalítica), o ânion superóxido ($O_2^{\bullet -}$) apresentou-se como principal agente oxidante nas reações.

Considerações Finais

O Ag_2MoO_4 foi sintetizado com sucesso por um método simples de precipitação controlada, produzindo molibdato de prata com suas duas fases, inclusive a α, que é metaestável e é raramente reportada. Vale pontuar que a atividade fotocatalítica do molibdato de prata sem tratamento térmico, sob luz visível, mostrou-se superior aos demais catalisadores estudados ($Ag_2MoO_4^{Calc.}$ e TiO_2-P25), devido à presença de α-Ag_2MoO_4. Em relação às reações de peroxidação e foto-peroxidação, bons resultados foram encontrados na ausência de luz ou na presença de luz visível. Já sob luz UV, intermediários marrom avermelhados foram observados e menores valores de mineralização foram obtidos. Além disso, ao longo das reações, a sensibilidade do PAN, em relação a fontes de luz e ao pH, ácido, ficaram bastante evidentes. Por fim, pode-se concluir que o Ag_2MoO_4 se mostrou um catalisador eficiente nos AOP estudados neste trabalho, especialmente para a peroxidação catalítica.

Palavras-chave: Ag_2MoO_4. Processos Avançados de Oxidação. Fotocatálise. Reações tipo Fenton. Pantoprazol.

ABSTRACT

In this work, silver molybdate (Ag_2MoO_4) was used as a catalyst in advanced oxidation processes (AOP) to degrade the pharmaceutical pantoprazole (PAN) in aqueous suspension, which is toxic and carcinogenic. The catalyst was synthesized by a controlled precipitation method and characterized by TGA/DTA, XRD, FTIR, FEG-SEM/EDS, BET, DRS and zeta potential. α-Ag_2MoO_4 and β-Ag_2MoO_4 were identified in crystalline structures of the butterfly-like particles, and the metastable α-Ag_2MoO_4 phase was completely converted to β-Ag_2MoO_4 by heat treatment at a temperature above 280 ºC. The band gap energy of the calcined Ag_2MoO_4 ($Ag_2MoO_4^{Calc.}$) (E_g = 3.25 eV) is slightly higher than that of the prepared catalyst (α-Ag_2MoO_4 + β-Ag_2MoO_4) (E_g = 3.09 eV), having higher responsive activity to visible light. Ag_2MoO_4 and $Ag_2MoO_4^{Calc.}$ showed superior photocatalytic activities than TiO_2-P25 under visible light. Under UV light, calcined and non-calcined catalyst exhibited similar catalytic activity in PAN degradation. However, as expected, under visible light Ag_2MoO_4 had better results (12% greater removal of TOC), due to its lower band gap. In addition, during photolysis reactions, it was observed that PAN is sensitive to light irradiation, especially UV (72-99%). The addition of H_2O_2 (as electron acceptor) increased the rate of mineralization in the presence of UV light, but no significant changes were observed when combined with VIS light. The results showed that the most efficient treatments for PAN mineralization were catalytic peroxidation and photoperoxidation under VIS light, which the compound was almost completely mineralized (> 95%). The study of the evaluation of reactive oxygen species showed that the superoxide anion ($O_2^{\bullet-}$) is the main radical responsible for the PAN degradation reaction in advanced oxidation processes.

Keywords: Ag_2MoO_4. Advanced Oxidation Processes. Photocatalysis. Peroxidation. Photo-peroxidation.

LIST OF FIGURES

LIST OF TABLES

LIST OF ABBREVIATIONS AND ACRONYMS

Abbreviation	Definition
AB	Acid blue
AO	Acid orange
AOP	Advanced Oxidation Processes
ATX	Aatrex
BET	Brunauer–Emmett–Teller
BJH	Barrett-Joyner-Halenda
BPA	Bisphenol A
BQ	p-benzoquinone
4-CP	4-clorophenol
CIP	Ciprofloxacin
CR	Congo red
CV	Crystal violet
DRS	UV-Vis Diffuse Reflectance Spectra
DT	Direct transition
DTA	Differential Thermal Analysis
EDS	Energy Dispersive Spectrometer
EY	Eosin Y
FEG-SEM	Field Emission Gun Scanning Electron Microscopy
FTIR	Fourier transform infrared
IT	Indirect transition
MB	Methylene blue
MO	Methyl orange
Na_2EDTA	Disodium ethylenediaminetetraacetate dihydrate
NaN_3	Sodium azide
NFC	Norfloxacin
PAN	Pantoprazole
PPI	Proton Pump Inhibitors
PVP	Polyvinylpyrrolidone
RhB	Rhodamine B
Rh6G	Rhodamine 6G
ROS	Reactive oxygen species
TBA	Tert-butyl alcohol
TC	Tetracylclines
TGA	Thermogravimetric Analysis
THC	Tetracylcline hydrochloride
TOC	Total Organic Carbon
XRD	X-ray diffraction

LIST OF SYMBOLS

Symbol	Meaning	Unit
A	A constant	cm^{-1}
α	Absorption coefficient	-
β	Length of the peak at half height of its maximum intensity	rad
C	Concentration	$mg \cdot L^{-1}$
C_0	Initial concentration	$mg \cdot L^{-1}$
e^-	Electron	-
E_g	Band gap	eV
E_{CB}	Conduction band	eV
E_{VB}	Valence band	eV
h	Plank's constant	eV·s
h^+	Photogenerated hole	-
K	Dimensionless shape factor	-
k_{app}	Kinetic pseudo-first order constant	min^{-1}
λ	Wavelength	nm
n	Reaction order	-
•OH	Hydroxyl radical	-
$O_2^{\bullet -}$	Superoxide anion radical	-
$^1O_2$	Singlet oxygen	-
$\bullet O_2H$	Hydroperoxyl radical	-
P/ P_0	Relative pressure	-
P_S	Average pore size	nm
$[PAN]_0$	Pantoprazole's initial concentration	$mg \cdot L^{-1}$
pH_0	Initial pH	-
•RO	Alkoxyl radical	-
S_{BET}	Surface area	$m^2 \cdot g^{-1}$
$\bullet SO_4^-$	Sulphate radical	-
t	Time	min
τ	Size of crystallite	nm
θ	Bragg's angle	rad
$[TOC]_0$	Initial total organic carbon	$mg \cdot L^{-1}$
V_P	Total pore volume	$cm^3 \cdot g^{-1}$
υ	Light frequency	Hz
χ	Electronegativity of semiconductor	eV

SUMMARY

1 INTRODUCTION

The discovery of semiconductor materials has revolutionized the technological industry, due to its unique properties, as: electric conductivity, electrons excitement, light emission and thermal energy conversion (NEAMEN, 2012). The demand for them is progressively increasing and many different materials are being developed recently (WORLD SEMICONDUCTORS TRADE STATISTCS, 2018).

Silver molybdate (Ag_2MoO_4) is one of the semiconductors that have recently received attention due to its high electrical conductivity, photoluminescence, antimicrobial activity, elevated energy storage performance and environmental friendly composition. (DRISCOLL; OZKAN, 1994; BHATTACHARYA; GHOSH, 2007; CUNHA et al., 2015).

Due to these characteristics, Ag_2MoO_4 has great potential, especially, for application in photocatalytic and Fenton-like reactions. (XU et al., 2015a; WANG et al., 2017; SOUSA et al., 2018; LI; LIU; LI, 2018; YANG et al., 2017a). Although these processes have been widely studied, there are still several limitations that restrain its diffusion in large scale to water and wastewater treatment.

In the photocatalytic degradation of pollutants from wastewater, most of photocatalysts have low activity in solar or visible light, and require the use of UV light. In consequence, the operation cost is high. Besides, under light irradiation, the efficiency is low due to the high electronic recombination rate (DI PAOLA et al., 2012). For Fenton-like reactions the main disadvantages are the waste sludge production, the narrow pH operation range (3 or lower) and low iron salts recyclability (MA et al., 2015).

Several new catalysts are being developed to overcome these problems (HONDOW; FULLER, 2014; MIAO et al., 2014; SHARMA; AHMAD; FLORA, 2018) and potential candidates to be use in wastewater treatment includes silver salts, bismuth oxide, zinc oxide, among others. The importance of developing more efficient, eco-friendly and low-cost catalysts is increasing, once Advanced Oxidation Processes (AOP) frequently achieve high degradation rate to remove emerging contaminants (TEODOSIU et al., 2018). Many of the traces of emerging contaminants found in water sources are remnant from daily products consume, such as personal care products, plasticizer, pesticides, surfactants, pharmaceuticals, etc. (WILKINSON et al., 2017). Up to now, there is no technology enough robust to be applied in large scale to remove emerging contaminants.

In particular, pharmaceuticals represent a great risk, since they are usually toxic, teratogenic and carcinogenic. Thus not only more monitoring and control measures are needed, but also further studies on their influence upon human health and environmental systems (KOOPAEI; ABDOLLAHI, 2017). Proton pump inhibitors (PPI), for example, are the most commonly medicines consumed worldwide and, yet, less than fifteen studies about its effects in water sources have been published in the last decade (SCOPUS, 2018). These pharmaceutical compounds are used for gastrointestinal disorders, peptic ulcer, gastroesophageal reflux disease, gastrointestinal complications and Zollinger-Ellison syndrome (RICHARDSON et al., 1998). It is worth mentioning that some side effects of the PPIs consumption may be: muscle cramps, diarrhea, nausea, dizziness, jittery feeling, confusion, headache, limp feeling, loss of appetite, memory problems, uneven heart beats, choking feeling, etc. (HERZIG et al., 2014).

Pantoprazole (PAN) is the second most consumed PPI in the world, just behind omeprazole (ORTIZ DE GARCÍA et al., 2013). According to KOSMA; LAMBROPOULOU; ALBANIS (2016), approximately 70-95% of the consumed PPI are excreted as inactive or pharmaceutically active metabolites in urine and feces. As a consequence, its presence in the environmental is not surprising, due to its stability and biodegradation resistance (ORTIZ DE GARCÍA et al. 2013). Some monitoring studies (NÖDLER et al., 2010; GRACIA-LOR et al., 2012; BOIX et al., 2015) have reported the presence of PAN in concentrations up to 0.18 $\mu g \cdot L^{-1}$ of this compound in effluent wastewaters. For this purpose, this study intends to contribute with a novel catalyst to be applied for removing PAN from water through advanced oxidation processes.

2 OBJECTIVES

2.1 GENERAL OBJECTIVE

The general goal of this study is synthetize, characterize and evaluate the catalytic activity of Ag_2MoO_4 as a heterogeneous catalyst in photocatalysis, catalyst peroxidation and catalyst photoperoxidation reactions, using pantoprazole as an organic contaminant of interest.

2.2 SPECIFIC OBJECTIVES

The specific goals of this work are described below:

- Prepare and characterize the Ag_2MoO_4 catalyst, obtained by controlled precipitation method;
- Investigate the degradation and mineralization of pantoprazole by non-catalytic reactions (photodegradation, oxygenation, peroxidation and adsorption);
- Investigate the degradation and mineralization of PAN by photocatalysis, catalyst peroxide oxidation and catalyst photoperoxide oxidation reactions;
- Compare the photocatalytic and photoperoxidation activity of Ag_2MoO_4 under UV and VIS light sources;
- Compare the photocatalytic performance of the synthesized Ag_2MoO_4 with the Ag_2MoO_4 after calcination treatment and the commercial TiO_2-P25 catalyst.
- Investigate the effect of some parameters (different electron acceptors and pH) on the PAN removal;
- Investigate which radicals are formed by Ag_2MoO_4 and propose a degradation mechanism for PAN.

3 LITERATURE REVIEW

3.1 ADVANCED OXIDATION PROCESSES

Advanced Oxidation Processes (AOPs) are techniques based on the in situ generation of strong oxidants, as reactive oxygen or free radical species, in order to promote the degradation of organic and inorganic compounds into nontoxic and less harmful molecules (SHARMA; AHMAD; FLORA, 2018). A great difference from these methods is the fact that they are not only able to oxidize persistent contaminants, which resist conventional treatments, but also mineralize them into CO_2 and H_2O (KARCI, 2014).

Reactive oxidizing species (ROS) are molecules that contain, at least, one unpaired electron, although hydroxyl radicals (•OH) are the most widely studied, other oxidants have also called attention, as: superoxide anion radical ($O_2^{\bullet -}$), singlet oxygen ($^1O_2$), hydroperoxyl radical ($^{\bullet}O_2H$), alkoxyl radical (•RO) and sulphate radical ($^{\bullet}SO_4^-$). (GUO et al., 2015; DEWIL et al., 2017; KANAKARAJU; GLASS; OELGEMÖLLER, 2018).

AOP can be categorized by its radicals formation type (Figure 1) being them coupled or not with catalysts, in four groups: chemical processes (ozonation, Fenton, peroxidation), photochemical processes (photolysis, photo-peroxidation, photocatalysis), physical processes (plasma, ultrasound, sonolysis, microwave, electron beam) and hybrid processes (sono-photolysis, photo-Fenton, photocatalytic ozonation, photoelectrocatalysis, sono-Fenton, etc.) (KANAKARAJU; GLASS; OELGEMÖLLER, 2018; MIKLOS et al., 2018; TROJANOWICZ et al., 2018).

Figure 1. AOP classification by process type.

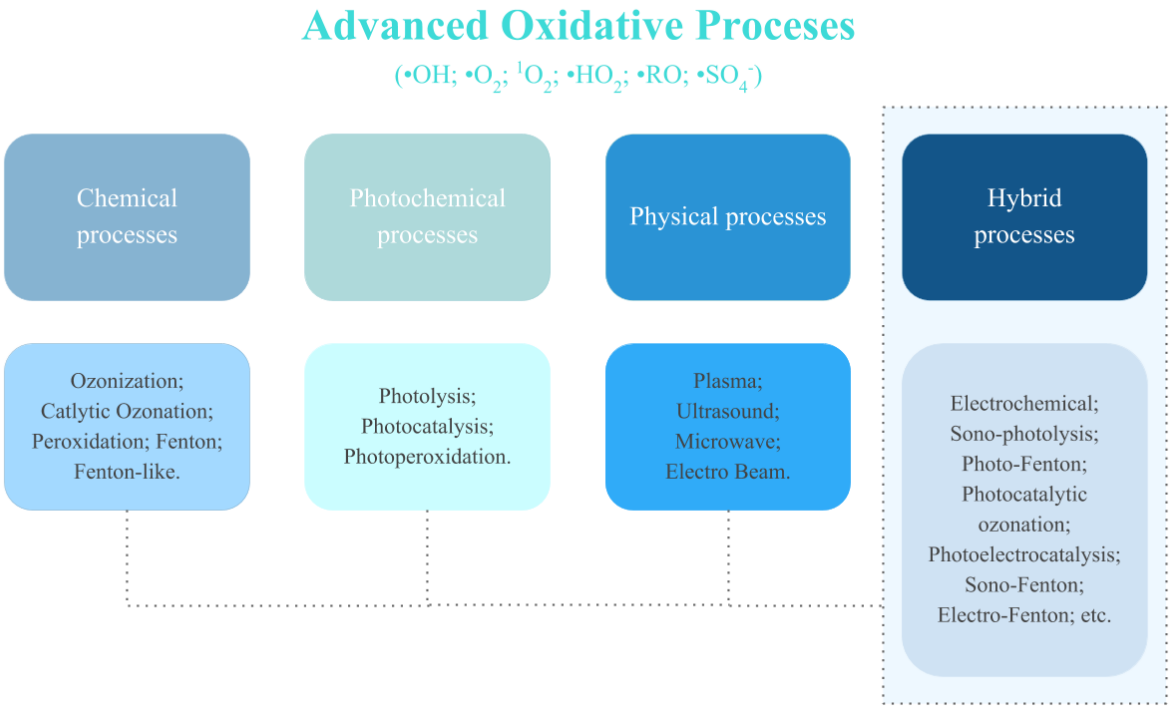

Source: Author's own elaboration.

Photocatalysis and Fenton oxidation techniques have attracted special attention in last few years, due to their high efficiency in degrading several organic pollutants, including recalcitrant compounds and micro-pollutants. Besides, their environmental friendly behavior and their great mineralization capacity also stand out (RODRIGUEZ-NARVAEZ et al., 2017). Although very promising, both still have limited applications, since some drawbacks remain an obstacle.

One of the biggest hindrance to spread out photocatalytic technology is associated to catalyst activation, since the majority of them show great performance just in the UV range. In this way, the operation requires electric energy and frequent lamps substitution, resulting in a high cost water treatment (MIKLOS et al., 2018). Furthermore, the electron recombination of these materials is also an undesirable issue (DI PAOLA et al., 2012). JIANG et al. (2017) affirmed that it is yet a challenge to develop a photocatalyst which is stable, abundant, efficient and with simple fabrication.

Fenton oxidation processes also have some disadvantages, such as the high amount of inorganic waste sludge produced after treatment, the very narrow and low pH operation range and low iron salts recyclability (MA et al., 2015). ANEGGI; TROVARELLI; GOI (2017) point out that one of the main obstacles for its diffusion in large scale are the iron sludge treatment, the chemicals consumption and pH adjust requeriments. For photo-Fenton processes, besides from the already cited Fenton's drawbacks, the high energy consumption associated to the UV light makes it even more expensive, difficulting its implementation (LOFRANO; MERIC, 2014).

Therefore, several new alternative catalysts are being studied to overcome these problems, in particular, by trying to lower the band gaps and by applying heterogeneous processes, in order to solve the sludge disposal, for both photocatalysis and Fenton, respectively (DEWIL et al., 2017).

3.1.1 Heterogeneous photocatalysis

Heterogeneous photocatalysis is an AOP that is been used in several different environmental applications, as, for example: water splitting, oxidation/mineralization of organic pollutants, reduction of hazardous metal contaminants, selective organic transformations and CO_2 reduction for fuel production (WEN et al., 2015). This method has been highlighted, due to its various advantages, as: high mineralization

potential of a wide range of organic compounds, no supplementation of additional electron acceptors is needed, environmentally friendly, the photocatalyst can be reused and, in some cases, solar energy can be used to activate the catalyst (DI PAOLA et al., 2012; GADGIL; IBRAYEV; NURAJE, 2016).

Photocatalytic reactions occur when a semiconductor material (photocatalyst) absorbs the photons provided from the light source and, if the energy is equal or superior to its bandgap, the catalyst is led to an excitation state. Bandgap can be defined as the energetic difference between the highest energy point of the semiconductor- so called valence band (VB) - and its lowest energy point- known as conduction band (CB) (NOGUEIRA; JARDIM, 1998; CHENG et al., 2018).

The photocatalyst activation is represented in Figure 2. Basically, an electron (e^-) is excited from the VB to the CB, as a result, a hole (h^+) is formed in the first region, forming the so called electron-hole pair. These species react with electrons acceptors/donors and then generate reactive radicals, which promote reduction reactions on the CB and oxidation reactions on the VB. However, if no reactions occur, the electron-hole pair recombines, releasing energy as heat (NOGUEIRA; JARDIM, 1998).

Figure 2. Representative scheme of a semiconductor being applied in heterogeneous photocatalysis.

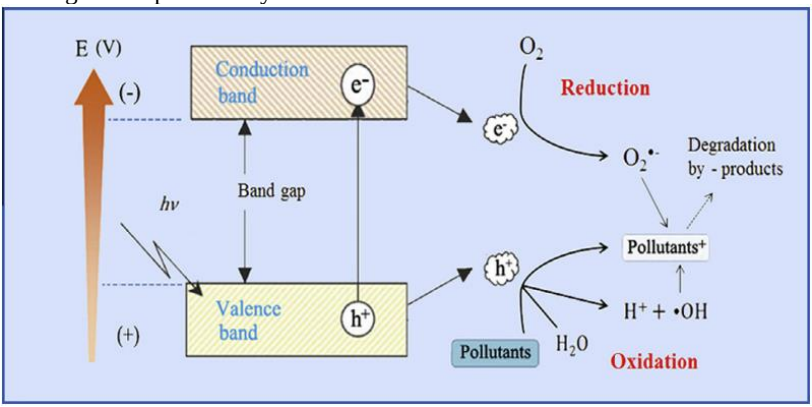

Source: Modified from CHENG et al., 2018.

If the irradiant energy either matches or exceeds the semiconductor's bandgap, the activation of the photocatalyst occurs after it absorbs the photons' quanta (Eq. I).

$$\text{Photocatalyst} + h\upsilon \rightarrow \text{Photoatalyst}\ (e^- + h^+) \quad \text{(I)}$$

After the photo-excitation in the presence of water, the photo generated holes (h^+) can promote several oxidation reactions (Equations II-IV), while e^- undergoes through reduction processes (Equations V-VII). This occurs by the reaction of these species with distinct adsorbed electrons acceptors and donors as O_2, H_2O or OH^-, producing various reactive oxygen species (ROS), such as $\bullet O_2^-$, •OH and hydrogen peroxide (H_2O_2) molecules (FUJISHIMA; ZHANG; TRYK, 2008; PRAKASH et al., 2018).

Oxidation reactions:

$$H_2O + h^+ \rightarrow \bullet OH + H^+ \quad \text{(II)}$$

$$OH^- + h^+ \rightarrow \bullet OH \quad \text{(III)}$$

$$\bullet OH + \bullet OH \rightarrow H_2O_2 \quad \text{(VI)}$$

Reduction reactions:

$$O_2 + e^- \rightarrow \bullet O_2^- \quad \text{(V)}$$

$$\bullet O_2^- + H^+ \rightarrow \bullet HO_2 \quad \text{(VI)}$$

$$\bullet HO_2 + H^+ + e^- \rightarrow H_2O_2 \quad \text{(VII)}$$

Although, many semiconductors' photocatalyt activity (such as: ZnO, ZnS, CdS, GaO, WO_3, Fe_2O_3, SnO_2 and NiO) have been investigated, titanium dioxide (TiO_2) is worldwide disseminated as the most appropriate photocatalyst, due to its characteristics, as high photoactivity, chemical inertness, non-toxicity, low cost and easy obtainment (CARP; HUISMAN, RELLER, 2004; AKPAN; HAMEED, 2009). However, its low quantum efficiency and high band gap (3.2 eV) really limits its use under visible light, which is unpleasant, since photocatalysis cost could lower significantly by the use of the reaching Earth's surface visible solar light (43%). That is much greater than the UV percentage (4%) (DI PAOLA et al., 2012; NIU, 2016).

Thus, in order to advance in this field, finding other catalysts with some of the main TiO_2 properties, but with lower band gap (such as Ag_2MoO_4) is still a priority.

3.1.2 Heterogeneous catalytic peroxidation (Fenton-like) and photo-peroxidation (photo-Fenton-like)

Hydrogen peroxide (H_2O_2) is an attractive oxidant, not only for its low cost but also for its environmental friendly behavior, although, it has

poor activity on its own (SUI et al., 2013). However, the discovery that ferrous ions (Fe^{+2}) could catalyze peroxide oxidation reactions (FENTON, 1895), really revolutionized the field, due to its enormous oxidizing potential. The main reactions involved in this procedure are described in the Equations VIII and IX, although some other competitive reactions have also been reported, as exposed in the Equations X, XI and XII. (FENTON, 1895; DE LAAT; GALLARD, 1999; NEYENS; BAEYENS, 2003).

$$Fe^{2+} + H_2O_2 \rightarrow Fe^{3+} + \bullet OH + OH^- \quad \text{(VIII)}$$

$$Fe^{3+} + H_2O_2 \rightarrow Fe^{2+} + \bullet HO_2 + H^+ \quad \text{(IX)}$$

$$\bullet OH + H_2O_2 \rightarrow H_2O + \bullet HO_2 \quad \text{(X)}$$

$$Fe^{2+} + \bullet OH \rightarrow Fe^{3+}\ OH^- \quad \text{(XI)}$$

$$\bullet OH + \bullet OH \rightarrow H_2O_2 \quad \text{(XII)}$$

To enhance the Fenton process efficiency, it can be combined to photochemical processes by the incidence of UV light source (photo-Fenton), which promotes a smaller catalyst loading, as well as a major •OH production, and, consequently to a major degradation of organic pollutants (ZEPP; FAUST; HOIGNÉ, 1992; WANG et al., 2016).

In conventional Fenton process, the degradation reactions are interrupted when all Fe^{2+} ions or H_2O_2 are consumed, while the Fe^{3+} ions remain almost inactive in the system. However, the introduction of a light source enables the regeneration of the ferrous ions (Fe^{2+}) from the ferric ions (Fe^{3+}) (Equation XIII), making it possible for the radical formation to continue (ZEPP; FAUST; HOIGNÉ, 1992; MIRZAEI et al., 2016).

$$Fe^{3+} + H_2O + h\upsilon \rightarrow Fe^{2+} + \bullet OH + H^+ \quad \text{(XIII)}$$

Furthermore, depending on the lamp's wavelength ($\lambda < 310$ nm) direct photolysis of H_2O_2 occurs (Equation XIV), generating more hydroxyl radicals to oxidize the contaminants (BABUPONNUSAMI; MUTHUKUMAR, 2014).

$$H_2O_2 + h\upsilon \rightarrow 2\ \bullet OH \quad \text{(XIV)}$$

Fenton process is one of the most attractive AOPs, once it is able to degrade several different organic contaminants as well as being low cost, high safety and of simple management, having even being implemented in some large scale systems, as wastewater and hospital effluent treatments (BAE et al., 2015; PERINI et al., 2018).

However, some disadvantages of the Fenton-like reactions, as: its operational pH (≈ 3), the waste sludge production and low recyclability, made it necessary to improve this process. A promising alternative for it is the use of non-ferrous catalysts in heterogeneous Fenton-like reactions. This kind of system has called attention, due to its easier recovery/separation of the catalyst, its reuse and its greater efficiency-consuming less H_2O_2 per mole of pollutant degraded (BABUPONNUSAMI; MUTHUKUMAR, 2014; BOKARE; CHOI, 2014).

Therefore, heterogeneous Fenton-like reactions, with non-ferrous materials have been widely studied as a solution for these drawbacks. Several works with a great variety of metals have already been published, such as: copper (Cu), manganese (Mn), cerium (Ce), cobalt (Co), aluminum (Al), chromium (Cr), ruthenium (Ru), as well as bimetallic combination of them and even their polyoxometalates (GALLARD; DE LAAT; LEGUBE, 1999; GOULD; GRIFFITH; SPIRO, 2001; WATTS et al., 2005; HECKERT; SEAL; SELF, 2008; BOKARE; CHOI, 2009; LING; WANG; PENG, 2010; BOKARE; CHOI, 2010; HU et al., 2011; WANG; SHIH, 2015).

Silver (Ag) and molybdenum (Mo) still have few reports in this field. As far as known by these authors, the use of Ag_2MoO_4 in peroxidation processes has not yet been reported, being one of the main motivations of this study. For further comparison, a summary of the existent results with both Ag and Mo as catalysts in peroxidation reactions are presented in Table 2, Table 3 and Table 4.

3.2 SILVER MOLYBDATE

Silver molybdate (Ag_2MoO_4) is an inorganic semiconductor with high electrical conductivity, photoluminescence, elevated energy storage performance, environmental green composition and non-toxic. It also has special characteristics such as antimicrobial, electrocatalyic and photocatalytic activities (BHATTACHARY; GHOSH, 2007; DE SANTANA et al., 2014; CUNHA et al., 2015; BAI; LU; LIU, et al., 2018; KUMAR et al., 2016).

Due to these characteristics, it has been applied in several different applications, as in: high-temperature lubricants (GULBIŃSKI; SUSZKO, 2006; LIU et al., 2013), ceramics (ZHOU et al., 2014), antibacterial materials (FABBRO et al., 2016), ion conducting glass (BHATTACHARYA; GHOSH, 2007; SANSON et al., 2007), photoswitches (CHENG et al., 2009), substrates to Raman Scattering

(FODJO et al., 2013), electrocatalysts (KUMAR et al., 2016), mercury oxidation catalyst (ZHAO et al., 2015) and photocatalysts (XU et al., 2015a; OLIVEIRA et al., 2017; WANG et al., 2017).

Ag_2MoO_4 crystal structure was firstly described by WYCKOFFL (1922). Further studies reported that this material exists in two distinct phases: α-Ag_2MoO_4 with a tetragonal structure and β-Ag_2MoO_4 with a cubic structure (WYCKOFFL, 1922; DONOHUE; SHAND, 1947; ARORA et al., 2012). It is known that α-Ag_2MoO_4 is a thermodynamically metastable phase, while β-Ag_2MoO_4 is the stable one. When exposed to temperatures higher than 280 ºC, the α-phase irreversibly transforms into β-phase (further about this issue is explored in section 4.1).

As photocatalyst, Ag_2MoO_4 has been highlighted, not only for the already properties mentioned, but also because low band gaps could be achieved, some reports even stand out its activity under visible light (WANG et al., 2017; ZHANG; MA, 2017a). Some authors have also studied its capability of radicals formation; holes (h^+), hydroxyl radicals (•OH) and superoxide anion radical ($\bullet O_2^-$) were detected as the main ROS contributors into the oxidation of organic compounds (XU et al., 2015a; DHANABAL; VELMATHI; BOSE, 2016; TANG et al., 2017; ZHANG; MA, 2017a; YANG et al., 2017a; LI; LIU; LI, 2018).

3.3 EMERGING CONTAMINANTS

The latest technological advances have turned possible to detect more deeply the concentration of organic pollutants in water resources, achieving ranges of $ng \cdot L^{-1}$ and $\mu g \cdot L^{-1}$. These compounds are being so called emerging contaminants (EC) or micro pollutants. Despite their low values, they have been recently recognized as possibly harmful and worrisome products on the water resources (POYNTON; ROBINSON, 2018). Furthermore, the extent of these products and their transformation by-products is unknown as well as their effect on human's health and environmental systems (RODRIGUEZ-NARVAEZ et al., 2017).

Although, the ECs disposal is not yet regulated, some directives have been released in Europe and in North America, with priority compounds, in order to try reducing its release in the environment. Furthermore, Canada and Switzerland are trying some new projects to develop strategies to treat ECs release in their wastewater treatment plants (EC, 2013; SCHÄRER; BLENY, 2015; MORALES-CASELLES et al., 2016; NORMAN NETWORK, 2018).

EC are natural or synthetically substances, generally, remnants from products of daily consume, as: personal care products, plasticizer, pesticides, surfactants, hormones, pharmaceuticals, etc. These products are, in general, resistant to natural attenuation and conventional water treatments, leading to their bioaccumulation in surface water, sand, sediments, soils, groundwaters and seas (RUHÍ et al., 2015; WILKINSON et al., 2017). TAHERAN et al. (2018) called this fact as "pseudo-persistency" and affirm that this condition is enough to promote adverse effects in several organisms.

3.3.1 Pharmaceutical compounds

Pharmaceuticals are biologically active compounds, which are known to alter the functioning of the metabolism of humans and animals. Firstly, drugs were obtained by solvent extraction of plants. Then, in the 19th century, synthetic drugs started to be developed, when liquid chloroform was applied for the first time as anesthetic drug (SNEADER, 2005). Great advances were obtained in this field, leading to the development of thousands of medicines, which continue to grow due to its increasing demand (TIWARI et al., 2017).

However, this elevated consume of pharmaceuticals has contributed to their presence in water resources (such as surface water, groundwater, wastewater and drinking water, as well). It's known that even in trace concentrations these contaminants can be toxic to the environment (MIRZAEI et al., 2016; KANAKARAJU; GLASS; OELGEMÖLLER, 2018). Moreover, drugs have potential of being teratogenic and carcinogenic, as well as occasioning side effects upon the organisms, due to their therapeutic properties and compositions (KOOPAEI; ABDOLLAHI, 2017; BASHEER, 2018).

The major source of pollution by pharmaceuticals comes from hospitals, industries, and households (Figure 3). The extended permanence of drugs in water sources is highly related to their low biodegrability and high persistence to conventional treatments, causing their extensive bioaccumulation in several aquatic and solid medias, interfering in their biota (YANG et al., 2017b). These properties may also cause an incomplete mineralization of these pollutants, enabling the formation of even more toxic sub-products (PAL et al., 2010; SHARMA; AHMAD; FLORA, 2018).

Figure 3. Sources and pathways of pharmaceuticals pollution (where, DWT is drinking water treatment and WWTP is wastewater treatment plant).

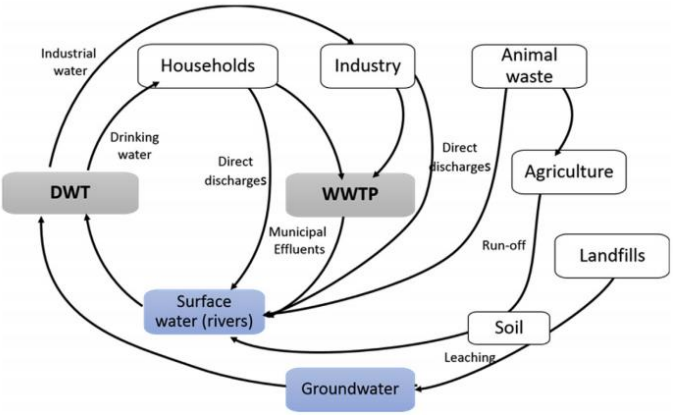

Source: TEODOSIU et al., (2018).

The natural removal of each pharmaceutical compound depends on their own characteristics, for example: biotransformation, volatilization, photolysis, hydrolysis, sedimentation, persistency and sorption propensity (TEODOSIU et al., 2018). As the removal of pharmaceuticals via hydrolysis, photolysis and biological treatments are infeasible, - once they normally represent insufficient mineralization - it becomes necessary to employ more effective solutions (RADJENOVIC et al., 2009; PAL et al., 2010; TROVÓ et al., 2012). Thus, AOP have emerged as an excellent alternative, since they are capable of removing several different and resistant organic contaminants with a reduced reaction time (SHARMA; AHMAD; FLORA, 2018).

Pharmaceuticals can be classified by its function in several groups. Some of the most consumed are: analgesics, antibiotics, antidepressants/anxiolytics, hormones, lipid regulators, and proton pump inhibitors (ORTIZ DE GARCÍA et al., 2013). According to KOSMA; LAMBROPOULOU; ALBANIS (2016) the last class should be monitored and evaluated more carefully, since their metabolites have been found in wastewaters. But, few is known about their effects in the environment.

3.3.2 Proton Pumps Inhibitors (PPI)

Proton pump inhibitors (PPI) are a medicine group that have as purpose irreversibly inhibit the H^+/K^+-adenosine triphosphatase (proton pump) enzyme production in the gastric system, catalyzing the exchange of H^+ and K^+ cations. Thus, these drugs are applied in treatment of gastrointestinal disorders, such as: esophagitis, peptic ulcer, gastroesophageal reflux disease, Helicobacter pylori infection, gastrointestinal complications, duodenal ulcer and Zollinger-Ellison syndrome. The main PPI are omeprazole, esomeprazole, lansoprazole, pantoprazole and rabeprazole (RICHARDSON et al., 1998; VAEZI; YANG; HOWDEN, 2017).

This drug class is one of the most commonly consumed worldwide, since they are also prescribed together with other medications such as antibiotics, for example (NEHRA et al., 2018). In 2015, these pharmaceuticals ranked in the top ten national health-related drugs expenditures (SCHUMOCK et al., 2016).

It is important to point out that the use of PPI may have several side effects, as: muscle cramps, diarrhea, nausea, dizziness, jittery feeling, confusion, headache, limp feeling, loss of appetite, memory problems, uneven heart beats, choking feeling, etc. (HERZIG et al., 2014). Moreover, studies reported that their long-term consumption may include other hazards, such as: risk of fractures, Campylobacter or Salmonella infection, small intestinal bacterial overgrowth, myocardial infarction, pneumonia, Clostridium difficile diarrhea, stroke, hypomagnesemia, vitamin B_{12} deficiency, anemia, chronic kidney disease, spontaneous bacterial peritonitis, and also dementia (LAHEIJ et al., 2004; BAVISHI; DUPONT, 2011; KWOK et al., 2012; LAM et al., 2013; LO; CHAN, 2013; CHEUNGPASITPORN et al., 2015; FURUYA-KANAMORI et al., 2015; HAENISCH et al., 2015; XU et al., 2015b; LAZARUS et al., 2016; ZHOU et al., 2016; VAEZI; YANG; HOWDEN, 2017).

According to SHI; KLOTZ (2008) approximately 70-95% of the consumed PPI are excreted as inactive or pharmaceutically active metabolites (such as hydroxyl-omeprazole, hydroxy-lansoprazole, desmethyl-pantoprazole) in urine and feces. Moreover, their transformation products have been found water resources (GRACIA-LOR; SANCHO; HERNÁNDEZ, 2011; BOIX et al., 2015). Although, just few studies of their monitoring have been published in the last decade, as shown in Figure 4 (SCOPUS, 2018).

Figure 4. Number of publications about PPI's presence in waters sources on the last decade.

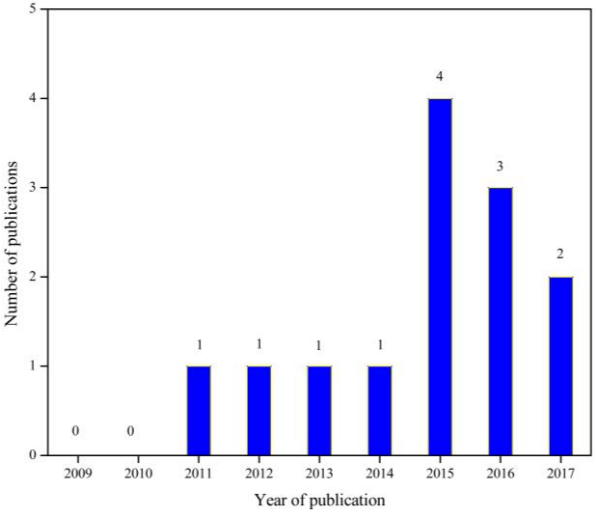

Source: SCOPUS, 2018. Advanced search in Scopus with title, abstract, keywords: "proton pump inhibitor" AND water AND environment.

3.3.3 Pantoprazole (PAN)

PAN (Figure 5) was reported as the top twenty selling drugs and as the second most consumed PPI worldwide, just behind omeprazole. It was estimated that, in 2009, 13.850–27.710 kg·day^{-1} of this drug were consumed (ORTIZ DE GARCÍA et al., 2013; ALI; AL-OTHMAN; ALHARBI, 2016).

Figure 5. Molecular formula of pantoprazole.

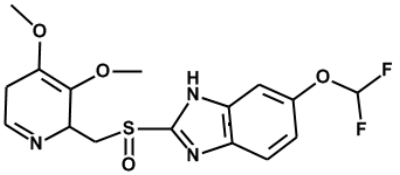

Source: Author's own elaboration.

In terms of persistence, ORTIZ DE GARCÍA et al. (2013) associated PAN to the maximum level of concern, due to its stability and biodegradation resistance. This fact is plausible, since this pharmaceutical was developed to be a PPI with enhanced stability (KATZ, 2000).

Furthermore, PAN may interfere in biological treatments, since it has high toxicity and carcinogenic characteristics (POWERS; LAWTON; MODLIN, 1995; GAN et al., 2017). Due to these characteristics, this drug has been found in some monitoring studies (more information is presented in section 4.3)

Although, PAN is a persistent emergent contaminant and its presence on the environment could cause a great impact- due to its large consumption-, efficient technologies to remove it from water sources have not yet been developed. So, this work is a first approach to the use of Ag_2MoO_4 on the AOP treatments of contaminated water or wastewater with PAN.

4 STATE OF ART

4.1 SILVER MOLYBDATE AS PHOTOCATALYST

In photocatalysis, Ag_2MoO_4 is being widely studied in the last decade as catalyst, for its already mentioned characteristics. It is possible to notice that β-Ag_2MoO_4 has been extensively more investigated than α-Ag_2MoO_4 (Table 1). Different techniques have been used to produce it, as: controlled precipitation (DHANABAL; VELMATHI; BOSE, 2016; CAO et al., 2017; WANG et al., 2017), hydrothermical (KUMAR et al., 2016; SOUSA et al., 2018), dynamic template route (JIANG et al., 2015), impregnation/calcination (ZHAO et al., 2015) and microwave-assisted (DE SANTANA et al., 2014; OLIVEIRA et al., 2017).

Besides that, the influence of many parameters in the obtainment of β-Ag_2MoO_4 has been studied, for example: pH (JIAN et al., 2017; YANG et al., 2017a; PANDIRI et al., 2018), autoclaving time and temperature (SOUSA et al., 2018), additives presence (JIANG et al., 2015; KUMAR et al., 2016; TANG et al., 2017; YANG et al., 2017a) and solvent media (CUNHA et al., 2015; XU et al., 2015a; FABBRO et al., 2018; LI; LIU; LI, 2018).

Thus, a large variety of β-Ag_2MoO_4 morphologies were obtained: flower-like, centered cubes, potato-like, microrods, nanoclusters, butterfly-like, coral-like, bud-like, spheres, micro polygonal particles, octahedral, nanowires, etc. (DE SANTANA et al., 2014; JIANG et al., 2015; NG; FAN, 2015; KUMAR et al., 2016; OLIVEIRA et al., 2017; WANG et al., 2017; YANG et al., 2017a; SOUSA et al., 2018).

However, the majority of these studies were only able to synthesize the β-phase of Ag_2MoO_4. It is known that metastable phases materials (as α-Ag_2MoO_4) exhibit different physical-chemical properties from their thermodynamically stable counterparts (CHEN et al., 1997). Due to the perspective of obtaining materials with novel properties and unique applications, a lot of research in this field has been made. Although, obtaining metastable phases remains a challenge, since they are prone to transform into their more stable phases, difficulting their achievement (LU et al., 2001).

Due to its stability, the β-phase was relatively easy obtained in mild conditions (JIANG et al., 2015; CAO et al., 2017; YANG et al., 2017a; ZHANG; MA, 2017b) while a theoretical study indicated that α-Ag_2MoO_4, could only be achieved when submitted to high hydrostatic pressures, since it is a metastable phase (BELTRÁN et al., 2014; CUNHA et al., 2015). This fact shows that α-Ag_2MoO_4 has a higher energy and,

consequently, a more excellent photocatalytic performance (WANG et al., 2017). However, recently, the synthesis of α-Ag_2MoO_4 by simple methodologies was reported (NG; FAN, 2015; WANG et al., 2017). The differential of these studies is the addition of an organic polymer as a stabilizer, in the studies both 2,3-Bis(2-pyridyl)pyrazine (DPP) and polyvinylpyrrolidone (PVP) were used.

PVP has been used as a stabilizer on several metallic nanoparticles synthesis, its polar groups interact with metal ions and form a complex (BONNEMAN et al., 2008). JIANG et al. (2004) proposed Ag^+ react with the lone electron pairs of both the oxygen and the nitrogen of the molecule (Figure 6).

Figure 6. Possible PVP and Ag^+ ions complexation.

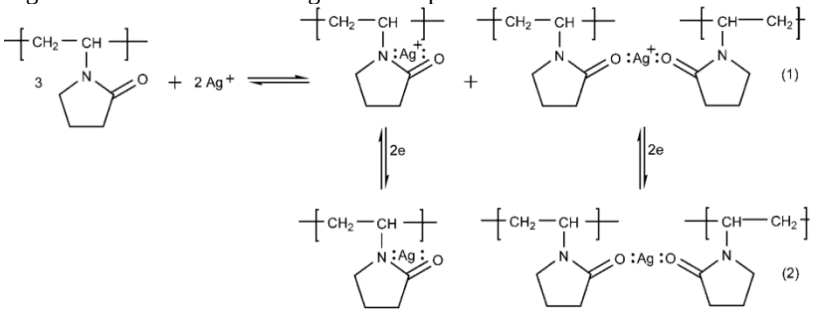

Source: JIANG et al., 2004.

The complex formation changes not only the particle size of the dispersed particles, but also the surface accessibility to them (TERANISHI; MIYAKE, 1998). The reason metal/organic stabilizer can change the final structure of the material, as reported by NG; FAN (2015), who obtained more α-phase by increasing DPP's concentration during their synthesis.

Moreover, interesting band gap results have been reported, some even lower than TiO_2 for instance, in particular for α-phase or mixtures of phases (NG; FAN, 2015; XU et al., 2015; DHANABAL; VELMATHI; BOSE, 2016; OLIVEIRA et al., 2017). The study of WANG et al. (2017) deserves to be highlighted, since the synthesized Ag_2MoO_4 (developed by a simple precipitation method under mild conditions) was able to degrade 95% of methylene blue (8 mg $\cdot L^{-1}$) in just 1 h under visible light. For this reason, and also due to the fact that these authors were able to obtain Ag_2MoO_4 with its both phases, this methodology was chosen for the catalyst synthesis.

Table 1. State of art of Ag_2MoO_4 synthesis and photocatalytic studies.

Catalyst Synthesis		**Characterizations**			**Photocatalysis reactions conditions**						**Reference**
Reactants	Methodology	Crystal Phases	Morphology (μm)	Band gap (eV)	Catalyst dosage ($mg \cdot L^{-1}$)	Light source (λ nm; power W)	Targeted Compound ($mg \cdot L^{-1}$)	Previous adsorption time (min)	Reaction time (min)	Compound removal (%)	
Na_2MoO_4; $AgNO_3$; Water media	Synthesis; Microwave-autoclaved (140 ºC, 1 h); Centrifugation; Washed (water and ethanol); Dried (70 ºC, 24 h)	β-phase	Nanorods (0.02-1)	3.15 (DT)			Not evaluated				DE SANTANA et al.,2014
Na_2MoO_4; CH_3COOAg Water media	Synthesis; Aging at 60 ºC (8 h); Centrifugation; Washed (water/acetone); Dried (room temperature, 12 h)	β-phase	Quasi-spherical (~4)	3.30 (IT)			Not evaluated.				CUNHA et al.,2015
Na_2MoO_4; CH_3COOAg Methanol media			Quasi-spherical (~1)	3.22 (IT)							
Na_2MoO_4; CH_3COOAg Ethanol media			Enlongated crystals (~5)	3.34 (IT)							
Na_2MoO_4; CH_3COOAg Propanol media			Enlongated crystals (~5.5)	3.36 (IT)							
Na_2MoO_4; CH_3COOAg 1-butanol media			Enlongated crystals (~6)	3.38 (IT)							

Source: Author's own elaboration.

Table 1 (continue)

Catalyst synthesis		Characterizations			Photocatalysis reactions conditions						Reference
Reactants	Methodology	Crystal Phases	Morphology (μm)	Band gap (eV)	Catalyst dosage ($mg \cdot L^{-1}$)	Light source (λ nm; power W)	Targeted Compound ($mg \cdot L^{-1}$)	Previous adsorption time (min)	Reaction time (min)	Compound removal (%)	
Na_2MoO_4; $AgNO_3$; Water media	Synthesis; Eggshell Membrane reactor; Aging (20 ºC, 24 h); Centrifugation; Washed (water and ethanol); Dried in dissector	β-phase	Dendritic nanocrystals	Not evaluated	4000	UV-VIS light (300-500; 500)	RhB (9.6)	Not specified	240	~100	JIANG et al., 2015
Na_2MoO_4; $AgNO_3$; Water media									270	~100	
Na_2MoO_4; $AgNO_3$; AM; Water media									180	~100	
Na_2MoO_4; $AgNO_3$; AM; PAM; Water media			Nanoclusters (0.05)						210	~100	
Na_2MoO_4; $AgNO_3$; Water media		β-phase	Irregular microparticles (2-4)	3.89 (IT)							
DPP/Na_2MoO_4 (0.15, 0.75 and 1.5) $AgNO_3$; Water media	Synthesis; Aging (1 h); Centrifugation; Washed (water)	α- and β-phase	Bud-like (0.2-0.55)	3.44 (IT)			Not evaluated				NG; FAN, 2015
		α- and β-phase	Spherical aggregates (0.9-0.98)	3.12 (IT)							
		α-phase	Spherical (0.01)	3.01 (IT)							

Source: Author's own elaboration.

Table 1 (continue)

Catalyst synthesis		Characterizations			Photocatalysis reactions conditions						Reference
Reactants	Methodology	Crystal Phases	Morphology (μm)	Band gap (eV)	Catalyst dosage ($mg \cdot L^{-1}$)	Light source (λ nm; power W)	Targeted Compound ($mg \cdot L^{-1}$)	Previous adsorption time (min)	Reaction time (min)	Compound removal (%)	
Na_2MoO_4; $AgNO_3$; Cyclohexane media	Synthesis; Aging (25 h); Centrifugation; Washed (water and ethanol); Dried (70 ºC, 4 h)	β-phase	Rod-like (0.2)	3.4 (DT)	1000	UV light (400; 300)	MB (4.8)	60	90	79	XU et al., 2015
$(NH_4)_2MoO_4$; $AgNO_3$; Water media	Synthesis; Adjusted pH (7.5) Aging (4 h); Centrifugation; Washed (water); Dried (100 ºC, 12 h)	β-phase	Agglomerated and irregular cubes (1.9-5.5)	3.05 (DT)	100	Visible light (420; 350)	MB (10)	30	180	72	DHANABAL; VELMATHI; BOSE, 2016
Na_2MoO_4; $AgNO_3$; Water media	Synthesis; Aging at 90 ºC (10 min); Centrifugation; Washed (water and ethanol); Dried (60 ºC, 12 h)	β-phase	Round-shaped (~1)	3.32 (IT)				Not evaluated			FABBRO et al., 2016
Na_2MoO_4; $AgNO_3$; Ethanol media				3.33 (IT)							
Na_2MoO_4; $AgNO_3$; Ammonia media				3.29 (IT)							

Source: Author's own elaboration.

Table 1 (continue)

Catalyst synthesis		Characterizations			Photocatalysis reactions conditions						Reference
Reactants	Methodology	Crystal Phases	Morphology (μm)	Band gap (eV)	Catalyst dosage ($mg \cdot L^{-1}$)	Light source (λ nm; power W)	Targeted Compound ($mg \cdot L^{-1}$)	Previous adsorption time (min)	Reaction time (min)	Compound removal (%)	
Na_2MoO_4; $AgNO_3$; Urea; Water media	Synthesis; Aging (30 min); Autoclaved (120 ºC, 8 h); Centrifugation; Washed (water and ethanol); Dried (80 ºC, overnight)	β-phase	Potato-like (1-2)	3.14 (DT)	50000	UV light (365; not specified)	CIP (20)	30	40	98	KUMAR et al., 2016
Na_2MoO_4; $AgNO_3$; PVP Water media	Synthesis; Microwave-autoclaved (150 ºC, 1 h); Centrifugation; Washed (water, ethanol and acetone); Dried (12 h)	β-phase	Spherical coral-like (4)	3.2 (DT)	1000	UV light (6 lamps, 254, 15)	RhB (10)	None	270	23	OLIVEIRA et al., 2017
Na_2MoO_4; $AgNO_3$; Water and ethanol media			Truncated cube (4)	3.4 (DT)						38	
H_2MoO_4; $AgNO_3$; Water media	Synthesis; Adjusted pH (8.5); Microwave-autoclaved (150 ºC, 1 h); Centrifugation; Washed (water and ethanol); Dried (12 h)		Alongated coral-like (width: 1; length 5)	3.4 (DT)						57	

Source: Author's own elaboration.

Table 1 (continue)

Catalyst synthesis		Characterizations			Photocatalysis reactions conditions						Reference
Reactants	Methodology	Crystal Phases	Morphology (μm)	Band gap (eV)	Catalyst dosage ($mg \cdot L^{-1}$)	Light source (λ nm; power W)	Targeted Compound ($mg \cdot L^{-1}$)	Previous adsorption time (min)	Reaction time (min)	Compound removal (%)	
Na_2MoO_4; $AgNO_3$; Water media	Synthesis; Centrifugation; Washed (water and ethanol); Dried (60 ºC,12 h)	β-phase	Not evaluated	3.38 (IT)	500	Visible light (420; 350)	RhB (10)	30	12	~0	CAO et al., 2017
$(NH_4)_2MoO_4$; $AgNO_3$; Water media	Synthesis; Adjusted pH (7); Aging (1 h); Autoclavated (160 ºC, 20 h); Centrifugation; Washed (water and ethanol); Dried 60 ºC (12 h)	β-phase	Aggregated spherical-like particles (5.5)	3.35 (IT)	500	Visible light (400; 500)	RhB (10)	30	120	11	JIN et al., 2017
MoO_3; $AgNO_3$; Water and ammonia media	Synthesis; Aging (6 h); Centrifugation; Washed (water); Dried (room temperature, overnight)	β-phase	Micro polygonal particles	3.24 (DT)	10	Visible light (420; 350)	RhB (9.6)	4	7	10	TANG et al., 2017

Source: Author's own elaboration.

Table 1 (continue)

Catalyst synthesis		Characterizations			Photocatalysis reactions conditions						Reference
Reactants	Methodology	Crystal Phases	Morphology (μm)	Band gap (eV)	Catalyst dosage ($mg \cdot L^{-1}$)	Light source (λ nm; power W)	Targeted Compound ($mg \cdot L^{-1}$)	Previous adsorption time (min)	Reaction time (min)	Compound removal (%)	
$(NH_4)_6Mo_7O_{24}$; CH_3COOAg; PVP; Water media	Synthesis; Centrifugation; Dried (60 ºC, 12 h)	α- and β-phase	Butterfly-like (2)	3.2 (DT)	1000	Visible light (410; 50)	MB (8)	None	60	95	WANG et al., 2017
$(NH_4)_6Mo_7O_{24}$; $AgNO_3$; SDS; Water media	Synthesis; Adjust pH (7) Autoclaved (160 ºC, 14 h); Centrifugation; Washed (water and ethanol); Dried (60 ºC, overnight)	β-phase	Octahedral (6-8)	3.15 (DT)	400	Visible light (420; 300)	RhB (9580)	30	150	60	YANG et al., 2017a
Na_2MoO_4; $AgNO_3$; Water media	Synthesis;; Aging (2 h); Centrifugation; Washed (water and ethanol); Dried (60 ºC, 24 h)	β-phase	Not evaluated	3.20 (DT)	600	Visible light (420; 300)	RhB (5); MO (6); MB (5)	30	60	21; 3; 73	ZHANG; MA, 2017a
Na_2MoO_4; $AgNO_3$; Water media	Synthesis; Aging (1 h); Centrifugation; Washed (water); Dried (60 ºC, 24 h)	β-phase	Irregular microparticles	3.19 (DT)	600	Visible light (420; 300)	RhB (10); MO (10); TCH (20)	30	60	15; ~0; 48	ZHANG; MA, 2017b

Source: Author's own elaboration.

Table 1 (continue)

Catalyst synthesis		**Characterizations**			**Photocatalysis reactions conditions**						**Reference**
Reactants	Methodology	Crystal Phases	Morphology (μm)	Band gap (eV)	Catalyst dosage ($mg \cdot L^{-1}$)	Light source (λ nm; power W)	Targeted Compound ($mg \cdot L^{-1}$)	Previous adsorption time (min)	Reaction time (min)	Compound removal (%)	
Na_2MoO_4; $AgNO_3$; Water media	Synthesis; Aging (1 h); Centrifugation; Washed (water and ethanol); Dried (60 ºC, 24 h)	β-phase	Not evaluated	3.26 (DT)	600	Visible light (420; 300)	RhB (10); MB (5)	30	60	15; 73	ZHANG; MA, 2017c
Na_2MoO_4; $AgNO_3$; PEG; Water media	Synthesis; Aging (10 min); Ultrasounded (15 min); Centrifugation; Washed (water and ethanol); Dried (60 ºC)	β-phase	Octahedral particles	3.05 (DT)	1000	Visible light (420; 300)	RhB (10); TC (10) 4-CP (10)	30	8; 40; 90	11; 21; 28	ALBULIZI et al., 2018
$(NH_4)_6Mo_7O_{24}$; CH_3COOAg; PVP; Water media	Synthesis; Centrifugation; Dried (60 ºC, 12 h)	α- and β-phase	Butterfly-like	3.22 (DT)	1000	Visible light (410; 50)	MB (20);	None	12	12	HUO et al., 2018
Na_2MoO_4; $AgNO_3$; Ethylene glicol media;	Synthesis; Aging (12 h); Centrifugation; Washed (water and ethanol); Dried (60 ºC, 8h)	β-phase	Agglomerated cubes (1)	3.28 (DT)	400	Visible light (420; 500)	CIP (10)	30	60	~0	LI; LIU; LI, 2018

Source: Author's own elaboration.

Table 1 (continue)

Catalyst synthesis		Characterizations			Photocatalysis reactions conditions						Reference
Reactants	Methodology	Crystal Phases	Morphology (μm)	Band gap (eV)	Catalyst dosage ($mg \cdot L^{-1}$)	Light source (λ nm; power W)	Targeted Compound ($mg \cdot L^{-1}$)	Previous adsorption time (min)	Reaction time (min)	Compound removal (%)	
MoO_3; $AgNO_3$; Water and ammonia media	Synthesis; Aging (6 h); Centrifugation; Washed (water); Dried (room temperature, overnight)	β-phase	Irregular particles	3.24 (DT)	Not evaluated						LIU et al., 2018a
Na_2MoO_4; $AgNO_3$; DPP; Water media	Synthesis; Aging at 90 ºC (80 min); Autoclavated (120 ºC, 8 h) Centrifugation; Washed (water and ethanol); Dried (80 ºC, 12h)	β-phase	Aglomarated regular spheres	3.26 (DT)	Not specified	Visible light (not specified)	4-CP (15); TC (8880)	None	60	~0; ~0	LIU et al., 2018b
$(NH_4)_2MoO_4$; $AgNO_3$; Water media	Synthesis; Adjusted pH (7); Autoclaved (140 ºC, 12h); Centrifugation; Washed (water); Dried 60 ºC	β-phase	Irregular microparticles	3.2 (IT)	1000	Visible light (380-840; 500)	MO (not specified)	30	180	20	PANDIRI et al., 2018

Source: Author's own elaboration.

Table 1 (continue)

Catalyst synthesis		Characterizations			Photocatalysis reactions conditions						Reference
Reactants	Methodology	Crystal Phases	Morphology (μm)	Band gap (eV)	Catalyst dosage ($mg \cdot L^{-1}$)	Light source (λ nm; power W)	Targeted Compound ($mg \cdot L^{-1}$)	Previous adsorption time (min)	Reaction time (min)	Compound removal (%)	
Na_2MoO_4; $AgNO_3$; PVP; Ethylene glycol media	Synthesis; Aging 70 ºC (12 h); Centrifugation; Washed (water); Dried (70 ºC)	β-phase	Not evaluated	3.31 (IT)	1000	Visible light (420, 500)	RhB (15)	30	35	3	QU et al., 2018
Na_2MoO_4; $AgNO_3$; Water media	Synthesis; Autoclaved (100 ºC; 120 ºC; 140 ºC or 160 ºC, 2h) Centrifugation; Washed (water and ethanol); Dried (75 ºC, 12h)	β-phase	Irregular microparticles	3.35 (IT)	1000	UV light (6 lamps, 254, 15)	RhB (4.8)	10	120	86	SOUSA et al., 2018
			Potato-like	3.34 (IT)						91	
				3.33 (IT)						97	
			"Coral" (0.1 - 17)	3.32 (IT)						90	
Na_2MoO_4; $AgNO_3$; Water media	Synthesis; Aging (1 h); Centrifugation; Dried (60 ºC, 12 h)	β-phase	Not evaluated	3.16 (IT)	250	Visible light (not especified, 300)	MO (10)	None	20	~0	WU et al., 2018

Source: Author's own elaboration.

Table 1 (continue)

Catalyst synthesis		**Characterizations**			**Photocatalysis reactions conditions**						**Reference**
Reactants	Methodology	Crystal Phases	Morphology (μm)	Band gap (eV)	Catalyst dosage ($mg \cdot L^{-1}$)	Light source (λ nm; power W)	Targeted Compound ($mg \cdot L^{-1}$)	Previous adsorption time (min)	Reaction time (min)	Compound removal (%)	
MoO_4; $AgNO_3$; Water media	Synthesis; Ajusted pH (9) Aging (24 h); Centrifugation; Washed (water); Dried (60 ºC, overnight)	β-phase	Irregular particles (1- 5)	3.16 (IT)	300	Visible light (420, 300)	RhB (10)	60	6	2	XIE et al., 2018
Na_2MoO_4; $AgNO_3$; Water media	Synthesis; Filtration; Washed (deionized water); Dried (60 ºC, 12 h)	β-phase	Potato-like (3-4)	3.32 (DT)	600	Visible light (420; 300)	RhB (10); MB (10); MO (10); NFC (10); THC (20)	30	90	15; 43.9; 10; ~0; 45	JIAO et al., 2019

Source: Author's own elaboration.

where: AM -acrylamide; BPA - Bisphenol A; 4-CP – 4-Clorophenol; CIP – Ciprofloxacin; DPP -2,3-Bis(2-pyridyl)pyrazine; DT – Direct transition; IT – Indirect transition; MB - Methylene blue; MO – Methyl orange; NFC – Norfloxacin; PAM - Polyacrylamide; PEG - Polyethylene glycol; PVP -polyvinylpyrrolidone; RhB - Rhodamine B; SDS - Sodium dodecyl sulfate; TC – Tetracylclines; THC - Tetracylcline hydrochloride.

Some conclusions can be punctuated according to above information. First of all, it can be noted that several factors affect the morphologies of Ag_2MoO_4 catalysts (in special pH, calcination conditions and synthesis dopants/stabilizers), which affects its photocatalytic activity and band gap, since the morphology of the particles influence on its specific area and crystallizability, which consequently, modifies the amount of active sites exposed (WANG et al., 2018). Moreover, an important observation is that there is not a consensus if Ag_2MoO_4 suffers direct transition (DT) or indirect transition (IT), having many reports with both approaches. And, at last, as already commented before, α-phase was synthesized by just a little number of authors, due to its metastability. Thus, due to its potential, it can be noted that more investigations about this catalyst are needed. α-Ag_2MoO_4 in special for its low band gap, which not only can be applied in photocatalysis, but also in other AOP.

4.2 FENTON AND PHOTO-FENTON-LIKE CATALYSTS BASED IN SILVER AND/OR MOLYBDENUM

Recently, the promising catalyst performance of Ag alone or as part of a composite with other oxides,- as CeO_2, Fe_3O_4, $CoFe_2O_4/Fe_2O_3$ and SiO_2/α-Fe_2O_3- in Fenton-like reactions have been reported (Table 2). For heterogeneous photo-peroxidation, in particular, spectacular results were found; since its incorporation lowered the catalysts band gaps and oxygen vacancies were observed (ANEGGI; TROVARELLI; GOI, 2017; UMA et al., 2017; BIAN et al., 2018; SALEH; TAUFIK, 2019).

Besides that, MA et al., (2017) and HUANG et al. (2018) used Ag_3PO_4 in photo-Fenton-like reactions under visible light and obtained promising degradation results of dyes and bisphenol A (BPA) ($\geq$ 60%), especially when applied as part of composites, in which ~100% of the contaminants were removed.

It's also important to point out that relevant results were published by HUANG et al. (2018), that synthesized the $Ag_3PO_4/NiFe_2O_4$ composite, where Ag_3PO_4 was used to produce H_2O_2 by photocatalysis throughout the reaction, providing a kind of "autonomous" photo-Fenton-like, once no additional H_2O_2 was added to the system.

Yet, for peroxidation reactions with Mo-based catalysts, published studies also reflect great degradation percentages in photo-peroxidation reactions, some even conducted under artificial sunlight or visible light (Table 3). Different molybdenum-based materials were applied on researches, citing: molybdenum disulfide (MoS_2) combined with ferrous oxides, polyoxometalates and iron molybdate ($Fe_2(MoO_4)_3$) (TIAN et al.,

2011; CHEN et al., 2013; POURAN et al., 2015; YANG et al., 2016; RASHAD et al., 2017; SAMAKCHI; CHAIBAKHSH; MORADI-SHOEILI, 2018).

A study that deserves highlight is the one of TIAN et al., (2011), that used $Fe_2(MoO_4)_3$ and found that in the pH range of 3-9 the contaminant's degradation efficiency was almost unchanged, solving one of the major problems of the original Fenton's method.

Another curious investigation was developed by WANG et al. (2019), the authors reported that MoS_2 alone or when combined with H_2O_2 or Fe^{+2}, separately, shows photoluminescent properties, but when it is combined with both Fenton reactants, this characteristic decreases due to the presence hydroxyl radicals.

As far as known by these authors, just one catalyst with both Ag and Mo in its composition has been used as photo-Fenton-like catalyst (Table 4). XIU et al. (2019) applied $Fe_3O_4/Ag/Bi_2MoO_6$ to degrade two recalcitrant pollutants (BPA and Aatrex) and could completely degrade them in 3 h of reaction under visible light. And, again, as HUANG et al. (2018), no H_2O_2 was added to the reaction, being the peroxidation process realized just with the produced H_2O_2 from photocatalysis associated reactions.

Table 2. Overview of Ag-based or Ag composites catalysts for Fenton-like and photo-Fenton-like reactions.

Fenton-like and photo-Fenton-like reactions conditions										Reference
Catalyst composition	Catalyst dosage (mg ·L^{-1})	H_2O_2 dosage (mmol ·L^{-1})	Targeted Compound (mg ·L^{-1})	Light Source (λ nm; Power W)	pH	Temperature (ºC)	Previous adsorption time (min)	Reaction time (min)	Compound removal (%)	
Ag/CeO	1000	49	Phenol (100)	None	2	70	None	120	~100	ANEGGI; TROVARELLI; GOI, 2017
g-C_3N_4/ Ag/FeOOH	1000	0.010	MO (10.7)	Visible light (420; 300)	7	Room temperature	30	60	90	HE et al., 2017
Ag/AgCl	1000	6	BPA (10)	Visible light (420; 500)	4	Not specified	30	180	~100	LIU et al., 2017a
Ag/AgCl/Fe-S								60	~100	
Ag_3PO_4	1000	98	RhB (4.8)	None	Not evaluated	Room temperature	30	35	62	MA et al., 2017
Ag_3PO_4/CuO								120	65	
Ag_3PO_4				Visible light (420; 300)				35	74	
Ag_3PO_4/CuO								20	~100	
Ag-SiO_2/Fe_2O_3	600	20	MB (10)	Visible light (415; not specified)	Not specified		30	90	~100	UMA et al., 2017
Ag/ $CeFe_2O_4$/Fe_2O_3	Not specified	195	Rh6G (5)	Artificial Sunlight (300-800; 300)	Not evaluated	Room temperature	30	60	~100	BIAN et al., 2018

Source: Author's own elaboration.

Table 2 (continued)

Fenton-like and photo-Fenton-like reactions conditions										Reference
Catalyst composition	Catalyst dosage (mg ·L^{-1})	H_2O_2 dosage (mmol ·L^{-1})	Targeted Compound (mg ·L^{-1})	Light Source (λ nm; Power W)	pH	Temperature (ºC)	Previous adsorption time (min)	Reaction time (min)	Compound removal (%)	
Ag_3PO_4	250	8 (own's reaction production)	MO (10) BPA (10)	Visible light (420; 300)	Not evaluated	30	30	30	60; 45	HUANG et al., 2018
Ag_3PO_4/ $NiFe_2O_4$		4 (own's reaction production)							95; ~100	
Ag-Fe_3O_4/ graphene	400	39	MO (20) MB (20) CV (20) MG (20) CR (20) EY (20)	UV-C light (not specified; 40)	5	Not specified		120	91; 97; 81; 89; 75; 70	SALEH; TAUFIK, 2019

Source: Author's own elaboration.

where: BPA - Bisphenol A; CR – Congo red ; CV - Crystal violet; EY – Eosin Y; MB - Methylene blue; MG – Malachite green; MO – Methyl orange; RhB - Rhodamine B Rh6G - Rhodamine 6G

Table 3. Overview of Mo-based or Mo composites catalysts for Fenton-like and photo-Fenton-like reactions.

Fenton-like and photo-Fenton-like reactions conditions										Reference
Catalyst composition	Catalyst dosage ($mg \cdot L^{-1}$)	H_2O_2 dosage ($mmol \cdot L^{-1}$)	Targeted Compound ($mg \cdot L^{-1}$)	Light Source (λ nm; Power W)	pH	Temperature (ºC)	Previous adsorption time (min)	Reaction time (min)	Compound removal (%)	
$3MoO_3$ $3MoO_3 + Fe_2O_3$ $Fe_2(MoO_4)_3$	1400	18	AO II (100)	None	6.7	30	60	60	8 10 94	TIAN et al., 2011
$Fe_{2.79}Nb_{0.171}Mo_{0.023}O_4$	1000	200	MB (100)	None	10	Room temperature	120	180	90	POURAN et al., 2015
MoS_2			MO (20)					20	10	
Fe_2O_3/MoS_2	333	130	MO (20); CR (50); RhB (20)	Artificial Sunlight (not specified; 300)	Not evaluated	Room temperature	30	10; 6; 6	10; ~100; ~100	YANG et al., 2016
$Fe_2(MoO_4)_3$	1000	40	RhB (10)	Artificial Sunlight (8 lamps; not specified; 8)	Not evaluated		30	60	97	RASHAD et al., 2017
$MoS_2/MnFe_2O_4$	60	59	AB 113 (25)	None Visible light (not specified; 50)	6.3	Not evaluated	15	42	39 ~100	SAMAKCHI; CHAIBAKHSH; MORADI-SHOELI, 2018
$MoS_2 + Fe^{+2}$	3	10-20000	None (only H_2O_2 detection)	None	3	Room temperature	None	10	Not evaluated	WANG et al., 2019

Source: Author's own elaboration.

where: AB – acid blue; AO – Acid Orange; CR – Congo red ; MB - Methylene blue; MO – Methyl orange; RhB - Rhodamine B

Table 4. Overview Ag/Mo composite catalysts for photo-Fenton-like reactions.

Fenton-like and photo-Fenton-like reactions conditions										**Reference**
Catalyst composition	Catalyst dosage (mg ·L^{-1})	H_2O_2 dosage (mmol ·L^{-1})	Targeted Compound (mg ·L^{-1})	Light Source (λ nm; Power W)	pH	Temperature (ºC)	Previous adsorption time (min)	Reaction time (min)	Compound removal (%)	
Bi_2MoO_6	700	0.3 (own's reaction production)	BPA (10) ATX (10)	Visible light (420; 300)	3	Room temperature	30	180	40; 29	XIU et al., 2019
Ag/Bi_2MoO_6									57; 62	
$Fe_3O_4/Ag/Bi_2MoO_6$									~100; ~100	

Source: Author's own elaboration.
where: BPA - Bisphenol A; ATX - Aatrex

Despite the promising results showed in this section, much more should be explored in this field, since there are just few published and recent reports in this area of work (less than 15 studies in 8 years). Overall, as noted, exceptional catalysts for AOP may arise for the combined use of both Ag/Mo-based, especially for Fenton-like processes. For these reasons, the authors decided to investigate for the first time, as far as known, the behavior of Ag_2MoO_4 in peroxidation and photo-peroxidation reactions.

4.3 PANTOPRAZOLE OCCURRENCE IN SURFACE WATER

The occurrence of PAN in the domestic wastewater effluent was first reported by GRACIA-LOR; SANCHO; HERNÁNDEZ in 2010. After that, several different water matrixes were investigated, as: influent and effluent wastewater treatments, seas, rivers, surface water and in drinking water, as well (Table 5).

In some monitoring investigations PAN wasn't detected (VAN NUJIS et al., 2010; BARREIRO; VANZOLINI; CASS, 2011), on the other hand, a concentration of 180 $ng \cdot L^{-1}$ of it has been found in domestic wastewater- this value would be enough to affect the aquatic environment (GRACIA-LOR; SANCHO; HERNÁNDEZ, 2010; GRACIA-LOR et al., 2012). LUQUE-ESPINAR et al. (2015) reported the presence of PAN in drinking water showing its persistence in water for consume, even after physical-chemical treatment.

Only one of these studies was reported in Brazil (São Carlos, SP-Brazil). BARREIRO; VANZOLINI; CASS (2011) have not detect PAN in Monjolinho river, but the limit of detection employed (200 $ng \cdot L^{-1}$) on their methodology was high for EC measurements.

At last, as summarized by Table 5, few authors have proposed to verify the presence of PAN in water sources, giving preference to other compounds. Thus, more studies about the adversities of PPI in the environment are still required.

Table 5. Summary of monitoring reports of PAN in water matrixes.

Matrix	Country of the study	Limit of Detection ($ng \cdot L^{-1}$)	Concentration ($ng \cdot L^{-1}$)	Reference
Influent wastewater; Effluent urban wastewater	Spain	66; 33	Not detected; 180	GRACIA-LOR; SANCHO; HERNÁNDEZ, 2010
Effluent wastewater; River; Sea water	Germany	36 4.8; 4.8;	149; 13; Not detected	NÖDLER et al., 2010
Influent wastewater	Belgium	1	Not detected	VAN NUJIS et al., 2010
Effluent wastewater; River water	Brazil	200	Not detected	BARREIRO; VANZOLINI; CASS, 2011
Effluent wastewater; River water	Spain	4; 2	36; 117	GRACIA-LOR; SANCHO; HERNÁNDEZ, 2011
Influent wastewater; Effluent wastewater	Spain	60; 4	Not detected; 10-180	GRACIA-LOR et al., 2012
Effluent wastewater; River water	Germany	-	Incomparable duplicates (samples were discarded)	HILLEBRAND et al., 2013
Effluent wastewater; Surface water	Spain	0.1	Not detected - 7; Not detected - 1	BOIX et al., 2015
Surface water; Drinking water	Spain	2	Not detected; 20-50	LUQUE-ESPINAR et al., 2015

Source: Author's own elaboration.

4.4 PANTOPRAZOLE DEGRADATION IN WATER

The removal of PAN from water has been poorly studied, as summarized in Table 6. ALI; AL-OTHMAN; ALHARBI (2016) developed adsorption with nano iron particles as treating procedure, being able to remove 89% of the compound under mild conditions (pH = 7, 25 ºC). Yet, GAN et al. (2017) promoted heterogeneous Fenton-like and photo-Fenton-like processes with Fe_3O_4/CeO_2 as catalyst, in 2 h, 98% of PAN was degraded in the proposed reactions, but just 53% of it was mineralized. So, it's important to notice that this is a promising alternative for PAN's degradation, although it's TOC removal can still be enhanced.

Table 6. Studies focused on the treatment of PAN.

Reactions conditions											Reference
Treatment applied	PAN's concentration (mg ·L^{-1})	Catalyst dosage (mg ·L^{-1})	H_2O_2 dosage (mmol ·L^{-1})	pH	Temperature (°C)	Light source (λ nm, Power W)	Adsorption time (min)	Reaction time (min)	Removal		
									HPLC (%)	TOC (%)	
Adsorption	0.05	1000	None	7	25	None	30	-	89	Not evaluated	ALI; AL-OTHMAN; ALHARBI (2016)
Heterogenous Fenton-like	20	2000	30	3.3	35	None	None	120	~98	53	GAN et al., 2017
Heterogenous photo-Fenton-like						UV light (254; 100)			~98	Not evaluated	
						VIS light (480; 100)			~98	Not evaluated	

Source: Author's own elaboration.

5 INNOVATIVE ASPECT OF THIS DISSERTATION

As shown in chapters 3 and 4, developing the Fenton process is still a challenge, being the heterogeneous Fenton-like a promising alternative to its application. For this reason, the major contribution of this master's thesis is directly attached to the unprecedented application of Ag_2MoO_4 in catalytic peroxide and photo-peroxide oxidation reactions.

Besides that, as presented in the state of art, PAN degradation has only been studies focus twice. Thus, this work intends to elucidate some questions about its behavior when submitted to different AOP.

So, in this sense, this study aims to clarify some open points in the literature:

- Can Ag_2MoO_4 be used as catalyst in peroxidation reactions?
- In which studied AOP is Ag_2MoO_4 the most promising to be applied in?
- Is the as-prepared catalyst active in both UV and VIS light?
- Is the organic contaminant degraded and mineralized by the proposed reactions?
- Does the degradation mechanism of the pollutant change, depending on the chosen AOP?

6 METHODOLOGY

6.1 CHEMICALS AND MATERIALS

Silver acetate ($AgC_2H_3O_2$, 98% purity), and polyvinylpyrrolidone (PVP, $M_w \approx 40000$ g·mol^{-1}) were obtained from NEON. Ammonium molybdate ($(NH_4)_6Mo_7O_{24}$, analytical purity), hydrogen peroxide (H_2O_2, 30%, analytical purity), sulfuric acid (H_2SO_4, 95-99%, analytical purity) and hydrochloric acid (HCl, 37%, analytical purity) were purchased from Vetec. Ammonium metavanadate (NH_4VO_3, analytical purity) was obtained from Sigma-Aldrich. The pharmaceutical pantoprazole (99,5% purity) was purchased by Pharmanostra. All reagents were used without any further purification.

6.2 CATALYST SYNTHESIS

The catalyst was synthesized by the modified method of WANG et al. (2017). The controlled precipitation (CP) technique was used and is next described in detail. Briefly, 1 mmol of $AgC_2H_3O_2$ was added in 50 ml of deionized water under continuous stirring. After its total dissolution, 7.4 mmol of PVP were added, this high concentration was applied, since some works- that applied lower proportions PVP/reactants- were not able to produce the α-phase on the synthesized Ag_2MoO_4 (OLIVEIRA et al., 2017; QU et al., 2018). After the complete homogenization of the solution, 2.5 mL of $(NH_4)_6Mo_7O_{24}$ (0.0285 M) were added drop by drop, forming a white precipitate. The stirring was let for 30 min further that, for the purpose of aging. The solids were filtered in PVDF membranes (Durapore, 0.22 μm pore diameter) and then dried at 60 ºC overnight. The as-prepared catalyst (Ag_2MoO_4) was thermally treated in a muffle for 3 h at 300 ºC, and the calcinated catalyst is named $Ag_2MoO_4^{Calc.}$. For the homogenization of the particles, all the catalyst batches were mixed and macerated together.

Figure 7 shows a scheme of the as mentioned Ag_2MoO_4 synthesis. The $AgC_2H_3O_2$ dissociates in Ag^+ and $C_2H_3O_2^-$, then the cations interact with the lone pair of the oxygen and nitrogen atoms present in the PVP molecule, forming a complex (Figure 7A). When $(NH_4)_6Mo_7O_{24}$ is added, the precipitation of the catalyst occurs ((Figure 7B). After, the solids were filtered ((Figure 7C) and dried ((Figure 7D).

Figure 7. Scheme of Ag_2MoO_4 synthesis, (A) $AgC_2H_3O_2$ and PVP are stirred forming $[Ag(PVP)]^+$ complex; (B) the Ag_2MoO_4 is formed by the addition of $(NH_4)_6Mo_7O_{24}$ and precipitates; (C) the solids are filtrated; (D) the catalyst is dried in oven.

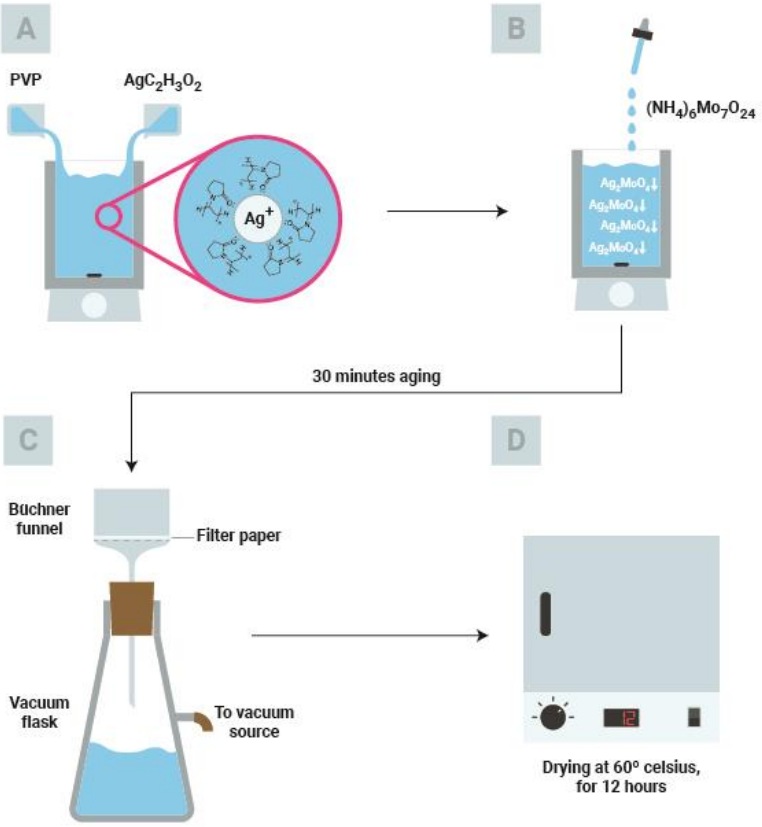

Source: Author's own elaboration.

6.3 CATALYST CHARACTERIZATION

6.3.1 Thermal behavior and phase change

Thermogravimetric analysis (TGA) and differential thermal analysis (DTA) were conducted in Shimazdu thermogravimeter (model DTG60/60H) (Shimadzu) in order to determine the catalyst's thermogravimetric profile and its phases transitions. The analysis preformed at heating a rate of 10

°C·min^{-1}, from room temperature environment to 350 °C, under inert atmosphere (N_2, 99.996% purity).

6.3.2 Crystallinity and phase composition

To identify the crystalline phases of the as-prepared powders and its composition, X-ray diffraction (XRD) data was collected using Rigaku Miniflex II, diffractometer with CuK∝ radiation (λ = 1.5418 Å) and sodium iodate detector coupled, operating at 30 kV potential difference and 15 mA electric current. The scanning range was from 10º to 90º, traveled at 0.05 °·s^{-1} speed. Samples did not require any previous preparation for analysis.

The crystallite sizes of each of the phases were estimated by Scherrer's equation (Equation XV), using their highest peaks as reference (SCHERRER, 1918):

$$\tau = \frac{K \cdot \lambda}{\beta \cdot \cos\theta} \qquad \text{(XV)}$$

where τ is mean size of crystallite, K is the dimensionless shape factor (typical 0.9 value was applied), λ is the X-ray wavelength (in nm), β is the length of the peak at half height of its maximum intensity (FWHM) in radians and θ is Bragg's angle.

6.3.3 Morphology and particles size

In order to analyze morphology of the particles and its size dimension, field emission gun scanning electron microscopy (FEG-SEM) was used, the microscope model is JEOL JSM-6701F, with energy dispersive spectrometer (EDS) coupled. For the analysis, the powder material was fixed in the metal stub with carbon tape and covered with gold, these procedures were realized to avoid interferences in the measurements and to enhance conductivity of the samples, respectively.

6.3.4 Surface area and porosity

The surface area (S_{BET}), average pore size (P_S) and total pore volume (V_P) were determined by nitrogen (N_2) adsorption-desorption isotherms at 77 K, analyses were obtained on an Autosorb 1C (Quantachrome, USA) adsorptionmeter. Degassing process was realized under vacuum at 60 °C for 24 h. The specific surface area was obtained by the Brunauer–Emmett–Teller (BET) method and pore size distribution was calculated by the Barrett-

Joyner-Halenda (BJH) method. The relative pressure (P/P_0) range adopted was from 0.05 to 1.

6.3.5 Vibrational behavior and bonds identification

The Fourier transform infrared (FTIR) spectrum in the range of 400 – 1100 cm^{-1} was taken using Agilent Technologies infra-red spectrophotometer (model Cary 600 Series). Potassium bromate (KBr) pellet was used as reference. For the samples analysis, they were mixed with KBr and, then, measured.

6.3.6 Optical properties

The UV-Vis diffuse reflectance spectra (DRS) were performed on Perkins Elmer UV/Vis/NIR Lambda 750, the wavelength range was varied from 300 to 800 nm. KBr was applied as the reference. For the analysis, a mixture of the sample and KBr was prepared and then pellets for the measurements were made.

The band gap energy (E_g) was determined using Tauc's equation (Tauc, 1968), Equation XVI:

$$\alpha h\nu = A\,(h\nu - E_g)^{n/2} \qquad \text{(XVI)}$$

where A, α, h, ν, and E_g are, in this order, a constant, the absorption coefficient, Planck's constant, the light frequency, and the band gap. The power index n varies depending on the type of electronic transition the semiconductor promotes, being equal to 1 for direct band-gaps materials and 4 for indirect band-gaps. For the synthesized Ag_2MoO_4, n value is 1.

The energies from the conduction band (E_{CB}) and the valence band (E_{VB}) were estimated by Mulliken's theory (Mulliken, 1934) Equations XVII and XVIII:

$$E_{VB} = \chi - E_C + 0.5E_g \qquad \text{(XVII)}$$
$$E_{CB} = E_{VB} - E_g \qquad \text{(XVIII)}$$

where, χ is the electronegativity of semiconductor, reported to be 5.92 eV for Ag_2MoO_4 (BAI; LU; LIU, et al., 2016) and E_C is the energy of free electrons on the hydrogen scale (~4.5 eV).

6.3.7 Electrical charge of the particles in suspension

Zeta potential analysis of the as-prepared catalyst was realized in Microtrac Stabino-Nanoflex (0.8 nm – 6.5 μm) with Dynamic Light

Scattering (DLS) at 180°. A solution of the Ag_2MoO_4 sample (150 ppm) was prepared with deionized water and then sonicated for 4 h (Unique – 25 kHz). The pH was varied from 3 to 10 with acidic (HCl, 0.1 M) and basic (NaOH, 0.1 M) solutions.

6.4 SLURY REACTIONS OPERATION CONDITIONS

All PAN degradation experiments, via AOP reactions, were performed isothermally (20 ºC) in a 1 L jacketed annular reactor, that was continuously stirred (~600 rpm, Dist, model DI-03), as described by VIEIRA et al., (2018). To start the experiment, 750 mL of pantoprazole solution (0.2 $g \cdot L^{-1}$, even though this concentration is higher than reported in aquatic environments, was used for the purpose of limit detection of the TOC equipment) was transferred to the reactor as well as the catalyst (0.5 $g \cdot L^{-1}$, this value was selected based on previous studies) (CAO et al., 2017; JIN et al., 2017).

Then, the adsorption step was realized. For the experiments that were submitted to this stage, they were maintained protected from light until the adsorption equilibrium was achieved (1 h for TiO_2-P25 and overnight for Ag_2MoO_4 and $Ag_2MoO_4^{Calc.}$). In order to start the reactions with similar conditions to those that were not submitted to adsorption- so the difference in the molecules concentration in the media would not affect the reaction conditions- the initial concentration of PAN on these reactions were higher (0.25 $g \cdot L^{-1}$ for TiO_2-P25, 0.3 $g \cdot L^{-1}$ for $Ag_2MoO_4^{Calc.}$ and 0.4 $g \cdot L^{-1}$ for Ag_2MoO_4).

After adsorption, in order to start photocatalysis reactions, the corresponding lamp medium-pressure mercury vapor UVA/VIS (200-800 nm, maximum peak at 368 nm, 41W, Osram) or a LED visible lamp (400–800 nm, 2W, Brilia) was lit (VIEIRA et al., 2018) and the air injection (0.168 $L \cdot min^{-1}$) was turned on.

In the peroxidation experiments, only Ag_2MoO_4 was used and no previous adsorption was realized. The initial H_2O_2 concentration was 0.5 $g \cdot L^{-1}$ (this value was established in order to guarantee H_2O_2 would be in excess in the media, approximately, 5 times higher than the theoretical minimum concentration). The photo-peroxidation reactions were performed just like the peroxidation ones in combination of the respective already described lamps.

In order to clarify each reaction conditions, a summary of the applied parameters is described in Table 7.

Table 7. Reactions conditions for each AOP performed.

Nomenclature	Catalyst dosage ($g \cdot L^{-1}$)	PAN concentration ($g \cdot L^{-1}$)	Preliminary adsorption (min)	O_2 injection ($L \cdot min^{-1}$)	H_2O_2 initial concentration ($g \cdot L^{-1}$)	Light source
Adsorption Ag_2MoO_4	Ag_2MoO_4 (0.5)	0.2	None	None	None	None
Adsorption $Ag_2MoO_4^{Calc.}$	$Ag_2MoO_4^{Calc.}$ (0.5)	0.2	None	None	None	None
O_2	None	0.2	None	0.168	None	None
H_2O_2	None	0.2	None	None	0.5	None
$Ag_2MoO_4 + H_2O_2$	Ag_2MoO_4 (0.5)	0.2	None	None	0.5	None
UV	None	0.2	None	None	None	UVA/VIS
UV + O_2	None	0.2	None	0.168	None	UVA/VIS
UV +H_2O_2	None	0.2	None	None	0.5	UVA/VIS
UV + Ag_2MoO_4 + O_2	Ag_2MoO_4 (0.5)	0.4	(12 h)	0.168	None	UVA/VIS
UV + $Ag_2MoO_4^{Calc.}$ + O_2	$Ag_2MoO_4^{Calc.}$ (0.5)	0.3	(12 h)	0.168	None	UVA/VIS
UV + Ag_2MoO_4 + H_2O_2	Ag_2MoO_4 (0.5)	0.2	None	None	0.5	UVA/VIS
UV + TiO_2-P25 + O_2	TiO_2-P25 (0.5)	0.25	(1 h)	0.168	None	UVA/VIS
VIS	None	0.2	None	None	None	VIS
VIS + O_2	None	0.2	None	0.168	None	VIS
VIS +H_2O_2	None	0.2	None		0.5	VIS
VIS + Ag_2MoO_4 + O_2	Ag_2MoO_4 (0.5)	0.4	(12 h)	0.168	None	VIS
VIS + $Ag_2MoO_4^{Calc.}$ + O_2	$Ag_2MoO_4^{Calc.}$ (0.5)	0.3	(12 h)	0.168	None	VIS
VIS + Ag_2MoO_4 + H_2O_2	Ag_2MoO_4 (0.5)	0.2	None	None	0.5	VIS
VIS + TiO_2-P25 + O_2	TiO_2-P25 (0.5)	0.25	(1 h)	0.168	None	VIS

Source: Author's own elaboration.

Aliquots were collected from the reactor in established time intervals, filtered and analyzed as described in the next section (6.5). The Figure 8 represents a scheme of the system used to realize the slurry reactions study.

Figure 8. Representation of the experiment's system, being (A) photocatalysis, (B) catalytic peroxidation and (C) catalytic photo peroxidation, where 1 is water inlet, 2 is the air bubbler, 3 is lamp, 4 is the sample collector, 5 is water outlet, 6 is the magnetic bar, 7 is the quartz tube, 8 is the stirrer and 9 is the H_2O_2 addition.

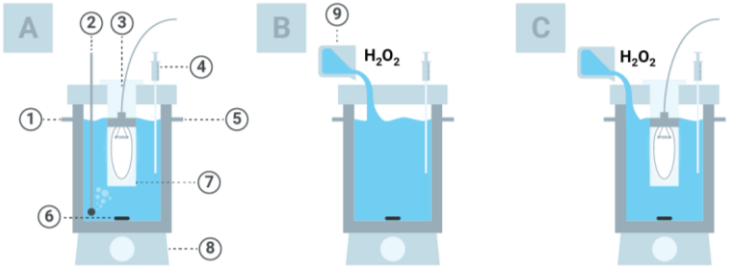

Source: Author's own elaboration.

6.5 ANALYTIC DETERMINATIONS

6.5.1 H_2O_2 concentration

H_2O_2 concentration was monitored by the metavanadate method (NOGUEIRA; OLIVEIRA; PATERLINI, 2005). Briefly, NH_4VO_3 was slowly added in deionized water at 50 ºC under magnetic stirring, until it reached the concentration of 6.2 mmol·L^{-1}. Then, a sulfuric acid solution (9 mol·L^{-1}) was added drop by drop, its final concentration was 0.058 mol·L^{-1}. After complete dissolution, the solution was cooled down and stored in amber glass bottles. The samples were diluted in 10 mL balloons (1:10) and read in UV-VIS spectrophotometer (HACH, model DR5000) at 450 nm wavelength.

The kinetic rates for the decomposition of H_2O_2 were calculated applying apparent pseudo-first order rate constant (k_{app}), described in Equation XIX.

$$-\ln (C/C_0) = k_{app} \cdot t \qquad \text{(XIX)}$$

where C, C_0, k_{app} and t are respectively, concentration of H_2O_2 in the media, the initial concentration of H_2O_2 in the solution, kinetic pseudo first-order constant and time.

6.5.2 pH

The pH of the samples was determined by the potentiometric method, using the pHmeter Q 400A (Quimis), which was previously calibrated with 4.0 and 7.0 buffer solutions.

6.5.3 PAN degradation and intermediates formation

The degradation analyses were conducted in UV-VIS spectrophotometer (HACH, model DR5000). The samples were diluted with deionizes water in a proportion 1:4 and read in the wavelength of maximum absorption wavelength of PAN, 289 nm. Some sub-products formation was also observed during the wavelength scanning, since new peaks were observed and the solution changed its color during some reactions.

6.5.4 Total Organic Carbon (TOC)

The mineralization was verified by TOC measurements, that were performed in TOC-VCPH analyzer (Shimadzu). Since the equipment's catalyst (Platinum, Pt) is deactivated in basic pH, the samples with this condition had its pH neutralized with a HCl solution (0.01 M) before reading. Samples with pH 7 or lower had not this previous treatment. The analysis is based on the combustion catalytic oxidation method, at 680 °C, coupled with a non-dispersive infrared detector.

6.5.5 Trapping experiments

Reactive species trapping experiments were performed for UV photocatalysis and catalytic peroxidation to investigate the ROS formation. The experimental procedures were realized as described in section 6.4, but, additionally, a reactive species scavenger was introduced in the reactor (10 mM) on the begging of the reaction. In particular, p-benzoquinone (BQ), sodium azide (NaN_3), disodium ethylenediaminetetraacetate dihydrate (Na_2EDTA) and tert-butyl alcohol (TBA) were employed as scavengers for, respectively, superoxide anion radicals ($\bullet O_2^-$), singlet oxygen ($^1O_2$), photogenerated holes (h^+) and hydroxyl radicals (•OH).

6.6 METHODOLOGY SUMMARY

In order to facilitate the understanding of the methodology applied in this study, its main information is described in the Figure 9.

Figure 9. Flowchart of the methodology used.

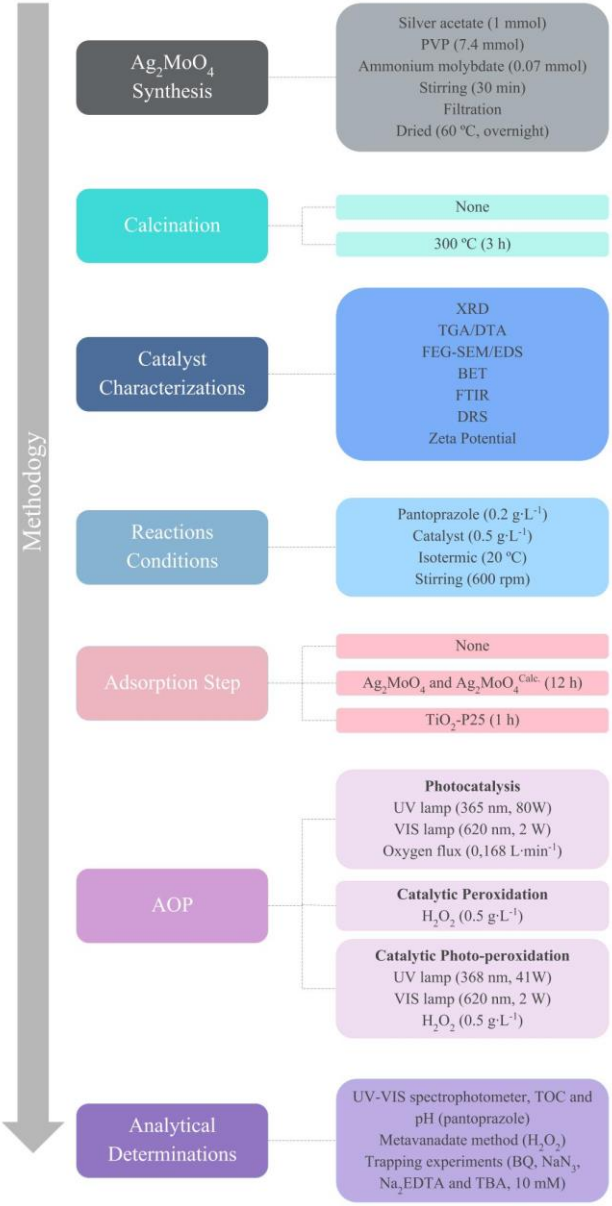

Source: Author's own elaboration.

7 RESULTS AND DISCUSSIONS

7.1 CHARACTERIZATION

Figure 10 shows the TGA and DTA curves of the as prepared Ag_2MoO_4. The TGA curve shows no significant weight loss in the temperature range from 40 to 350 ºC. However, two exothermic peaks were detected in the DTA. The first one, at 272 ºC, can be attributed to the phase change from α-Ag_2MoO_4 to β-Ag_2MoO_4 (BELTRÁN et al., 2014). The other one, at 318 ºC, is an unknown peak, that must be further studied, this result is similar to results reported by MOURA et al. (2016).

Figure 10. TGA and DTA curves of the as prepared silver molybdate.

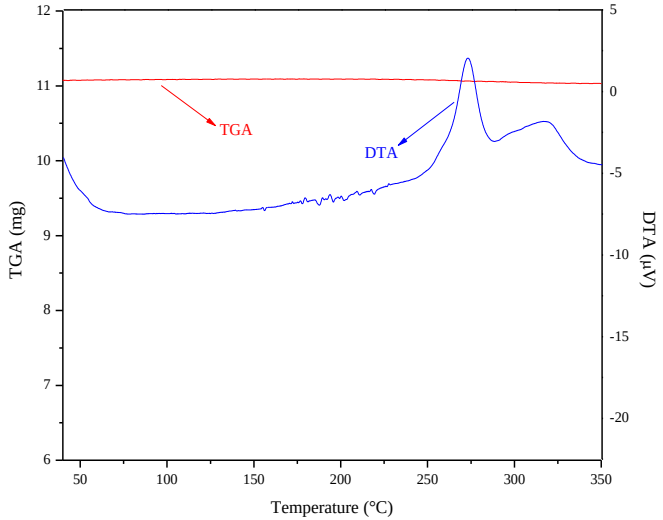

Source: Author's own elaboration.

The XRD results of the as-prepared and the calcined samples are displayed at Figure 11. The high crystallinity of the samples was evidenced by the existence of high intense and sharp peaks. For the non-treated sample (Ag_2MoO_4, a), the peaks 2θ = 14.70º, 22.97º, 27.47º, 29.86º, 32.69º, 34.87º, 36.02º, 36.33º, 37.79º, 40.40º, 41.54º, 43.33º, 44.79º, 49.59º 52.52º, 55.02º, 58.37º and 60.68º are indexed with the reflections (111), (210), (212), (004), (310), (302), (312), (204), (320), (115), (400), (205), (402), (305), (423), (502), (424), (503) and (440) of tetragonal α-Ag_2MoO_4 (JCPDS 21-1340). The other identified peaks of (a) 16.58º, 27.14º, 31.94º, 33.42º, 38.74º, 42.30º, 47.93º, 50.95º, 55.86º,

58.69º, 63.15º, 65.67º and 66.62º match to the crystal planes (111), (220), (311), (222), (400), (331), (422), (511), (440), (531), (620), (533) and (622) of cubic β-Ag_2MoO_4 (JCPDS 08-0473). After calcination at 300 ºC under air atmosphere ($Ag_2MoO_4^{Calc.}$, b), a complete phase transformation (α-Ag_2MoO_4 → β-Ag_2MoO_4) occurred, since all the peaks (2θ = 16.45º, 27.09º, 31.89º, 33.37º, 38.70º, 42.23º, 47.89º, 51.02º, 55.82º, 63.11º, 65.74º and 66.69º) correspond only to the reflections of β-Ag_2MoO_4 (JCPDS 08-0473).

Figure 11. XRD pattern of the synthesized Ag_2MoO_4 (a) and $Ag_2MoO_4^{Calc.}$ (b).

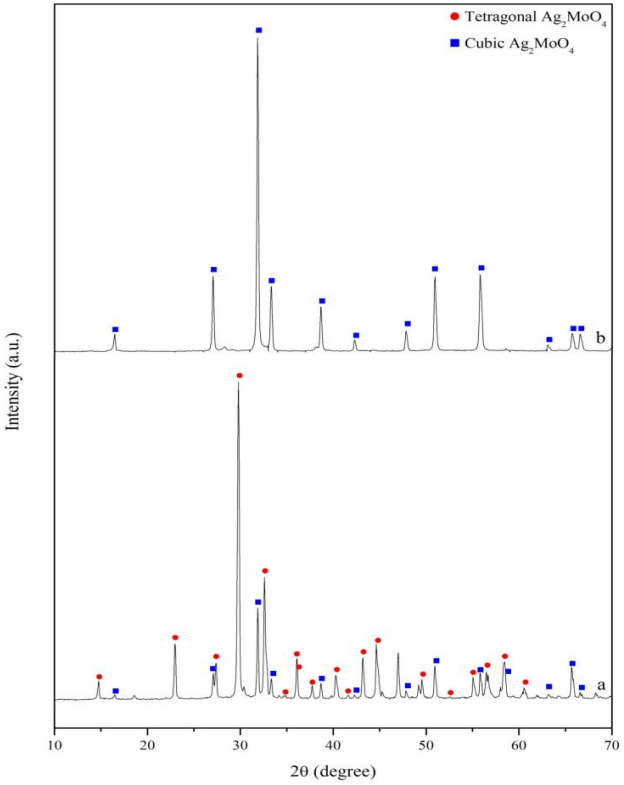

Source: Author's own elaboration.

The as-synthesized material is composed by both α and β Ag_2MoO_4 phases. The presence of high concentration of PVP during the preparation of the catalyst has contributed to the formation of two Ag_2MoO phases (NG; FAN, 2015). PVP is a stabilizer on several metallic nanoparticles synthesis, since its polar groups, specially C=O, interact

with metal ions and form a complex (JIANG et al., 2004; BONNEMAN et al., 2008), its presence on the synthesis changes the dispersion of the particles as well as the access to them (TERANISHI; MIYAKE, 1998).

The obtained crystallite sizes (Equation XV) for α and β phases of the as-prepared catalyst were, respectively, 46 nm and 41 nm, while 39 nm was obtained for the calcinated sample, similar from one another.

The morphology of the Ag_2MoO_4 catalyst was investigated by FEG-SEM images (Figure 12). Figure 12A shows agglomerates of smooth particles that have irregular forms and sizes (ranging from 1 to 5 μm). It can be observed the presence of some butterfly-like structures Ag_2MoO_4 consisted of four united petals. When the structures are carefully analyzed (Figure 12B), tiny butterfly-like or petals parted from one another can be detected. This can be explained by the additional maceration that was developed in other to homogenize all the synthesized catalyst.

Figure 12. (A) FEG-SEM images of Ag_2MoO_4 and (B) amplification of a butterfly-like structure.

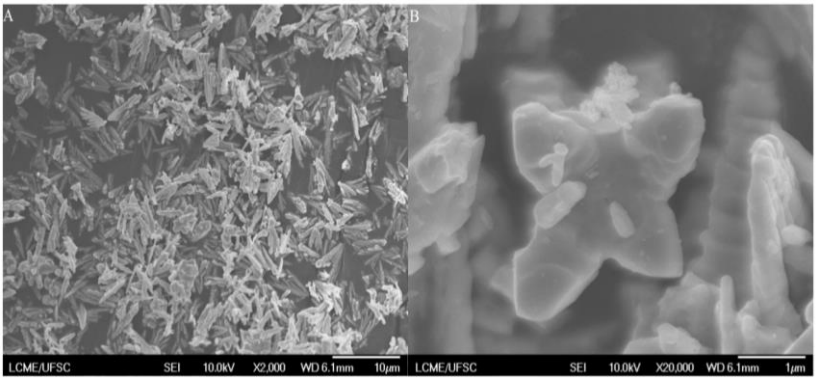

Source: Author's own elaboration.

The elemental composition of Ag_2MoO_4 was also analyzed by EDS (Table 8). Only oxygen (O), molybdenum (Mo) and silver (Ag) were observed in the surface of the catalyst, showing that the sample contained no pronounced impurities. Meanwhile, the molar proportion of Ag:Mo was found out to be approximately 2:1.

Table 8. Summary of EDS results of the synthesized Ag_2MoO_4.

Element	Peak (keV)	Apparent concentration	Wt (%)
O	0.6	0.15	18.4
Mo	2.4	0.32	26.3
Ag	3.0	0.67	55.3
Total			100

Source: Author's own elaboration.

The N_2 adsorption–desorption isotherms of the as-prepared sample at 77 K (Figure 13) showed a discrete H3-hysteresis, indicative of slit-shaped type pores, and its format is typical of mesoporous materials that could be classified as type IV (THOMMES et al., 2015). The corresponding S_{BET}, pore volume (V_P) and average pore size (P_S) of the sample are, respectively, 1.9 $m^2 \cdot g^{-1}$, 0.003 $cm^3 \cdot g^{-1}$ and 5.9 nm. This specific area results were similar to the already reported 2.6 (HUO et al., 2018) and 2.3 $m^2 \cdot g^{-1}$ (LI et al., 2018) values, indicating that the coexistence of the two phases of Ag_2MoO_4 is not a significant parameter to provide differences in the textural characteristics.

Figure 13. N_2 adsorption–desorption isotherms of Ag_2MoO_4 catalyst at 77 K.

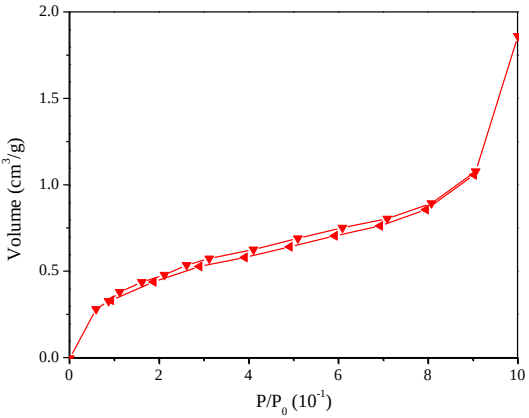

Source: Author's own elaboration.

FTIR spectra (Figure 14) of the Ag_2MoO_4 (a) and $Ag_2MoO_4^{Calc.}$ (b) samples exhibit the expected characteristic peaks at 823 and 824 cm^{-1}, respectively, corresponding to the anti-symmetric stretch vibrations of O-Mo-O in Ag_2MoO_4. The other two peaks of each sample- 1647 and 3442 cm^{-1} for (a) and 1643 and 3404 cm^{-1} for (b)- correspond to the bending vibration of absorbed water and surface hydroxyl O-H stretching, respectively.

Figure 14. FTIR spectra of Ag_2MoO_4 (a), and $Ag_2MoO_4^{Calc.}$ (b).

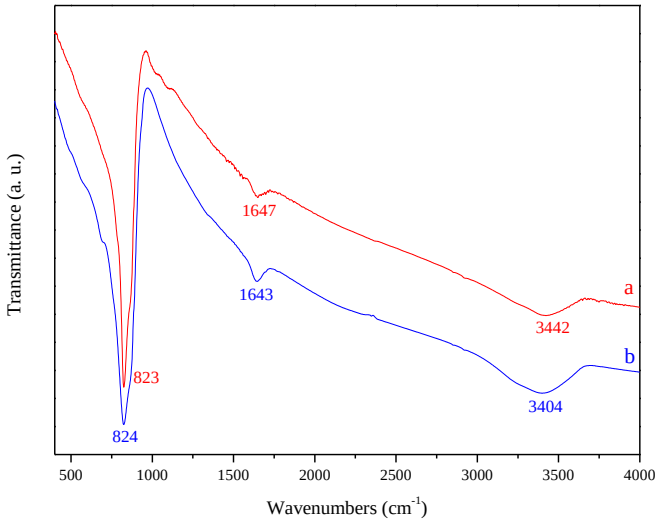

Source: Author's own elaboration.

The as-prepared and calcinated Ag_2MoO_4 UV-VIS reflectance spectra are shown in Figure 15A and a maximum peak in ~320 nm is observed for both samples. The absorption edge of the catalysts is near to 465 nm, indicating potential application in the visible region for catalytic purposes.

Considering direct transitions (Equation XVI), the plot of $(\alpha h\upsilon)^2$ versus $h\upsilon$ (Figure 15B) was used to calculate the band gaps. The values obtained are E_g = 3.09 eV, and E_g = 3.25 eV, for Ag_2MoO_4 and $Ag_2MoO_4^{Calc.}$, respectively. The first value is lower than those reported by other authors for different particle's morphology (XU et al., 2015; CAO et al., 2017; OLIVEIRA et al., 2017). The decreasing in the E_g can be attributed to structural defects at medium range and local bond distortions, which yield localized electronic levels within the forbidden band gap (SOUSA et al., 2018), this is expected by the coexistence of

both α-Ag_2MoO_4 and β-Ag_2MoO_4 phases, which are formed by the presence of the PVP during the synthesis. For the treated catalyst, E_g was comparable to some other literature results and its higher value was expected, since it was already reported that β-Ag_2MoO_4 possess higher band gaps then α-Ag_2MoO_4, due to its configuration (NG; FAN, 2015; ZHANG; MA, 2017a; LI; LIU; LI, 2018).

Figure 15. (A) UV–Vis diffuse reflectance spectra and (B) plots of $(\alpha h\upsilon)^2$ versus energy (hυ) of Ag_2MoO_4, where (a) is Ag_2MoO_4 and (b) is $Ag_2MoO_4^{Calc}$.

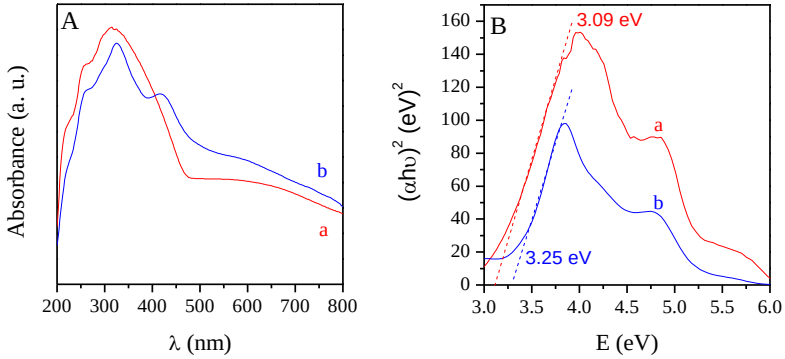

Source: Author's own elaboration.

The calculated values for E_{CB} and E_{VB} (Equations XVII and XVIII) are -0.12 eV and 2.96 eV, respectively, for the as-prepared Ag_2MoO_4, and -0.21 eV and 3.05 eV, respectively, for the calcined sample.

For a given photocatalytic redox reaction, the redox potential of the CB should be more negative than the electron acceptor redox potential, while the valence band of the VB should be more positive than the oxidation potential of the oxidizable chemical compounds. Therefore, ROS could be formed in the presence of different electron acceptors as well as the Ag_2MoO_4 phase.

The potential zeta data of the as-synthesized Ag_2MoO_4 sample (Figure 16) shows that the particle is negatively charged in all the measured pHs (3-10). The pH of the isoeletric point was not detected. It's also important to point out that, from pH 5 to 10, the potential zeta is lower than -30 mV, being considered as a stable colloidal suspension (RIDDICK, 1968).

Figure 16. Potential zeta curve of the as prepared catalyst.

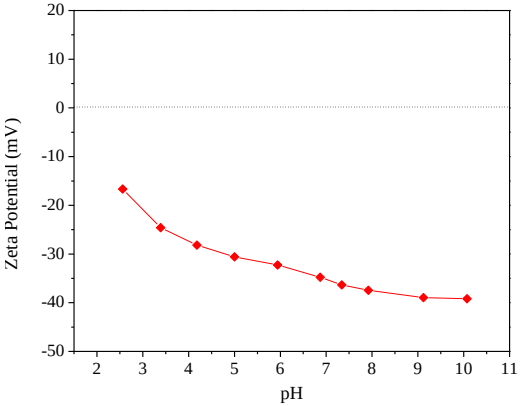

Source: Author's own elaboration.

7.2 NON-PHOTOCHEMICAL REACTIONS

The preliminary tests on PAN's removal by non-catalytic and non-photochemical methods, through 8 h of reaction, are reported in Figure 17.

Figure 17. C/C_0 (A) and TOC/TOC_0 (B) versus time for non-photochemical reactions, where (a) Adsorption Ag_2MoO_4, (b) Adsorption $Ag_2MoO_4^{Calc.}$, (c) O_2 and (d) H_2O_2.

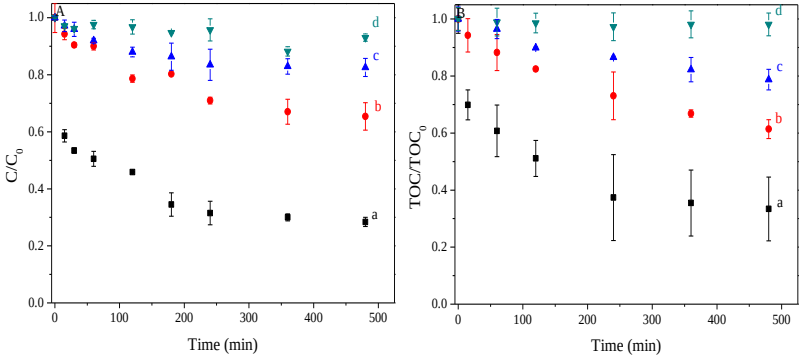

Source: Author's own elaboration.

Great adsorption was obtained by Ag_2MoO_4 (71.6%), however for $Ag_2MoO_4^{Calc}$ this result was much inferior (34.5%). The adsorption capacity of the as-prepared catalyst (280 $mg \cdot g^{-1}$) was more than the

double of $Ag_2MoO_4^{Calc.}$ (138 $mg \cdot g^{-1}$). So, even though Ag_2MoO_4 presented low S_{BET}, it's noticeable that other factors (as pores shape, V_P, roughness, surface structure, among others) influence in the adsorption process.

In relation to the oxidizing agents applied on their own, it can be seen that low degradation values were achieved, for O_2, approximately ~17%, and for H_2O_2, in particular, the reaction showed really poor removal (less than 10%). But, at the same time, oxygen reaction was able to mineralize almost the same amount of PAN it degraded.

7.3 PHOTOLYSIS REACTIONS

In Figure 18A, it is noticeable that UV light reactions (a-c), combined or not with electrons acceptors, were able to degrade PAN. This UV sensitivity has also been described by RAFFIN et al. (2008). The obtained rates were 72%, 83% and 99%, respectively, for UV, UV + O_2 and UV + H_2O_2, showing that UV light was able to decompose H_2O_2 in hydroxyl radicals (further will be discussed in section 6.5.1). However, just UV-peroxidation process was able to achieve considerable mineralization results (Figure 18B), this fact suggests that sub-products with lower degradability are formed when exposed to UV light. Also, it is important to point out the importance of the oxidizing potential of the oxidants applied, since the TOC removal was ~40% higher for H_2O_2 than for O_2.

Yet for VIS (d-f), no significant variances on PAN's concentration were detected for VIS light itself or when combined with hydrogen peroxide- indicating that this light source hadn't energy enough to excite the H_2O_2 molecule, promoting its low decomposition. On the other hand, the reaction VIS + O_2 showed up as one of the best treatments in terms of photolysis (64%). It can be noted that this result is achieved by a combination of both processes, once not only VIS alone didn't degrade the pollutant and just O_2 itself was, approximately, 3 times less effective than when they were applied together. It is known that PAN is sensitive to light and to oxidizing species as well, being the main explanation to this result (DHURKE; KUSHWAHA; DESAI, 2013).

Figure 18. C/C_0 (A) and TOC/TOC_0 (B) versus time for photolysis reactions, where (a) UV, (b) UV + $O_2^{\cdot}$, (c) UV + H_2O_2, (d) VIS, (e) VIS + O_2 and (f) VIS + H_2O_2.

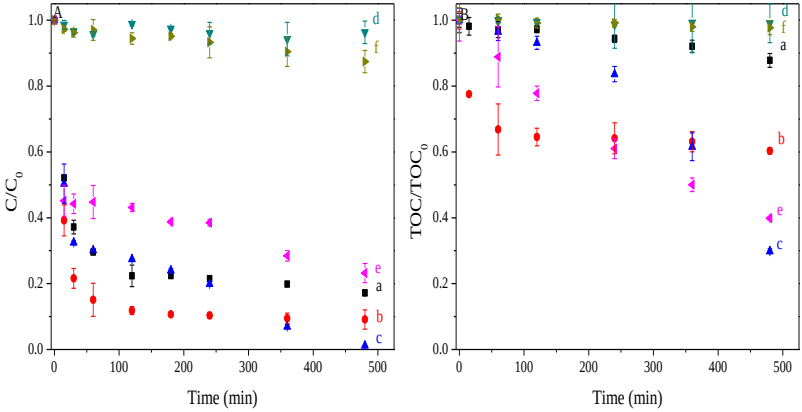

Source: Author's own elaboration.

7.4 PHOTOCATALYSIS REACTIONS

As can be observed in Figure 19, all photocatalysis under UV light were able to reach high degradation values (> 90%). Besides, the mineralization rates of PAN were at least 20% greater when compared to UV or UV + O_2 processes, with the catalyst introduction, being the best result achieved by TiO_2-P25 (99% of UV_{289} removal and 84% TOC removal). Also, it is important to point out that, under UV light, Ag_2MoO_4 and $Ag_2MoO_4^{Calc.}$ showed very similar behavior, having similar activation.

Yet, the PAN degradation by VIS photocatalysis, showed both silver molybtade catalysts presented better performance than TiO_2-P25, which was significantly reduced (~24%), showing its high band gap was not completely activated by VIS light.

Furthermore, under visible light it was possible to observe a greater difference on photocatalytic activity from Ag_2MoO_4 and $Ag_2MoO_4^{Calc.}$, since the catalyst with just β-phase was able to remove 62%, while the one with both phases was able to remove 75% of the contaminant, agreeing with the already presented results of band gap. So, Ag_2MoO_4 stands out as one of the best analyzed photocatalysts, showing ~10% difference from the best treatment evaluated so far (TiO_2-P25 under UV light).

As a final observation, is important to point out that Ag_2MoO_4 under VIS presented a better performance, this can be attributed to PAN's transformation under UV light (reported in the last section), that probably had less adsorption affinity with the catalyst, reducing its degradation rate a little.

Figure 19. C/C_0 (A) and TOC/TOC_0 (B) versus time for photocatalysis reactions, where (a) UV+ Ag_2MoO_4 + O_2, (b) UV + $Ag_2MoO_4^{Calc.}$ + O_2, (c) UV + TiO_2-P25 + O_2, (d) VIS + Ag_2MoO_4 +O_2, (e) VIS + $Ag_2MoO_4^{Calc.}$ + O_2 and (f) VIS + TiO_2-P25 + O_2.

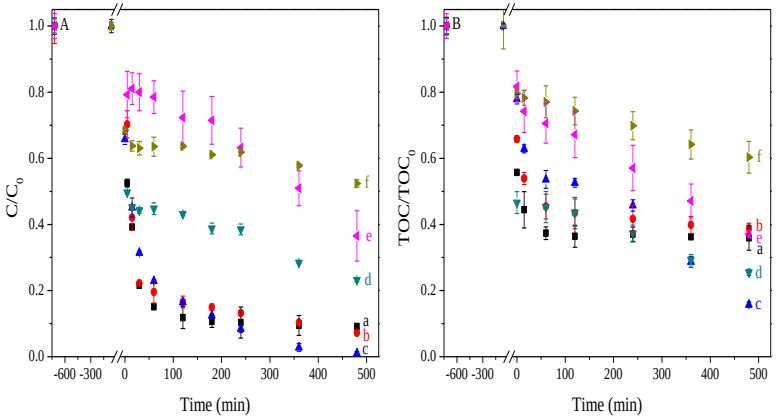

Source: Author's own elaboration.

7.5 PEROXIDATION AND PHOTO-PEROXIDATION REACTIONS

Ag_2MoO_4 had a surprisingly high activity for catalytic peroxidation reactions (Figure 20), since peroxide couldn't oxidize PAN by itself (Figure 17), although when Ag_2MoO_4 is added, the reaction occurs really fast and the mineralization process accompanies its curve tendency (Figure 20B). Besides after 8 h, 98% of degradation and 94% of mineralization were obtained, but it's important to point out that, in 15 min, UV_{289} removal and TOC removal were, respectively, 95% and 89%.

For photo-peroxidation under VIS light, little effect was noticed with the light introduction, since this reaction presented similar removals after 8 h. However, this process still is not efficient as the one in the dark. It can be noted that, in the applied conditions, this process is slower, once 86% of mineralization were achieved only after 120 min, while in the absence of light better values were reached in only 15 min. Again, the

major reason is the by-products formation of PAN under light, changing the adsorbent/pollutant interaction, reducing its kinetics.

Yet, for UV photo-Fenton-like processes, as in other reactions under UV light, a high degradation percentage was obtained (85%), but poor mineralization (32%). In section 7.6.2, some points about UV reactions and the observation of some PAN's intermediates formation will be highlighted.

Figure 20. C/C_0 (A) and TOC/TOC_0 (B) versus time for peroxidation and photo-peroxidation reactions, where (a) $Ag_2MoO_4 + H_2O_2$, (b) UV + $Ag_2MoO_4 + H_2O_2$ and (c) VIS + $Ag_2MoO_4 + H_2O_2$.

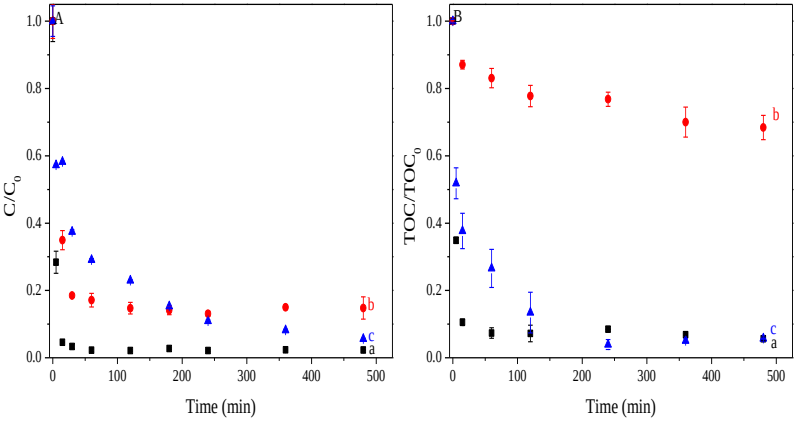

Source: Author's own elaboration.

7.6 REACTIONS SUMMARY

This section is dedicated to highlight the most important observations made in the AOP reactions studied in this work, as well as to analyze some other overall results of the performed degradations essays.

7.6.1 Hydrogen peroxide analyses

The first point to be further discussed is the hydrogen peroxide behavior in the Fenton-like reactions. Primarily, aside from H_2O_2 itself and H_2O_2 combined with visible light, all the other reactions were able to decompose hydrogen peroxide (Figure 21A). In Ag_2MoO_4 peroxidation, in particular, peroxide was rapidly consumed in the beginning of the

reaction, so, by this decay is acceptable to assume that the catalyst is able to promote OH• radicals formation.

Moreover, hydrogen peroxide concentration decreases as PAN is degraded, and the pseudo-first order kinetic model was well fitted for each treatment (Figure 21B). The highest kinetic constant was found for catalytic peroxidation, as expected, since this was the reaction that faster degraded PAN in this study.

Figure 21. Hydrogen peroxide concentration through the reaction (A) and pseudo-first-order reaction adjusts, where: (a) H_2O_2, (b) UV + H_2O_2, (c) VIS + H_2O_2, (d) Ag_2MoO_4 + H_2O_2, (e) UV + Ag_2MoO_4 + H_2O_2 and (f) VIS + Ag_2MoO_4 + H_2O_2.

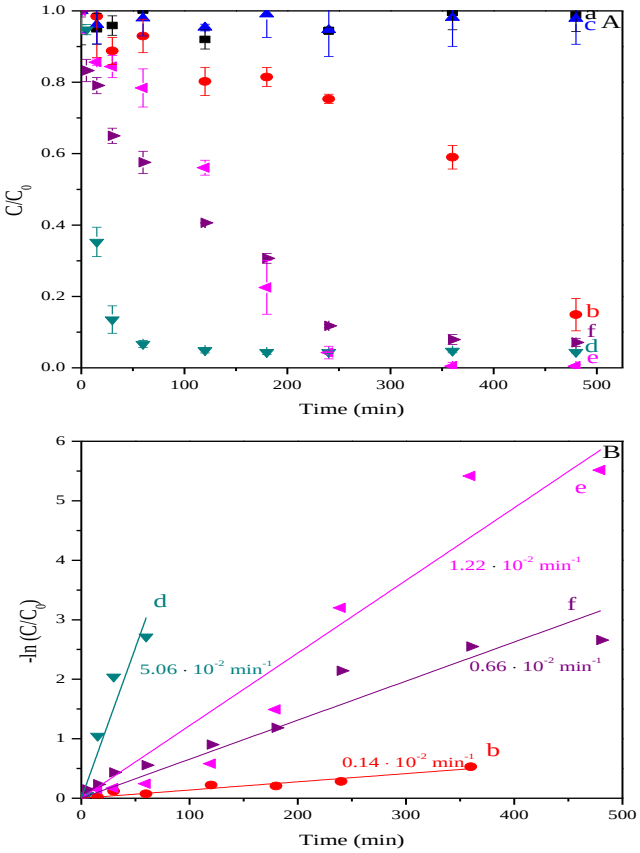

Source: Author's own elaboration.

In order to evaluate the efficiency of the processes in terms of H_2O_2 expenditure, the total amount of hydrogen peroxide consumed by TOC removed was calculated (Table 9). It can be seen that, in the applied conditions, the catalytic peroxidation under dark or under VIS showed up as the most economic treatments, this fact is very promising, since one of the biggest drawbacks for photo-Fenton-like reactions operation in high scale is the cost with UV light, which would be unnecessary in this case.

Table 9. Pseudo first order kinetic constant to H_2O_2 decomposition under different AOP treatment (pH_0 = 9.15; solid dosage = 0.5 $g \cdot L^{-1}$).

AOP applied to PAN degradation	Pseudo first order kinetic constant for H_2O_2 decomposition ($10^{-2} \cdot min^{-1}$)	mol H_2O_2 consumed / mol TOC removed	
		2 h	8 h
H_2O_2	~0	-	-
UV + H_2O_2	0.14 ± 0.01	159	68
VIS + H_2O_2	~0	-	-
Ag_2MoO_4 + H_2O_2	5.06 ± 0.51	58	58
UV + Ag_2MoO_4 + H_2O_2	1.22 ± 0.09	110	184
VIS + Ag_2MoO_4 + H_2O_2	0.66 ± 0.04	40	58

Source: Author's own elaboration.

7.6.2 Overall observations on PAN's degradation

It's important to elucidate here that the kinetic PAN's degradation constants were calculated, but they did not fit well to the pseudo-linear model neither for the initial speeds nor for the entire reaction, so they were presented in the APPENDIX A of this work (Figure A1-A4). So, the removal in specific times was calculated to evaluate the degradation and mineralization results of the applied treatments all together (Figure 22).

As observed previously, PAN was quite resistant to degradation under visible light and by H_2O_2 oxidation, while it was adsorbed in an appreciable amount on the as-prepared Ag_2MoO_4. Also, both silver molybdate catalyst were capable of performing photocatalysis under VIS light. However, catalytic peroxidation showed up as the best treatment studied, especially when comparing the procedures for 2 h of reaction (Figure 22A).

Figure 22. Degradation and mineralization of PAN after 2 h (A) and 8 h (B) treatments under similar experimental conditions (pH_0 = 9.15; $[PAN]_0$ = 0.2 $g \cdot L^{-1}$; $[TOC]_0$ = 0.1 $g \cdot L^{-1}$; solid dosage (when applied) = 0.5 $g \cdot L^{-1}$).

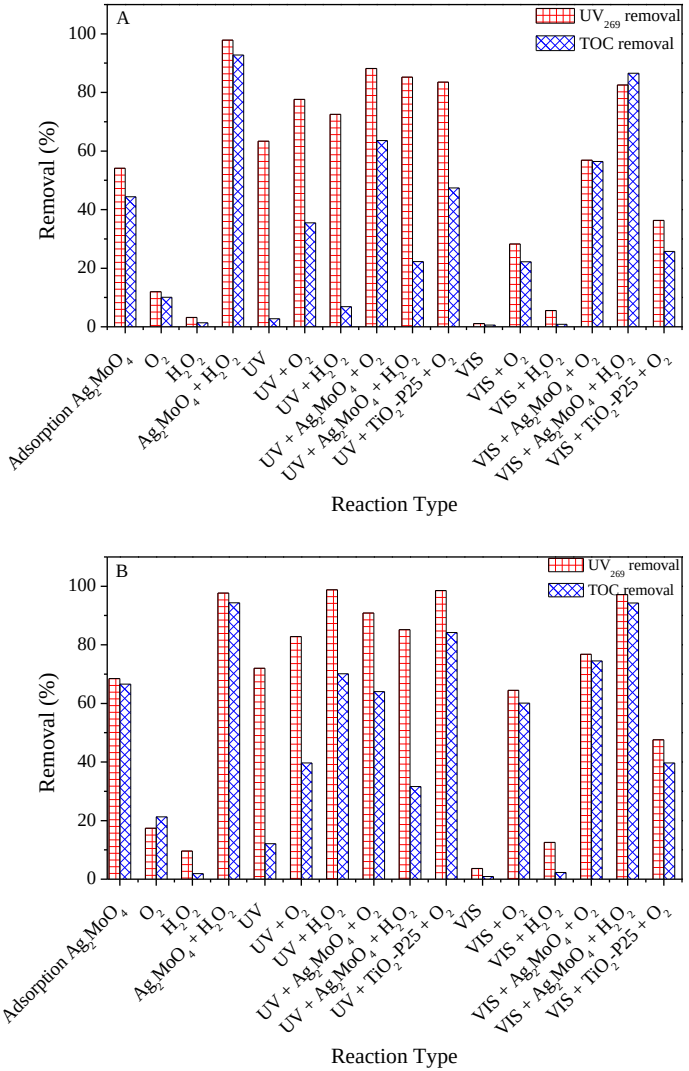

Source: Author's own elaboration.

On the other hand, the UV light irradiation causes considerable degradation, without mineralization (RAFFIN et al., 2008). Thus, it is assumable that sub-products of PAN are formed during its photolysis, which could be more resistant or less reactive in the presence of the catalyst, since low TOC removal were obtained. As evidence of these intermediates formation, scanning spectrums were realized (Figure 23).

Figure 23. Scanning spectras from 200-900 nm for UV + Ag_2MoO_4 + O_2 (A) and UV + Ag_2MoO_4 + H_2O_2 (B).

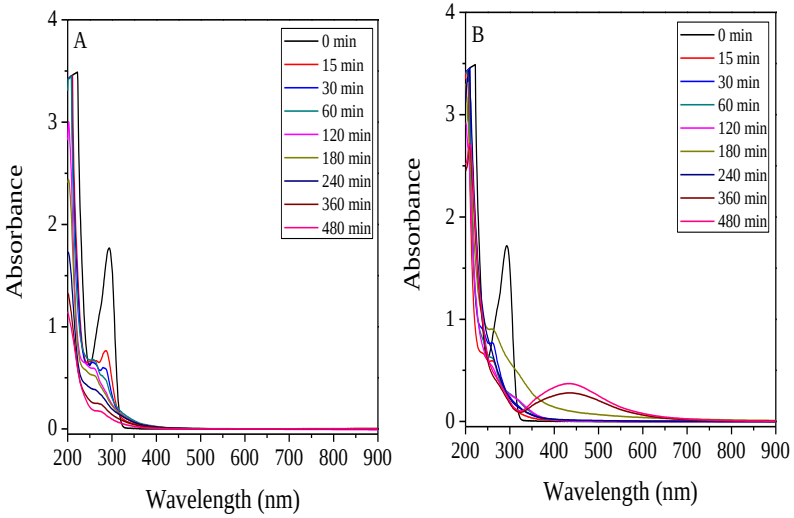

Source: Author's own elaboration.

For Ag_2MoO_4 photocatalysis under UV light (Figure 23A), it can be noted some new peaks appearances, specially, for 15 min and 30 min times. Besides, the solution started transparent, but for the filtered samples from 15 to 60 min became yellow, after these points, for higher times of reaction, the solution returned to be transparent. This fact shows the presence of oxidation by-products in the begging of the reaction and their posterior degradation. All the other UV reactions presented similar behavior (Figure B3, APPENDIX B), aside from UV photo-peroxidation. In this process- besides the yellow sub-products- from 6 to 8 h of the reaction, it turned into a reddish brown color, suggesting this reaction forms different ROS from the other UV-based reactions.

In order to compare that not all processes form this kind of sub-products, the spectra of catalytic peroxidation is presented in Figure 24,

in it can observed that only the PAN's peaks are diminishing. All the other scanning spectrums of the investigated procedures are presented in Figure B1-B3 in APPENDIX B.

Figure 24. Scanning spectrum from 200-900 nm for catalytic peroxidation.

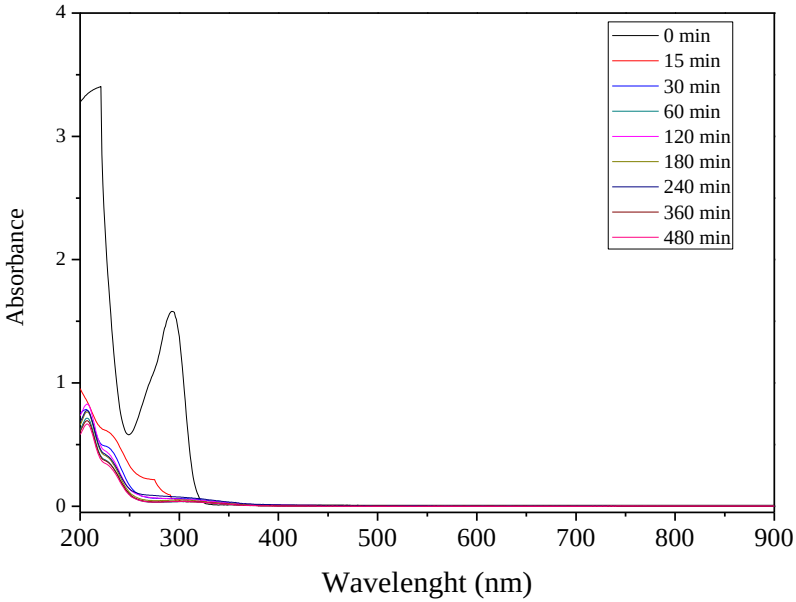

Source: Author's own elaboration.

Moreover, in all treatments applied in this study, the PAN degradation is accomplished by a decrease on the pH, as shown in Figure 25. It is known that the optimal pH for PAN degradation is under acidic conditions, since the constant rate increases with the increasing of the H^+ concentration. Also, PAN is unstable under acidic conditions, causing its degradation, but without its mineralization (DHURKE; KUSHWAHA; DESAI, 2013).

Figure 25. pH behavior through the time the preformed reactions, where: (a) Adsorption Ag_2MoO_4, (b) Adsorption $Ag_2MoO_4^{Calc.}$, (c) O_2, (d) H_2O_2, (e) $Ag_2MoO_4 + H_2O_2$, (f) VIS, (g) VIS + O_2, (h) VIS + H_2O_2, (i) VIS + Ag_2MoO_4 + O_2, (j) VIS + $Ag_2MoO_4^{Calc.}$ + O_2, (k) VIS + Ag_2MoO_4 + H_2O_2, (l) UV, (m) UV + O_2, (n) UV + H_2O_2, (o) UV + Ag_2MoO_4 + O_2, (p) UV + + $Ag_2MoO_4^{Calc.}$ + O_2 and (q) UV + Ag_2MoO_4 + H_2O_2.

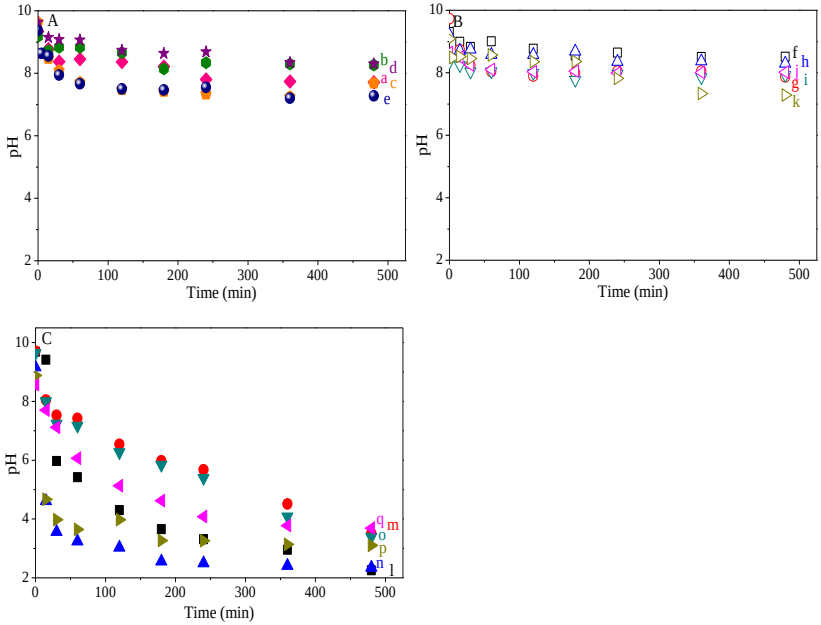

Source: Author's own elaboration.

Figure 22 shows that the highest TOC removal is found by the catalytic peroxidation. So, it is possible to assume that the decrease of the pH caused by PAN degradation using light-enhanced processes contributes to PAN degradation, but low mineralization efficiency, indicating that different ROS are formed.

7.6.3 Radical scavengers analyses

Firstly, trapping experiments were conducted for the as prepared Ag_2MoO_4 UV photocatalysis, to evaluate the different oxidizing radicals formation (Figure 26). It can be seen that the addition of BQ into the

reaction mixture considerably decreases the PAN's degradation rate, i.e., O_2•$^-$ radical is relevant in the photocatalytic process. Other authors have already reported the formation of this radical by Ag_2MoO_4 (CAO et al., 2017; ALBULIZI et al., 2018; QU et al., 2018).

Figure 26. Trapping results for UV photocatalysis throughout time: C/C_0 versus time (A) and degradation values after 8 h of reaction (B), where (a) is no scavenger, (b) is BQ, (c) is NaN_3 (d) is Na_2EDTA and (e) is TBA.

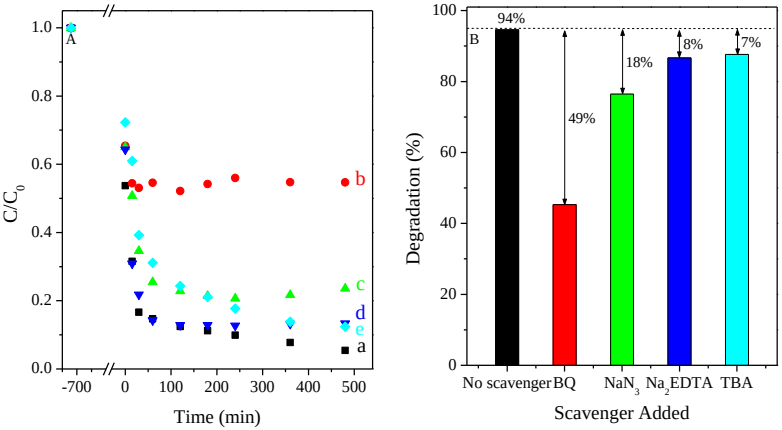

Source: Author's own elaboration.

Moreover, all the trappers addition inhibited photocatlysis (Figure 26B). However, when Na_2EDTA (h^+ scavenger) or TBA (•OH scavenger) were added to the system, PAN removal is only slightly affected. This behavior could be ascribed to the limitation of e^-/h^+ recombination (causing the electrons to react more with O_2, facilitating O_2•$^-$ formation) and to the low •OH generation (due to the reaction between O_2•$^-$ and H^+), respectively (LIU et al., 2017b). Thus, the major influencing radicals on photocatalysis were found to be O_2•$^-$ (BQ) and $^1O_2$ (NaN_3).

Additionally, since catalytic peroxidation presented the best results trapping experiments were realized in order to analyze the ROS formed and suggest possible mechanisms for PAN's removal.

It's possible to see that all the added trappers greatly affected the reaction kinetics (Figure 27A), indicating that the ROS O_2•$^-$ (BQ), $^1O_2$ (NaN_3) and •OH (TBA) radicals are formed throughout this process. By these results, it's possible to assume that the amount of •OH radicals produced on the solid surface, by the H_2O_2 decomposition, may be higher than that formed under UV light. In terms of inhibition, at the end of the process (Figure 27B), the major one was from BQ (82%), demonstrating

$O_2^{\bullet-}$ plays important part on the oxidation reactions, as in photocalysis. Although the contribution of singlet oxygen and hydroxyl radical can't be overlooked, once high difference in the degradations responses were observed.

Figure 27. Trapping results for catalytic peroxidation throughout time: C/C_0 versus time (A) and degradation values after 8 h of reaction (B), where (a) is no scavenger, (b) is BQ, (c) is NaN_3 and (d) is TBA.

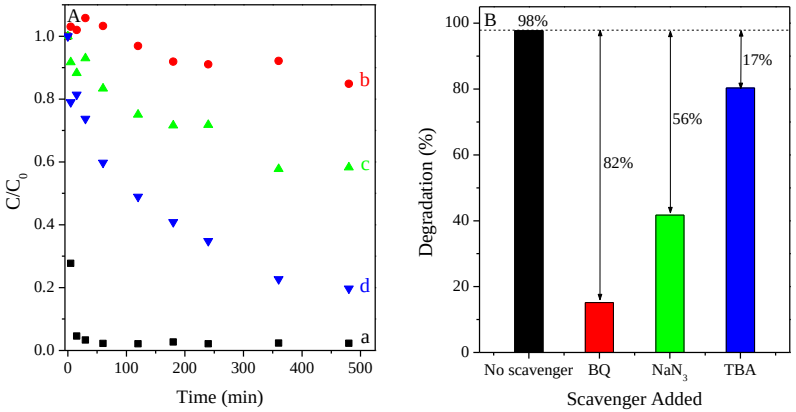

Source: Author's own elaboration.

Furthermore, in the photocatalytic reactions, molecular oxygen is used as electron acceptor, which is reduced to produce superoxide ion $O_2^{\bullet-}$. However, the potential of the conduction band of Ag_2MoO_4 (-0.12 eV) could not be sufficiently negative to reduce molecular oxygen to allow its reduction (< -0.13 eV). So, a more efficient electron acceptor, such as hydrogen peroxide, would be required to the photocatalytic degradation of PAN using Ag_2MoO_4 (YAN et al., 2013).

Thus, the mechanism of PAN degradation and mineralization is complex due to the formation of several ROS. The importance of •OH radical is understandable because of its high oxidizing power. However, with other ROS species such as $^1O_2$ and $O_2^{\bullet-}$ very little work has been carried out to understand their formation in a photocatalytic/catalytic oxidation system. Moreover, $O_2^{\bullet-}$ can be quickly converted to $^1O_2$ (JEDSUKONTORN et al., 2016), resulting in its lower concentration in the catalytic system. A possible degradation mechanism is shown in Equations from XX to XXIX.

$Ag_2MoO_4 + H_2O_2 \rightarrow [(Ag_2MoO_4 \bullet H_2O_2]_{ads}$ (XX)

$[(Ag_2MoO_4) \bullet H_2O_2]_{ads} + H^+ \rightarrow Ag_2MoO_4 + \bullet OH + H_2O$ (XXI)

$\bullet OH + H_2O_2 \rightarrow H_2O + \bullet O_2H$ (XXII)

$\bullet OH + \bullet OH \rightarrow H_2O + \frac{1}{2}(O_2 + {}^1O_2)$ (XXIII)

$\bullet O_2H + \bullet O_2H \rightarrow H_2O + O_2 + {}^1O_2$ (XXIV)

$\bullet O_2H \rightarrow H^+ + O_2\bullet^-$ (XXV)

$\bullet O_2H + OH^- \rightarrow O_2\bullet^- + H_2O$ (XXVI)

$\bullet OH + \bullet O_2H \rightarrow H_2O + \frac{1}{2}(O_2 + {}^1O_2)$ (XXVII)

$PAN + O_2\bullet^-/{}^1O_2/\bullet OH \rightarrow$ Intermediates (XXVIII)

$Intermediates + O_2\bullet^-/{}^1O_2/\bullet OH \rightarrow CO_2 + H_2O$ (XXIX)

8 CONCLUSIONS

In this work, Ag_2MoO_4 with both α and β-phases was successfully synthesized by a simple controlled precipitation method. Also, after calcination ($Ag_2MoO_4^{Calc.}$), the catalyst presented just the β-phase, showing a complete phase transformation. Due to this change, a higher band gap was found for $Ag_2MoO_4^{Calc.}$, demonstrating the presence of α-phase plays important part on lowering its value. Furthermore, other characterizations (as morphology, superficial area, FTIR and zeta potential) were similar to results already reported in the literature.

Besides, Ag_2MoO_4 had a greater adsorption performance, reducing in ~67% the PAN's concentration in 8 h. In terms of the other non-catalytic reactions, almost none degradation was observed in the reactions of only peroxide itself or peroxide combined with VIS light. Yet, the pharmaceutical reacted little with O_2, being able to mineralize up to 17% of it. Additionally, for UV and UV + O_2 high degradation values were obtained, but poor PAN mineralization. Moreover, UV peroxidation, presented the second highest TOC removal among the UV-based reactions (just lower than TiO_2-P25 photocatalysis), achieving 99% of degradation and 70% of mineralization. Also, sub-products were noted when PAN was exposed to UV light, since colorful compounds were observed in the scanning spectrums.

As photocatalyst, Ag_2MoO_4 had inferior performance under UV light when compared to TiO_2-P25, but higher activity when exposed to VIS light. It's also important to point out that VIS photolysis reactions presented similar results to those obtained with $Ag_2MoO_4^{Calc.}$, but Ag_2MoO_4 enhanced in 12% the PAN's TOC removal. On the other hand, no significant change was noticeable among both silver molybdates behavior in the UV photocatalysis, however the two catalysts enhanced in, at least, 20% the PAN's mineralization when compared to UV photolysis. Yellow intermediates were identified in this reaction as well.

Yet, as catalyst in peroxidation and VIS photo-peroxidation processes, Ag_2MoO_4 showed its greatest performance, leading to an almost complete PAN mineralization. Although, in the absence of light. the pollutant's decrease was achieved much faster (90% in 15 min), reinforcing that PAN is very sensible to light, making it possible to assume some resistant by-products are formed. In UV photo-Fenton-like, the reaction showed similar results to the other UV-based reactions (high degradation values and little mineralization), although some distinct reddish brown sub-products were detected.

In addition, from PAN's sensitivity to light, it was also possible to note it had high degradability under acid pH, however, again- aside from PAN instability- poor TOC removal was obtained. Thus, being one of the main explanations why UV reactions were not able to promote elevated TOC removals of PAN.

Furthermore, the radicals formed throughout the reactions were studied with trapping experiments. It was observed that $O_2\bullet^-$ and $^1O_2$ radicals performed important roles on the oxidation reactions to both UV photocatalysis and catalytic peroxidation with Ag_2MoO_4 as catalyst. Even though, the other two applied trappers (for h^+ and •OH) also inhibited the reactions, but just slightly, indicating they influence less in the investigated processes.

Overall, it can be concluded that the novel application of Ag_2MoO_4 as catalyst for peroxide oxidation reactions is not only an efficient process but also a promising one. Thus, its use should be further investigated with other contaminants and, also, $Ag_2MoO_4^{Calc.}$ performance should also be evaluated.

REFERERENCES

AKPAN, U. G.; HAMEED, B. H. Parameters affecting the photocatalytic degradation of dyes using TiO_2-based photocatalysts: A review. **Journal of Hazardous Materials**, v. 170, p. 502-529, 2009.

ALBULIZI, A.; KADEER, K.; ZHOU, L.; TURSUN, Y.; DILINUER, T. *In situ* anion exchange synthesis of β-Ag_2MoO_4/AgBr heterojunctions with enhanced photocatalytic activity and stability. **Journal of the Taiwan Institute of Chemical Engineers**, v. 88, p. 243-251, 2018.

ALI, I.; AL-OTHMAN, Z. A.; ALHARBI, O. M. L. Uptake of pantoprazole drug residue from water using novel synthesized composite iron nano adsorbent. **Journal of Molecular Liquids**, v. 218, p. 465-472, 2016.

ANEGGI, E.; TROVARELLI, A.; GOI, D. Degradation of phenol in wastewaters via heterogeneous Fenton-like Ag/CeO_2 catalyst. **Journal of Environmental Chemical Engineering**, v. 5, p. 1159-1165, 2017.

ARORA, A. K.; NITHYA, R.; MISRA, S.; YAGI, T. Behavior of silver molybdate at high-pressure. **Journal of Solid State Chemistry**, v.196, p. 391-397, 2012.

BABUPONNUSAMI, A.; MUTHUKUMAR, K. A review on Fenton and improvements to the Fenton process for wastewater treatment. **Journal of Environmental Chemical Engineering**, v. 2, p. 557-572, 2014.

BAE, W.; WON, H.; HWANG, B.; TOLEDO, R. A. de; CHUNG, J.; KWON, K.; SHIM, H. Characterization of refractory matters in dyeing wastewater during a full-scale Fenton process following pure-oxygen activated sludge treatment. **Journal of Hazardous Materials**, v. 287, p. 421-428, 2015.

BAI, Y. Y.; LU, Y.; LIU, J. K. An efficient photocatalyst for degradation of various organic dyes: Ag/Ag_2MoO_4–AgBr composite. **Industrial & Engineering Chemistry Research**, v. 307, p. 26-35, 2016.

BARREIRO, J. C.; VANZOLINI, K. L.; CASS, Q. B. Direct injection of native aqueous matrices by achiral–chiral chromatography ion trap mass spectrometry for simultaneous quantification of pantoprazole and lansoprazole enantiomers fractions. **Journal of Chromatography A**, v. 1218, p. 2865-2870, 2011.

BASHEER, A. A. New generation nano-adsorbents for the removal of emerging contaminants in water. **Journal of Molecular Liquids**, v. 261, p. 583-593, 2018.

BAVISHI, C.; DUPONT, H. L. Systematic review: the use of proton pump inhibitors and increased susceptibility to enteric infection. **Alimentary Pharmacology & Therapeutics**, v. 34, p. 1269-1281, 2011.

BELTRÁN, A.; GRACIA, L.; LONGO, E.; ANDRÉS, J. First-Principles Study of Pressure-Induced Phase Transitions and Electronic Properties of Ag_2MoO_4. **Journal of Physical Chemistry C**, v. 118, p. 3724-3732, 2014.

BHATTACHARYA, S.; GHOSH, A. Silver molybdate nanoparticles, nanowires, and nanorods embedded in glass nanocomposites. **Physical Review B**, v. 75, p.1-4, 2007.

BIAN, L.; LIU, Y.; ZHU, G.; YAN, G.; ZHANG, J.; YUAN, A. $Ag@CoFe_2O_4/Fe_2O_3$ nanorod arrays on carbon fiber cloth as SERS substrate and photo-Fenton catalyst for detection and degradation of R6G. **Ceramics International**, v. 44, p. 7580-7587, 2018.

BOIX, C.; IBÁÑEZ, M.; SANCHO, J. V.; RAMBLA, J.; ARANDA, J. L.; BALLESTER, S.; HERNÁNDEZ, F. Fast determination of 40 drugs in water using lparge volume direct injection liquid chromatography–tandem mass spectrometry. **Talanta**, v. 131, p. 719-727, 2015.

BOKARE, A. D.; CHOI, W. Zero-valent aluminum for oxidative transformation of aqueous organic pollutants. **Environmental Science & Technology**, v. 41, p. 7130-7135, 2009.

BOKARE, A. D.; CHOI, W. Chromate-induced activation of hydrogen peroxide for oxidative degradation of aqueous organic pollutants. **Environmental Science & Technology**, v. 44, p. 7232-7237, 2010.

BOKARE, A. D.; CHOI, W. Review of iron-free Fenton-like systems for activating H_2O_2 in advanced oxidation processes. **Journal of Hazardous Materials**, v. 275, p. 121-135, 2014.

BONNEMANN, H.; NAGABHUSHANA, K. S. Metal Nanoclusters in Catalysis and Material Science: The Issue of Size Control. CHAPTER 2 - Metal Nanoclusters: Synthesis and Strategies for their Size Control. **Elsevier Science**. 28 p., 2008.

CAO, W.; AN, Y.; CHEN, L.; QI, Z. Visible-light-driven Ag_2MoO_4/Ag_3PO_4 composites with enhanced photocatalytic activity. **Journal of Alloys and Compounds**, v. 701, p. 350-357, 2017.

CARP, O.; HUISMAN, C. L.; RELLER, A. Photoinduced reactivity of titanium dioxide. **Progress in Solid State Chemistry**, v. 32, p. 33-177, 2004.

CHEN, C. C.; HERHOLD, A. B.; JOHNSON, C. S.; ALIVISATOS, A. P. Size Dependence of Structural Metastability in Semiconductor Nanocrystals. **Science**, v. 276, p. 398-401, 1997.

CHEN, X.; SOUVANHTHONG, B.; WANG, H.; ZHENG, H.; WANG, X.; HUO, M. Polyoxometalate-based Ionic liquid as thermoregulated and environmentally friendly catalyst for starch oxidation. **Applied Catalysis B: Environmental**, v. 138-139, p. 161-166, 2013.

CHENG, L.; SHAO, Q.; SHAO, M.; WEI, X.; WU, Z. Photoswitches of one-dimensional Ag_2MO_4 (M = Cr, Mo, W). **The Journal Physical Chemistry C**, v. 113, p. 1764-1768, 2009.

CHENG, M.; ZENG, G.; HUANG, D.; LAI, C.; XU, P.; ZHANG, C.; LIU, Y. Hydroxyl radicals based advanced oxidation processes (AOPs) for remediation of soils contaminated with organic compounds: A review. **Chemical Engineering Journal**, v. 284, p. 582-598, 2018.

CHEUNGPASITPORN, W.; THONGPRAYOON, C.; KITTANAMONGKOLCHAI, W.; SRIVALI, N.; EDMONDS, P. J.; UNGPRASERT, P.; O'CORRAGAIN, O. A.; KORPAISARN, S.; ERICKSON, S. B. Proton pump inhibitors linked to hypomagnesemia: a

systematic review and meta-analysis of observational studies. **Renal Failure**, v. 37, n. 7, p. 1237-1241, 2015.
CUNHA, F. S.; SCZANCOSKI, J. C.; NOGUEIRA, I. C.; DE OLIVEIRA, V. G.; LUSTOSA, S. M. C.; LONGO, E.; CAVALCANTE, L. S. Structural, morphological and optical investigation of β-Ag_2MoO_4 microcrystals obtained with different polar solvents. **CrystEngComm**, v. 17, p.8207-8211, 2015.

DE LAAT, J.; GALLARD, H. Catalytic Decomposition of Hydrogen Peroxide by Fe(III) in Homogeneous Aqueous Solution: Mechanism and Kinetic Modeling. **Environmental Science & Technology**, v. 33, n. 16, p. 2726-2732, 1999.

DE SANTANA, Y. V. B.; GOMES, J. E. C.; MATOS, L.; CRUVINEL, G. H.; PERRIN, A.; PERRIN, C.; ANDRES, J.; VARELA, J. A.; LONGO, E. Silver Molybdate and Silver Tungstate Nanocomposites with Enhanced Photoluminescence. **Nanomaterials and Nanotechnology**, v. 4, n. 22, p. 1-10, 2014.

DEWIL, R.; MANTZAVINOS, D.; POULIOS, I.; RODRIGO, M. A. New perspectives for Advanced Oxidation Processes. **Journal of Environmental Management**, v. 195, p. 93-99, 2017.

DHANABAL, R.; VELMATHI, S.; BOSE, A. C. High-efficiency new visible-light driven Ag_2MoO_4–Ag_3PO_4 composite photocatalyst towards degradation of industrial dyes. **Catalysis Science & Technology**, v. 6, p. 8449-8463, 2016.

DHURKE, R.; KUSHWAHA, I.; DESAI, B. G. Improvement in Photostability of Pantoprazole Sodium by Microencapsulation. **PDA Journal of Pharmaceutical Science and Technology**, v. 67, p. 43-52, 2013.

DI PAOLA, A.; GARCÍA-LÓPEZ, E.; MARCÌ, G.; PALMISANO, L. A survey of photocatalytic materials for environmental remediation. **Journal of Hazardous Materials**, v. 211, p. 3-29, 2012.

DISCROLL, S. A.; OZKAN, U. S. Isotopic Labeling Studies on Oxidative Coupling of Methane over Alkali Promoted Molybdate Catalysts. **Studies in Surface Science and Catalysis**, v. 82, p. 367-375, 1994.

DONOHUE, J.; SHAND, W. J. The Determination of the Interatomic Distances in Silver Molybdate, Ag_2MoO_4. **Journal of American Chemical Society**, v. 69, p. 222-223, 1947.

EC, The European Parlament and the Council of the European Union, 2013. Directive 2013/39/EU. **Official Journal of European Union**, v. 226, p. 1–17, 2013.

FABBRO, M. T.; FOGGI, C. C.; SANTOS, L. P. S.; GRACIA, L.; PERRIN, C.; VERGANI, C. E.; MACHADO, A. L.; ANDRÉS, J.; CORDONCILLO, E.; LONGO, E. Synthesis, antifungal evaluation and optical properties of silver molybdate microcrystals in different solvents: a combined experimental and theoretical study. **Dalton Transactions**, v. 45, n. 26, p. 10736-10743, 2016.

FENTON, H. J. H. Oxidation of tartaric acid in presence of iron. **Journal of Chemical Society, Transactions**, v. 65, p. 899-910, 1895.

FODJO, E. K.; LI, D.W.; MARIUS, N. P.; ALBERT, T.; LONG, Y. T. Low temperature synthesis and SERS application of silver molybdenum oxides. **Journal of Materials Chemistry A**, v. 1, p. 2558-2566, 2013.

FUJISHIMA, A.; ZHANG, X.; TRYK, D. A. TiO_2 photocatalysis and related surface phenomena. **Surface Science Reports**, v. 63, p. 515–582, 2008.

FURUYA-KANAMORI, L.; STONE, J. C.; CLARK, J.; MCKENZIE, S. J.; YAKOB, L.; PATERSON, D. L.; RILEY, T. V.; DOI, S. A. R.; CLEMENTS, A. C. Comorbidities, Exposure to Medications, and the Risk of Community-Acquired *Clostridium difficile* Infection: A systematic Review and Meta-analysis. **Infection Control & Hospital Epidemiology**, v. 36, n. 2, p. 132-141, 2015.

GADGIL, T.; IBRAYEV, N.; NURAJE, N. Heterogeneous Photocatalysis: From Fundamentals to Green Applications, Chapter 2 – Photocatalytuc Water Oxidation. **Springer**, 29 p., 2016.

GALLARD, H.; DE LAAT, J.; LEGUBE, B. Comparative study of the rate of decomposition of H_2O_2 and of atrazine by Fe(III)/H_2O_2,

Cu(II)/H_2O_2, Fe(III)/Cu(II)/H_2O_2. **Revue des sciences de l'eau**, v. 12, p. 713–728, 1999.

GAN, G.; ZHAO, P.; ZHANG, X.; LIU, J.; LIU, J.; ZHANG, C.; HOU, X. Degradation of Pantoprazole in aqueous solution using magnetic nanoscaled Fe_3O_4/CeO_2 composite: Effect of system parameters and degradation pathway. **Journal of Alloys and Compounds**, v. 725, p. 472-483, 2017.

GRACIA-LOR, E.; SANCHO, J. V.; HERNÁNDEZ, F. Simultaneous determination of acidic, neutral and basic pharmaceuticals in urban wastewater by ultra high-pressure liquid chromatography-tandem mass spectrometry. **Journal of Chromatography A**, v. 1217, p. 622–632, 2010.

GRACIA-LOR, E.; SANCHO, J. V.; HERNÁNDEZ, F. Multi-class determination of around 50 pharmaceuticals, including 26 antibiotics, in environmental and wastewater samples by ultra-high performance liquid chromatography-tandem mass spectrometry. **Journal of Chromatography A**, v. 1218, p. 2264–2275, 2011.

GRACIA-LOR, E.; SANCHO, J. V.; SERRANO, R.; HERNÁNDEZ, F. Occurrence and removal of pharmaceuticals in wastewater treatment plants at the Spanish Mediterranean area of Valencia. **Chemosphere**, v. 87, p. 453-462, 2012.

GOULD, D. M.; GRIFFITH, W. P.; SPIRO, M. Polyoxometalate catalysis of dye bleaching by hydrogen peroxide. **Journal of Molecular Catalysis A: Chemical**. v.175, p. 289–291, 2001.

GULBIŃSKI, W.; SUSZKO, T. Thin films of MoO_3–Ag_2O binary oxides – the high temperature lubricants. **Wear**, v. 261, p.867-873, 2006.

GUO, X.; LI, Q.; ZHANG, M.; LONG, M.; KONG, L.; ZHOU, Q.; SHAO, H.; HU, W.; WEI, T. Enhanced photocatalytic performance of N-nitrosodimethylamine on TiO_2 nanotube based on the role of singlet oxygen. **Chemosphere**, v. 120, p. 521-526, 2015.

HAENISCH, B.; VON HOLT, K.; WIESE, B.; PROKEIN, J.; LANGE, C.; ERNST, A.; BRETTSCHNEIDER, C.; KÖNIG, H. H.; WERLE, J.;

WEYERER, S.; LUPPA, M.; RIEDEL-HELLER, S. G.; FUCHS, A.; PENTZEK, M.; WEEG, D.; BICKEL, H.; BROICH, K.; JESSEN, F.; MAIER, W.; SCHERER, M. Risk of dementia in elderly patients with the use of proton pump inhibitors. **European Archives of Psychiatry and Clinical Neuroscience**, v. 265, n. 5, p. 419-428, 2015.

HE, D.; CHEN, Y.; SITU, Y.; ZHONG, L.; HUANG, H. Synthesis of ternary g-C_3N_4/Ag/-FeOOH photocatalyst: An integrated heterogeneous Fenton-like system for effectively degradation of azo dye methyl orange under visible light. **Applied Surface Science**, v. 425, p. 862-872, 2017.

HECKERT, E. G.; SEAL, S.; SELF, W. T. Fenton-like reaction catalyzed by the rare earth inner transition metal cerium. **Environmental Science & Technology**, v. 42, p. 5014–5019, 2008.

HERZIG, S. J.; DOUGTHTY, C.; LAHOTI, S.; MARCHINA, S.; SANAN, N.; FENG, W.; KUMAR, S. Acid-Suppressive Medication Use in Acute Stroke and Hospital-Acquired Pneumonia. **American Neurological Association**, v. 76, p. 712-718, 2014.

HILLEBRAND, O.; MUSALLAM, S.; SCHERER, L.; NÖDLER, K.; LICHA, T. The challenge of sample-stabilisation in the era of multi-residue analytical methods: A practical guideline for the stabilisation of 46 organic micropollutants in aqueous samples. **Science of the Total Environment**, v. 454-455, p. 289-298, 2013.

HONDOW, N.; FULLER, R.O. The use of preformed nanoparticles in the production of heterogeneous catalysts. **Journal of Colloid and Interface Science**, v. 417, p. 396-401, 2014.

HU, Z.; LEUNG, C. F.; TSANG, Y. K.; DU, H.; LIANG, H.; QIU, Y.; LAU, T. C. A recyclable polymer-supported ruthenium catalyst for the oxidative degradation of bisphenol A in water using hydrogen peroxide. **New Journal of Chemistry**, v. 35, p.149–155, 2011.

HUANG, S.; XU, Y.; ZHOU, T.; XIE, M.; MA, Y.; LIU, Q.; JING, L.; XU, H.; LI, H. Constructing magnetic catalysts with in-situ solid-liquid interfacial photo-Fenton-like reaction over Ag_3PO_4@$NiFe_2O_4$ composites. **Applied Catalysis B: Environmental**, v. 225, p. 40-50, 2018.

HUO, Y.; WANG, Z.; ZHANG, J.; LIANG, C.; DAI, K.; Ag SPR-promoted 2D porous g-C_3N_4/Ag_2MoO_4 composites for enhanced photocatalytic performance towards methylene blue degradation. **Applied Surface Science**, v. 459, p. 271-280, 2018.

JEDSUKONTORN, T.; MEEYOO, V.; SAITO, N.; HUNSOM, M. Effect of electron acceptors H_2O_2 and O_2 on the generated reactive oxygen species $^1O_2$ and $OH^\bullet$ in TiO_2-catalyzed photocatalytic oxidation of glycerol. **Chinese Journal of Catalysis**, v. 37, p. 1975-1981, 2016.

JIAO, Z.; ZHANG, J.; LIU, Z.; MA, Z. Ag/AgCl/Ag_2MoO_4 composites for visible-light-driven photocatalysis**. Journal of Photochemistry & Photobiology A: Chemistry**, v. 371, p. 67-75, 2019.

JIANG, P.; LI, S. Y.; XIE, S. S.; GAO, Y.; SONG, L. Machinable long PVP-stabilized silver nanowires. **Chemistry**, v. 10, p. 4817–4821, 2004.

JIANG, H.; LIU, J. K.; WANG, J. D.; LU, Y.; YANG, X. H. Thermal perturbation nucleation and growth of silver molybdate nanoclusters by a dynamic template route. **CrystEngComm**, v. 17, p. 5511- 5521, 2015.

JIANG, L.; YUAN, X.; PANA, Y.; LIANGA, J.; ZENGA, G.; WUA, Z.; WANGA, H. Doping of graphitic carbon nitride for photocatalysis: A review. **Applied Catalysis B: Environmental**, v. 217, p. 388-406, 2017.

JIN, J.; LIANG, Q.; SONG, Y.; XU, S.; LI, Z.; YAO, C. Hydrothermal synthesis of g-C_3N_4/Ag_2MoO_4 nanocomposites for improved visible light photocatalytic performance. **Journal of Alloys and Compounds**, v. 726, p. 221-229, 2017.

KANAKARAJU, D.; GLASS, B. D.; OELGEMÖLLER, M. Advanced oxidation process-mediated removal of pharmaceuticals from water: A review. **Journal of Environmental Management**, v. 219, p. 189-207, 2018.

KARCI, A. Degradation of chlorophenols and alkylphenol ethoxylates, two representative textile chemicals, in water by advanced oxidation processes: The state of the art on transformation products and toxicity. **Chemosphere**, v. 99, p. 1-18, 2014.

KATZ, P. O. Pharmacologic Basis of Pantoprazole Dosing. **Current Therapeutic Research**, v. 61, n. 8, p. 507-522, 2000.

KOOPAEI, N. N.; ABDOLLAHI, M. Health risks associated with the pharmaceuticals in wastewater. **DARU Journal of Pharmaceuticals Sciences**, v. 25, n. 9, p. 1-7, 2017

KOSMA, C. I.; LAMBROPOULOU, D. A.; ALBANIS, T. A. Analysis, occurrence, fate and risks of proton pump inhibitors, their metabolites and transformation products in aquatic environment: A review. **Science of the Total Environment**, v. 569-570, p.732-750, 2016.

KUMAR, J. K.; KARTHIK, R.; CHEN, S. M.; MUTHURAJ, V.; KARUPPIAH, C. Fabrication of potato-like silver molybdate microstructures for photocatalytic degradation of chronic toxicity ciprofloxacin and highly selective electrochemical detection of H_2O_2. **Scientific Reports**, v. 6, n. 34149, p. 1 – 13, 2016.

KWOK, C. S.; ARTHUR, A. K.; ANIBUEZE, C.I.; SINGH, S.; CAVALLAZZI, R.; LOKE, Y. K. Risk of *Clostridium difficile* infection with acid suppressing drugs and antibiotics: meta-analysis. **American Journal of Gastroenterology**, v. 107, n. 7, p. 1011-1019, 2012.

LAHEIJ, R. J.; STURKENBOOM, M. C.; HASSING, R. J.; DIELEMAN, J.; STRICKER B. H.; JANSEN, J. B. Risk of community-acquired pneumonia and use of gastric acid-suppressive drugs. **JAMA**, v. 292, n. 16, p. 1955-1960, 2004.

LAM, J. R.; SCHNEIDER, J. L.; ZHAO, W.; CORLEY, D. A. Proton pump inhibitor and histamine 2 receptor antagonist use and vitamin B_{12} deficiency. **JAMA**, v. 310, n. 22, p. 2435-2442, 2013.

LAZARUS, B.; CHEN, Y.; WILSON, F. P.; SANG, Y.; CHANG, A. R.; CORESH, J.; GRAMS, M. E. Proton pump inhibitor use and the risk of chronic kidney disease. **JAMA Internal Medicine**, v. 176, n. 2, p. 238-246, 2016.

LI, J.; LIU, F.; LI, Y. Fabrication of an Ag/Ag_2MoO_4 plasmonic photocatalyst with enhanced photocatalytic performance for the degradation of ciprofloxacin. **NJC**, v. 42, p. 12054-12061, 2018.

LING, S. K.; WANG, S.; PENG, Y. Oxidative degradation of dyes in water using Co^{2+}/H_2O_2 and Co^{2+}/peroxymonosulfate. **Journal of Hazardous Materials**, v. 178, p. 359–385, 2010.

LIU, E.; GAO, Y.; JIA, J.; BAI, Y. Friction and Wear Behaviors of Ni-based Composites Containing Graphite/Ag_2MoO_4 Lubricants. **Tribology Letters**, v. 50, p. 313–322, 2013.

LIU, Y.; MAO, Y.; TANG, X.; XU, Y.; LI, C.; LI, F. Synthesis of Ag/AgCl/Fe-S plasmonic catalyst for bisphenol A degradation in heterogeneous photo-Fenton system under visible light irradiation. **Chinese Journal of Catalysis**, v. 38, p. 1726-1735, 2017a.

LIU, T.; WANG, L.; LU, X.; FAN, J.; CAI, X.; GAO, B.; MIAO, R.; WANG, J.; LV, Y. Comparative study of the photocatalytic performance for the degradation of different dyes by $ZnIn_2S_4$: adsorption, active species, and pathways. **RSC Advances**, v. 7, p. 12292-12300, 2017b.

LIU, W.; SHEN, J.; YANG, X.; LIU, Q.; TANG, H. Dual Z-scheme g-C_3N_4/Ag_3PO_4/Ag_2MoO_4 ternary composite photocatalyst for solar oxygen evolution from water splitting. **Applied Surface Science**, v. 456, p. 369-378, 2018a.

LIU, X.; LI, W.; LI, H.; REN, C.; LI, X.; ZHAO, Y. Efficient Fe_3O_4-C_3N_4-Ag_2MoO_4 ternary photocatalyst: Synthesis, outstanding light harvesting, and superior hydroxyl radical productivity for boosted photocatalytic performance. **Applied Catalysis A: General**, v. 568, p. 54-63, 2018b.

LO, W. K.; CHAN, W. W. Proton pump inhibitor use and the risk of small intestinal bacterial overgrowth: a meta-analysis. **Clinical Gastroenterology and Hepatology**, v. 11, n. 5, p. 483-490, 2013.

LOFRANO, G. MERIC, S. A comprehensive approach to winery wastewater treatment: a review of the state-of the-art. **Desalination and Water Treatment**, v. 57, n. 7, p. 3011-3028, 2014.

LU, J.; QI, P.; PENG, Y.; MENG, Z.; YANG, Z.; YU, W.; QIAN, Y. Metastable MnS Crystallites through Solvothermal Synthesis. **Chemistry of Materials**, v. 13, p. 2169-2172, 2001.

LUQUE-ESPINAR, J. A.; NAVAS, N.; CHICA-OLMO, M.; CANTARERO-MALAGÓN, S.; CHICA-RIVAS, L. Seasonal occurrence and distribution of a group of ECs in the water resources of Granada city metropolitan areas (South of Spain): pollution of raw drinking water. **Journal of Hydrology**, v. 531, 612–625, 2015.

MA, Z.; REN, L.; XING, S.; WU, Y.; GAO, Y. Sodium Dodecyl Sulfate Modified $FeCo_2O_4$ with Enhanced Fenton-Like Activity at Neutral pH. **The Journal of Physical Chemistry C**, v. 119, n. 40, p. 23068-23074, 2015.

MA, P.; YU, Y.; XIE, J.; FU, Z. Ag_3PO_4/CuO composites utilizing the synergistic effect of photocatalysis and Fenton-like catalysis to dispose organic pollutants. **Advanced Powder Technology**, v. 28, p. 2797-2804, 2017.

MIAO, X. J.; WANG, N. N.; ZHAO, S. S.; PAN, W. Q.; WANG, P. Treatment of PNP wastewater by microwave assisted Cu(II)-Fenton catalytic oxidation process. **Chinese Journal of Environmental Engineering**. v. 8, p. 2299–2305, 2014.

MIKLOS, D. B.; REMY, C.; JEKEL, M.; LINDEN, K. G.; DREWES, J. E.; HÜBNER, U. Evaluation of advanced oxidation processes for water and wastewater treatment e A critical review. **Water Research**, v. 139, p. 118-131, 2018.

MIRZAEI, A. M.; CHEN, Z.; HAGHIGHAT, F.; YERUSHALMI, L. Removal of pharmaceuticals from water by homo/heterogonous Fenton-type processes - A review. **Chemosphere**, v. 174, p. 665-688, 2017.

MORALES-CASELLES, C.; GAO, W.; ROSS, P. S.; FANNING, L. Emerging Contaminants of Concern in Canadian Harbours: A case study of Halifax Harbour. **Marine Affairs Program Technical Report**, n. 15, 49 p., 2016.

MOURA, J. V. B.; DA SILVA FILHO, J. G.; FREIRE, P. T. C.; LUZ-LIMA, C.; PINHEIRO, G. S.; VIANA, B. C.; MENDES FILHO, J.; SOUZA-FILHO, A. G.; SARAIVA, G. D. Phonon properties of β-Ag_2MoO_4: Raman spectroscopy and *ab initio* calculations. **Vibrational Spectroscopy**, v. 86, p. 97-102, 2016.

MULLIKEN, R. S. A new electroaffinity scale; Together with data on valence states and on valence ionization potentials and electron affinities. **The Journal of Chemical Physics**, v. 11, p. 782-793, 1934.

NEAMEN, D. A. Semiconductor physics and devices: basic principles. **McGraw-Hill**, 566 p., 2012.

NEHRA, A. K.; JEFFREY, A. A.; LOFTUS, C. G.; NEHRA, V. Proton Pump Inhibitors: Review of Emerging Concerns. **Mayo Clinic Proceedings**, v. 93, n. 2, p. 240-246, 2018.

NEYENS, E.; BAEYENS, J. A review of classic Fenton's peroxidation as an advanced oxidation technique. **Journal of Hazardous Materials**, v. 98, p. 33-50, 2003.

NG, C. H. B.; FAN, W. Y. Uncovering Metastable α-Ag_2MoO_4 Phase Under Ambient Conditions. Overcoming High Pressures by 2,3-Bis(2-pyridyl)pyrazine Doping. **Crystal Growth & Design**, v. 15, p. 3032-3037, 2015.

NIU, G. Plant Factory: An Indoor Vertical Farming System for Efficient Quality Food Production, Chapter 7 – Light. **Elsevier**, 14 p., 2016.

NÖDLER, K.; LICHA, T.; BESTER, K.; SAUTER, M. Development of a multi-residue analytical method, based on liquid chromatography–tandem mass spectrometry, for the simultaneous determination of 46 micro-contaminants in aqueous samples. **Journal of Chromatography A**, v. 1217, p. 6511-6521, 2010.

NOGUEIRA, R. F. P.; JARDIM, W. F. A fotocatálise heterogênea e sua aplicação ambiental. **Química nova**, v. 21, p. 69-72, 1998.

NOGUEIRA, R. F. P.; OLIVEIRA, M. C.; PATERLINI, W. C. Simple and fast spectrophotometric determination of H_2O_2 in photo-Fenton reactions using metavanadate. **Talanta**, v. 66, p. 86-91, 2005.

NORMAN NETWORK. **Emerging substances**. Available in: https://www.norman-network.net/?q=node/19}. Access in: 01 December 2018.

OLIVEIRA, C. A.; VOLANTI, D. P.; NOGUEIRA, A. E.; ZAMPERINI, C. A.; VERGANI, C. E.; LONGO, E. Well-designed β-Ag_2MoO_4 crystals with photocatalytic and antibacterial activity. **Materials and Design**, v. 115, p. 73-81, 2017.

ORTIZ DE GARCÍA, S.; PINTO, G. P.; ENCIMA, P. G.; MATA, R. I. Consumption and occurrence of pharmaceutical and personal care products in the aquatic environment in Spain. **Science of the Total Environment**, v. 444, p. 451-465, 2013.

PANDIRI, M.; VELCHURI, R.; GUNDEBOINA, R.; MUGA, V. A facile *in-situ* hydrothermal route to construct a well-aligned β-Ag_2MoO_4/g-C_3N_4 heterojunction with enhanced visible light photodegradation: Mechanistic views. **Journal of Photochemistry & Photobiology A: Chemistry**, v. 360, p. 231-241, 2018.

PAL, A.; GIN, K. Y. H.; LIN, A. Y. C.; REINHARD, M. Impacts of emerging organic contaminants on freshwater resources: Review of recent occurrences, sources, fate and effects. **Science of the Total Environment**, v. 408, p. 6062-6069, 2010.

PERINI, J. A. L.; TONETTI, A. L.; VIDAL, C.; MONTAGNER, C. C.; NOGUEIRA, R. F. P. Simultaneous degradation of ciprofloxacin, amoxicillin, sulfathiazole and sulfamethazine, and disinfection of hospital effluent after biological treatment via photo-Fenton process under ultraviolet germicidal irradiation. **Applied Catalysis B: Environmental**, v. 224, p. 761-771, 2018.

POURAN, S. R.; AZIZ, A. R. A.; DAUD, W. M. A. W.; SHAFEEYAN, M. S. Effects of niobium and molybdenum impregnation on adsorption capacity and Fenton catalytic activity of magnetite. **RSC Advances**, v. 5, p. 87535-87549, 2015.

POWERS, R. E.; LAWTON, G. P.; MODLIN, I. M. Genotoxicity, carcinogenicity and acid-suppressing medications. **Pharmacology & Therapeutics**, v. 65, n. 3, p. 303-317, 1995.

POYNTON, H. C.; ROBINSON, W. E. Green Chemistry. Chapter 3.7-Contaminants of Emerging Concern, With an Emphasis on Nanomaterials and Pharmaceuticals. **Elsevier**, 26 p., 2018.

PRAKASH, J.; SUN, S.; SWART, H. C.; GUPTA, R. K. Noble metals-TiO_2 nanocomposites: From fundamental mechanisms to photocatalysis, surface enhanced Raman scattering and antibacterial applications. **Applied Materials Today**, v. 11, p. 82-135, 2018.

QU, J.; WANG, X.; ZHANG, Y.; YUAN, G. Multifuncional Ag nanoparticles in heterostructured Ag_2MoO_4/Ag/AgBr cubes with boosted photocatalytic performances. **Solar Energy**, v. 170, p. 124-131, 2018.

RADJENOVIC, J.; SIRTORI, C.; PETROVIC, M.; BARCELÓ, D.; MALATO, S. Solar photocatalytic degradation of persistent pharmaceuticals at pilot-scale: Kinetics and characterization of major intermediate products. **Applied Catalysis B: Environmental**, v. 89, p. 255-264, 2009.

RAFFIN, R. P.; COLOMÉ, L. M.; SCHAPOVAL, E. E.; POHLMANN, A. R.; GUTERRES, S. S. Increasing sodium pantoprazole photostability by microencapsulation: effect of the polymer and the preparation technique. **European Journal of Pharmaceutics and Biopharmaceutics**, v. 69, p. 1014-1018, 2008.

RASHAD, M. M.; Ibrahim, A. A.; RAYAN, D. A.; SANAD, M. M. S.; HELMY, I. M. Photo-Fenton-like degradation of Rhodamine B dye from waste water using iron molybdate catalyst under visible light irradiation. **Environmental Nanotechnology, Monitoring & Management**, v. 8, p. 175-186, 2017.

RICHARDSON, P.; HAWKEY, C. J.; STACK, W. A. Proton Pump Inhibitors. **Drugs**, v. 56, p. 307-335, 1998.

RIDDICK, T. M. Control of colloid stability through zeta potential. **Wynnewood, Pa.**, 372 p., 1968.

RODRIGUEZ-NARVAEZ, O. M.; PERALTA-HERNANDEZ, J. M.; GOONETILLEKE, A.; BANDALA, E. R. Treatment technologies for emerging contaminants in water: A review. **Chemical Engineering Journal**, v. 323, p. 361-380, 2017.

RUHÍ, A.; ACUÑA, V.; BARCELÓ, D.; HUERTA, B.; MOR, J. R.; RODRÍGUEZ-MOZAZ, S.; SABATER, S. Bioaccumulation and

trophic magnification of pharmaceuticals and endocrine disruptors in a Mediterranean river food web. **Science of the Total Environment**, v. 540, p. 250-259, 2015.

SALEH, R.; TAUFIK, A. Ultraviolet-light-assisted heterogeneous Fenton reaction of Ag-Fe_3O_4/graphene composites for the degradation of organic dyes. **Journal of Environmental Chemical Engineering**, in press, accepted manuscript, 2019.

SAMAKCHI, S.; CHAIBAKHSH, N.; MORADI-SHOEILI, Z. Synthesis of MoS_2/$MnFe_2O_4$ nanocomposite with highly efficient catalytic performance in visible light photo-Fenton-like process. **Journal of Photochemistry & Photobiology A: Chemistry**, v. 367, p. 420-428, 2018.

SANSON, A.; ROCCA, F.; ARMELLINI, C.; AHMED, S.; GRISENTI, R. Local study on the MoO_4 units in AgI-doped silver molybdate glasses. **Journal of Non-Crystalline Solids**, v. 354, p. 94-97, 2007.

SCHÄRER, M.; BLENY, H. Elimination of micropollutants-the Swiss approach. Final Conference. **Transnational Action Program on Emerging Substances**, 2015.

SCHUMOCK, G. T.; LI, E. C.; SUDA, K. J.; WIEST, M. D.; STUBBINGS, J. A.; MATUSIAK, L. M.; HUNKLER, R. J.; VERMEULEN, L. C. National trends in prescription drug expenditures and projections for 2016. **American Journal of Health-System Pharmacy**, v. 73, n. 14, p. 1058-1075, 2016.

SCOPUS. Document Search. **Advanced search in Scopus with title, abstract, keywords: "proton pump inhibitor" AND water AND environment**. Available in: {https://www.scopus.com/results/results.uri?numberOfFields=2&src=s&clickedLink=&edit=&editSaveSearch=&origin=searchbasic&authorTab=&affiliationTab=&advancedTab=&scint=1&menu=search&tablin=&searchterm1=%22proton+pump+inhibitor%22+&field1=TITLE_ABS_KEY&connector=AND&searchterm2=water&field2=TITLE_ABS_KEY&connectors=AND&searchTerms=environment&fields=TITLE_ABS_KEY&dateType=Publication_Date_Type&yearFrom=2009&yearTo=Present&loadDate=7&documenttype=All&accessTypes=All&resetFormLink=&st1=%22proton+pump+inhibitor%22+&st2=water&sot=b&sdt=

b&sl=96&s=%28TITLE-ABS-KEY%28%22proton+pump+inhibitor%22+%29+AND+TITLE-ABS-KEY%28water%29AND+TITLE-ABS-KEY%28environment%29%29&sid=11b31ff35e5d4361663d6f560bd087ad&searchId=11b31ff35e5d4361663d6f560bd087ad&txGid=c360aa790ae313987a1e919e15400ccc&sort=plf-f&originationType=b&rr=}. Access in: 02 December 2018.

SHARMA, A.; AHMAD, J.; FLORA, S. J. S. Application of advanced oxidation processes and toxicity assessment of transformation products. **Environmental Research**, v. 167, p. 223-233, 2018.

SHI, S.; KLOTZ, U. Proton pump inhibitors: an update of their clinical use and pharmacokinetics. **European Journal of Clinical Pharmacology**, v. 64, p. 935–951, 2008.

SINGH, D. P.; SIROTA, B.; TALPATRA, S.; KOHLI, P.; REBHOLZ, C.; AOUADI, S. M. Broom-like and flower-like heterostructures of silver molybdate through pH controlled self-assembly. **Journal of Nanoparticle Research**, v. 14, n. 781, p. 1-11, 2012.

SNEADER, W. **Drug discovery: a history**. John Wiley & Sons, Ltd, 469 p., 2005.

SOUSA G. S.; NOBRE, F. X.; ARAÚJO, E. A. J.; SAMBRANO, J. R.; ALBUQUERQUE, A. R.; BINDÁ, R. S.; COUCEIRO, P. R. C.; BRITO, W. R.; CAVALCANTE, L. S.; SANTOS, M. R. M. C.; MATOS, J. M. E. Hydrothermal synthesis, structural characterization and photocatalytic properties of β-Ag_2MoO_4 microcrystals: Correlation between experimental and theoretical data. **Arabian Journal of Chemistry**, in press, 2018.

SUI, M.; SHE, L.; SHENG, L.; WEI, J.; ZHANG, L.; HUANG, S. Ordered mesoporous manganese oxide as catalyst for hydrogen peroxide oxidation of norfloxacin in water. **Chinese Journal of Catalysis**, v. 34, p. 536-541, 2013.

TAHERAN, M.; NAGHDI, M.; BRAR, S. K.; VERMA, M.; SURAMPALLI, R. Y. Emerging contaminants: Here today, there tomorrow!. **Environmental Nanotechnology, Monitoring & Management**, v. 10, p. 122-126, 2018.

TANG, H.; LU, A.; LI, L.; ZHOU, W.; XIE, Z.; ZHANG, L. Highly antibacterial materials constructed from silver molybdate nanoparticles immobilized in chitin matrix. **Chemical Engineering Journal**, v. 234, p. 124-131, 2013.

TANG, H.; FU, Y.; CHANG, S.; XIE, S.; TANG, G. Construction of Ag_3PO_4/Ag_2MoO_4 Z-scheme heterogeneous photocatalyst for the remediation of organic pollutants. **Chinese Journal of Catalysis**, v. 38, p. 337-347, 2017.

TAUC, J. Optical properties and electronic structure of amorphous Ge and Si. **Materials Research Bulletin**, v. 3, p. 37-46, 1968.

TEODOSIU, C.; GILCA, A. F.; BARJOVEANUA, G.; FIOR, S. Emerging pollutants removal through advanced drinking water treatment: A review on processes and environmental performances assessment. **Journal of Cleaner Production**, v. 197, p. 1210-1221, 2018.

TERANISHI, T.; MIYAKE, M. Size Control of Palladium Nanoparticles and Their Crystal Structures. **Chemistry of Materials**, v. 10, p. 594–600, 1998.

THOMMES, M.; KANEKO, K.; NEIMARK, A.V.; OLIVIER, J. P.; RODRIGUEZ-REINOSO, F.; ROUQUEROL, J.; SING, K. S. W. Physisorption of gases, with special reference to the evaluation of surface area and pore size distribution (IUPAC Technical Report). **IUPAC technical report. Pure and Applied Chemistry**. 20 p., 2015.

TIAN, S. H.; TU, Y. T.; CHEN, D. S.; CHEN, X.; XIONG, Y. Degradation of Acid Orange II at neutral pH using $Fe_2(MoO_4)_3$ as a heterogeneous Fenton-like catalyst. **Chemical Engineering Journal**, v. 169, p. 31-37, 2011.

TIWARI, B.; SELLAMUTHU, B.; OUARDA, Y.; DROGUI, P.; TYAGI, R. D.; BUELNA, G. Review on fate and mechanism of removal of pharmaceutical pollutants from wastewater using biological approach. **Bioresource Technology**, v. 224, p. 1-12, 2017.

TROJANOWICZ, M.; BOJANOWSKA-CZAJKA, A.; BARTOSIEWICZ, I.; KULISA, K. Advanced Oxidation/Reduction

Processes treatment for aqueousperfluorooctanoate (PFOA) and perfluorooctanesulfonate (PFOS) – A review of recent advances. **Chemical Engineering Journal**, v. 336, p. 170-199, 2018.

TROVÓ, A. G.; NOGUEIRA, R. F. P.; AGÜERA, A.; FERNANDEZ-ALBA, A. R.; MALATO, S. Paracetamol degradation intermediates and toxicity during photo-Fenton treatment using different iron species. **Water research**, v. 46, p. 5374-5380, 2012.

UMA, K.; ARJUN, N.; PAN, G. T.; YANG, T. C. K. The photodeposition of surface plasmon Ag metal on SiO_2@-Fe_2O_3 nanocomposites sphere for enhancement of the photo-Fenton behavior. **Applied Surface Science**, v. 425, p. 377-383, 2017.

VAEZI, M. F.; YANG, Y. X.; HOWDEN, C. W. REVIEWS IN BASIC AND CLINICAL GASTROENTEROLOGYAND HEPATOLOGY. **Gastroenterology**, v. 153, p. 35-48, 2017.

VAN NUJIS, A. L. N.; TARCOMNICU, I.; SIMONS, W.; BERVOETS, L.; BLUST, R.; JORENS, P. G.; NEELS, H.; COVACI, A. Optimization and validation of a hydrophilic interaction liquid chromatography-tandem mass spectrometry method for the determination of 13 top-prescribed pharmaceuticals in influent wastewater. **Analytical and Bioanalytical Chemistry**, v. 398, 2211–2222, 2010.

VIEIRA, G. B.; JOSÉ, H. J.; PETERSON, M.; BALDISSARELLI, V. Z.; ALVAREZ, P.; MOREIRA, R. F. P. M. CeO_2/TiO_2 nanostructures enhance adsorption and Photocatalytic degradation of organic compounds in aqueous suspension. **Journal of Photochemistry and Photobiology A: Chemistry**, v. 353, p. 325-336, 2018.

WANG, Y.; LIU, Y.; LU, X.; LI, Z.; ZHANG, H.; CUI, X.; ZHANG, Y.; SHI, F.; DENG, Y. Silver-molybdate electrocatalysts for oxygen reduction reaction in alkaline media. **Electrochemistry Communications**, v. 20, p. 171-174, 2012.

WANG, C.; SHIH, Y. Degradation and detoxification of diazinon by sono-Fenton and sono-Fenton-like processes. **Separation and Purification Technology**. v. 140, p. 6-12, 2015.

WANG, N.; ZHENG, T.; ZHANG, G.; WANG, P. A review on Fenton-like processes for organic wastewater treatment. **Journal of Environmental Chemical Engineering**, v. 4, p. 762-787, 2016.

WANG, Z.; DAI, K.; LIANG, C.; ZHANG, J.; ZHU, G. Facile synthesis of novel butterfly-like Ag_2MoO_4 nanosheets for visible-light driven photocatalysis. **Materials Letters**. v. 196, p. 373-376, 2017.

WANG, L.; ZHAO, J.; LIU, H.; HUANG, J. Design, modification and application of semiconductor photocatalysts. **Journal of the Taiwan Institute of Chemical Engineers**, v. 93, p. 590-602, 2018.

WANG, T.; HU, X.; ZHANG, X.; CAO, H.; HUANG, Y.; FENG, P. MoS_2 QDs co-catalytic Fenton reaction for highly sensitive photoluminescence sensing of H_2O_2 and glucose. **Analytical Methods**, v. 6, p. 65670-65682, 2019.

WATTS, R. J.; SARASA, J.; LOGE, F. J.; TEEL, A. L. Oxidative and reductive pathways in manganese-catalyzed Fenton's reaction. **Journal of Environmental Engineering**. v.131, p. 158–164, 2005.

WEN, J.; LI, X.; LIU, W.; FANG, Y.; XIE, J.; XU, Y. Photocatalysis fundamentals and surface modification of TiO_2 nanomaterials. **Chinese Journal of Catalysis**, v. 36, p. 2049-2070, 2015.

WILKINSON, J.; HOODA, P. S.; BARKER, J.; BARTON, S.; SWINDEN, J. Occurrence, fate and transformation of emerging contaminants in water: An overarching review of the field. **Environmental Pollution**, v. 231, p. 954-970, 2017.

WORLD SEMICONDUCTORS TRADE STATISTCS, **WSTS Semiconductor Market Forecast Spring 2018**. Available in: https://www.wsts.org/76/103/WSTS-Semiconductor-Market-Forecast-Spring-2018}. Access in: 17 November 2018.
WU, M.; LV, H.; WANG, T.; AO, Z.; SUN, H.; WANG, C.; AN, T.; WANG, S. Ag_2MoO_4 nanoparticles encapsulated in g-C_3N_4 for sunlight photodegradation of pollutants. **Catalysis Today**, v. 315, p. 205-212, 2018.

WYCKOFFL, R. W. G. The crystal structure of silver molybdate. **Journal of American Chemical Society**, v. 44, p. 1994-1998, 1922.

XIE, Y.; DAI, Y.; YUAN, X.; JIANG, L.; ZHOU, L.; WU, Z.; ZHANG, J.; WANG, H.; XIONG, T. Insight on the plasmonic Z-scheme mechanism underlying the highly efficient photocatalytic activity of silver molybdate/silver vanadate composite in rhodamine B degradation. **Journal of Colloid and Interface Science**, v. 530, p. 493-504, 2018.

XIU, Z.; CAO, Y.; XING, Z.; ZHAO, T.; LI, Z.; ZHOU, W. Wide spectral response photothermal catalysis-fenton coupling systems with 3D hierarchical Fe_3O_4/Ag/Bi_2MoO_6 ternary hetero-superstructural magnetic microspheres for efficient high-toxic organic pollutants removal**. Journal of Colloid and Interface Science**, v. 533, p. 24-33, 2019.

XU, D., CHENG, B.; ZHANG, J.; WANG, W.; YU, J.; HO, W. Photocatalytic activity of Ag_2MO_4 (M = Cr, Mo, W) photocatalysts. **Journal of Materials Chemistry A**, v. 3, p. 20153-20166, 2015a.

XU, H. B.; WANG, H. D.; LI, C. H.; YE, S.; DONG, M. S.; XIA, Q. J.; ZHANG, A. Q.; PAN, K.; GE, X. L. DONG, J. H. Proton pump inhibitor use and risk of spontaneous bacterial peritonitis in cirrhotic patients: a systematic review and meta-analysis. **Genetics and Molecular Research**, v. 14, p. 7490-7501, 2015b.

YAN, H.; WANG, X.; YAO, M.; YAO, X. Band structure design of semiconductors for enhanced photocatalytic activity: The case of TiO_2, **Progress in Natural Science: Materials International**, v. 23, p. 402-407, 2013.

YANG, X.; SUN, H.; ZHANG, L.; ZHAO, L.; LIAN, J.; JIANG, Q. High Efficient Photo-Fenton Catalyst of α-Fe_2O_3/MoS_2 Hierarchical Nanoheterostructures: Reutilization for Supercapacitors. **Scientific Reports**, v. 6, n. 31591, p. 1-12, 2016.

YANG, X.; WANG, Y.; XU, X.; QU, Y.; DING, H.; CHEN, H. Surface plasmon resonance-induced visible-light photocatalytic performance of silver/silver molybdate composites. **Chinese Journal of Catalysis**, v. 38, p. 260-269, 2017a.

YANG, Y.; O. K. Y. S.; KIM, K. H.; KWON, E. E.; TSANG, Y. F. Occurrences and removal of pharmaceuticals and personal care products

(PPCPs) in drinking water and water/sewage treatment plants: A review. **Science of the Total Environment**, v. 596-597, p. 303-320, 2017b.

ZEPP, R. G.; FAUST, B. C.; HOIGNÉ, J. Hydroxyl radical formation in aqueous reactions (pH 3–8) of iron(II) with hydrogen peroxide: the Photo-Fenton reaction. **Environmental Science & Technology**, v. 26, p. 313–319, 1992.

ZHANG, J.; MA, Z. Novel β-Ag_2MoO_4 /g-C_3N_4 heterojunction catalysts with highly enhanced visible-light-driven photocatalytic activity. **RSC Advances**, v. 7, p. 2163-2171, 2017a.

ZHANG, J.; MA, Z. AgI/β-Ag_2MoO_4 heterojunctions with enhanced visible-light-driven catalytic activity**. Journal of the Taiwan Institute of Chemical Engineers**, v. 81, p. 225-231, 2017b.

ZHANG, J.; MA, Z. Flower-like Ag_2MoO_4/Bi_2MoO_6 heterojunctions with enhanced photocatalytic activity under visible light irradiation. **Journal of the Taiwan Institute of Chemical Engineers**, v. 71, p. 156-164, 2017c.

ZHAO, S.; LI, Z.; QU, Z.; YAN, N.; HUANG, W.; CHEN, W.; XU, H. Co-benefit of Ag and Mo for the catalytic oxidation of elemental mercury. **Fuel**, v. 158, p. 891-897, 2015.

ZHOU, D.; LI, W. B.; PANG, L. X.; GUO, J.; QI, Z. M.; SHAO, T.; YUE, Z. X.; YAO, X. Sintering behavior and dielectric properties of ultra-low temperature fired silver molybdate ceramics. **Journal of the American Ceramic Society**, v. 97, p. 3597-3601, 2014.

ZHOU, B.; HUANG, Y.; LI, H.; SUN, W.; LIU, J. Proton-pump inhibitors and risk of fractures: an update meta-analysis. **Osteoporosis International**, v. 27, n. 1, p. 339-347, 2016.

APPENDIX A - Degradation rate constants

Figure A 1. Kinetic rates for non-photochemical processes, where (a) Adsorption Ag_2MoO_4, (b) Adsorption $Ag_2MoO_4^{Calc.}$, (c) O_2 and (d) H_2O_2.

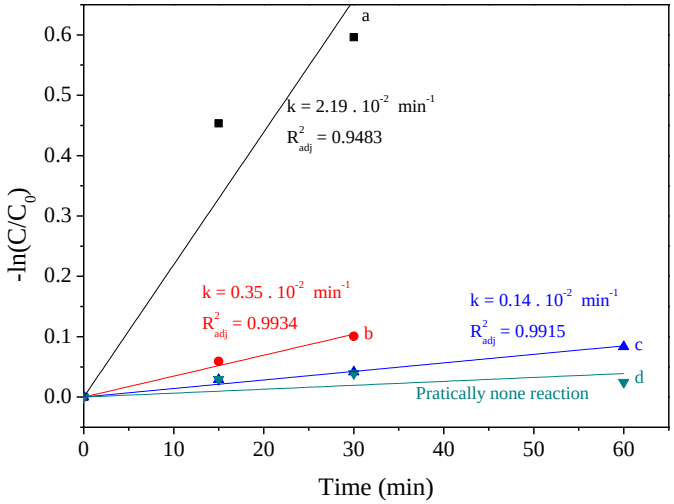

Source: Author's own elaboration.

Figure A 2. Kinetic rates for photolysis, where (a) UV, (b) UV + O_2, (c) UV + H_2O_2, (d) VIS, (e) VIS + O_2 and (f) VIS + H_2O_2.

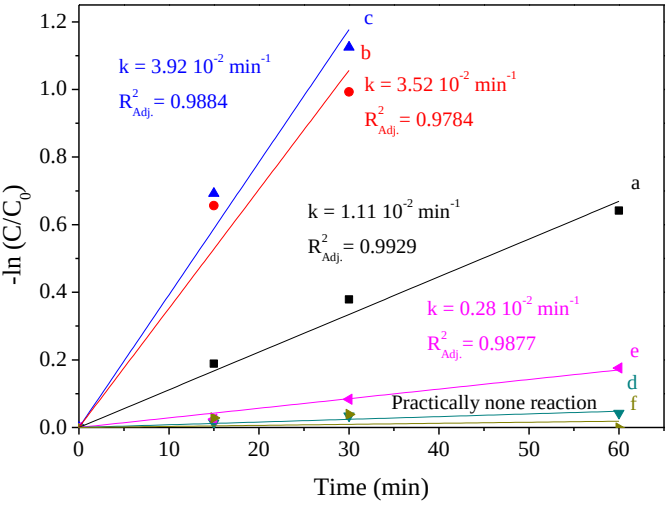

Source: Author's own elaboration.

Figure A 3. Kinetic rates for photocatalysis, where (a) UV + Ag_2MoO_4 + O_2, (b) UV + $Ag_2MoO_4^{Calc.}$ + O_2, (c) UV + TiO_2-P25+ O_2, (d) VIS + Ag_2MoO_4 + O_2, (e) VIS + $Ag_2MoO_4^{Calc.}$ + O_2 and (f) VIS + TiO_2-P25+ O_2.

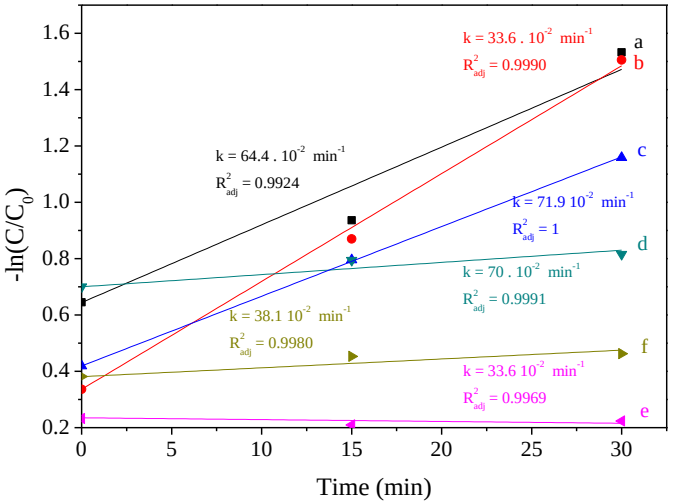

Source: Author's own elaboration.

Figure A 4. Kinetic rates for catalytic peroxidation and photo-peroxidation reactions, where (a) Ag_2MoO_4 + H_2O_2, (b) UV + Ag_2MoO_4 + H_2O_2 and (c) VIS + Ag_2MoO_4 + H_2O_2.

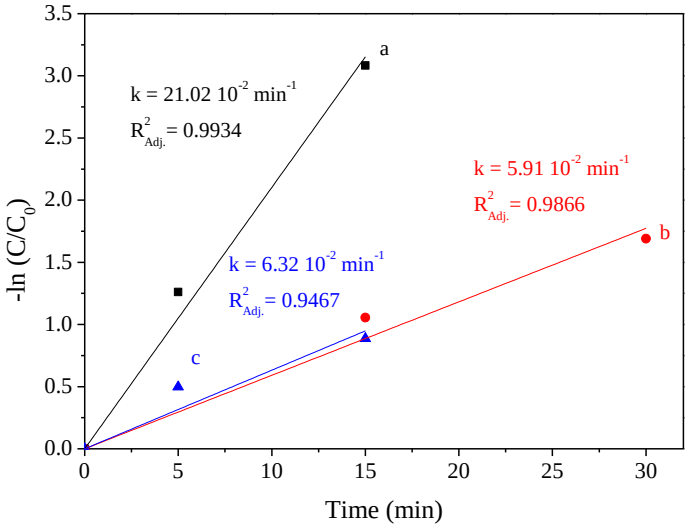

Source: Author's own elaboration.

APPENDIX B - Scanning spectrums

Figure B 1. Scanning spectrums of adsorption Ag_2MoO_4 (A), adsorption $Ag_2MoO_4^{Calc.}$ (B), O_2 (C) and H_2O_2 (D).

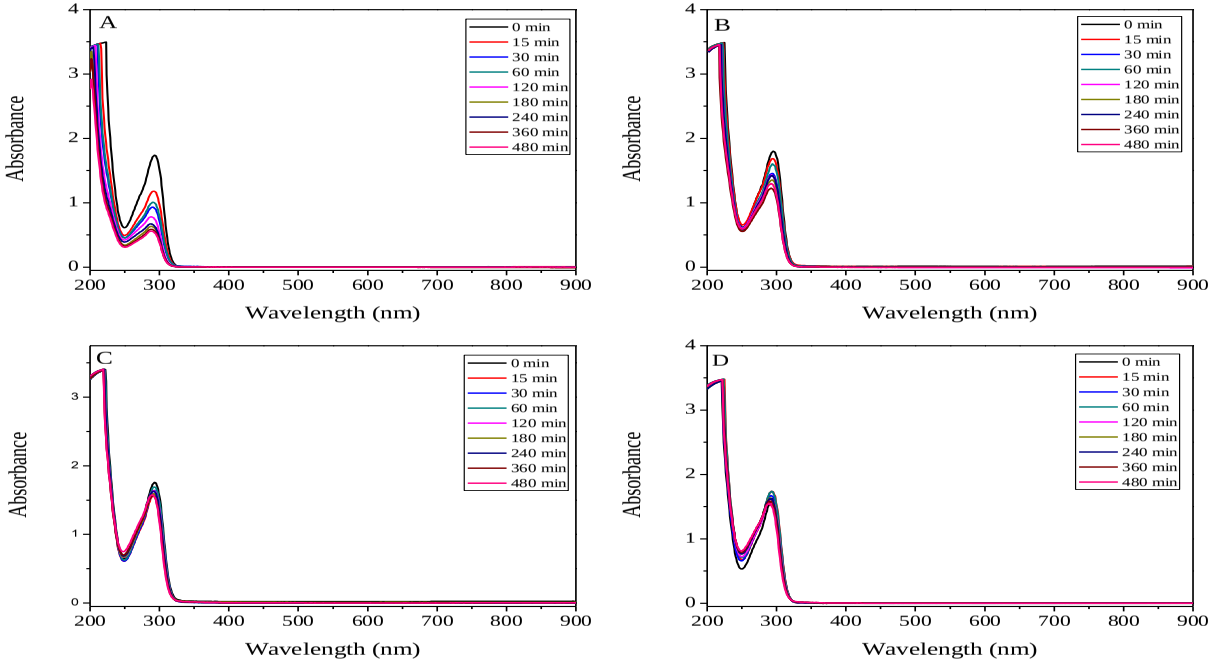

Source: Author's own elaboration.

Figure B 2. Scanning spectrums of VIS (A) VIS + O_2 (B), VIS + H_2O_2 (C), VIS + Ag_2MoO_4 + O_2 (D) VIS + $Ag_2MoO_4^{Calc.}$ + O_2 (E), VIS + TiO_2-P25 + O_2 (F) and VIS + Ag_2MoO_4 + H_2O_2 (G).

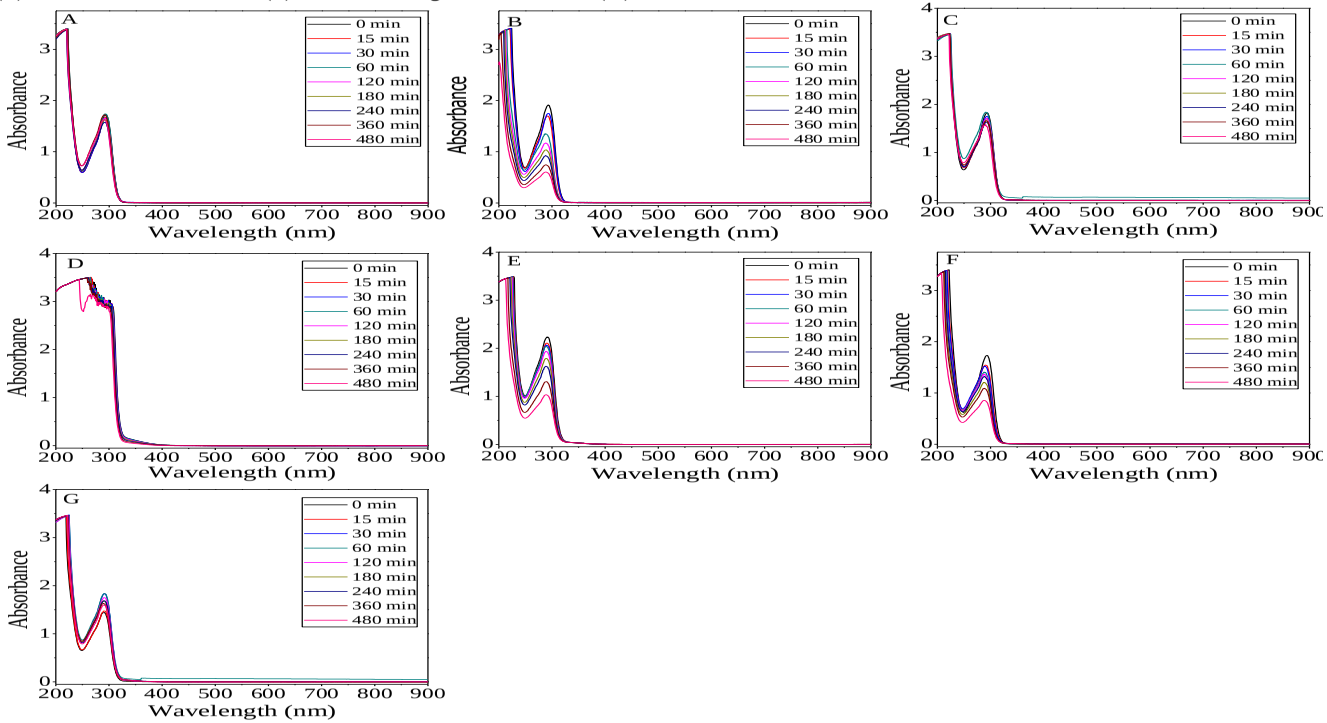

Source: Author's own elaboration.

Figure B 3. Scanning spectrums of UV (A), UV + O_2 (B), UV + H_2O_2 (C), UV + $Ag_2MoO_4^{Calc.}$ + O_2 (D) and UV + TiO_2-P25 + O_2.

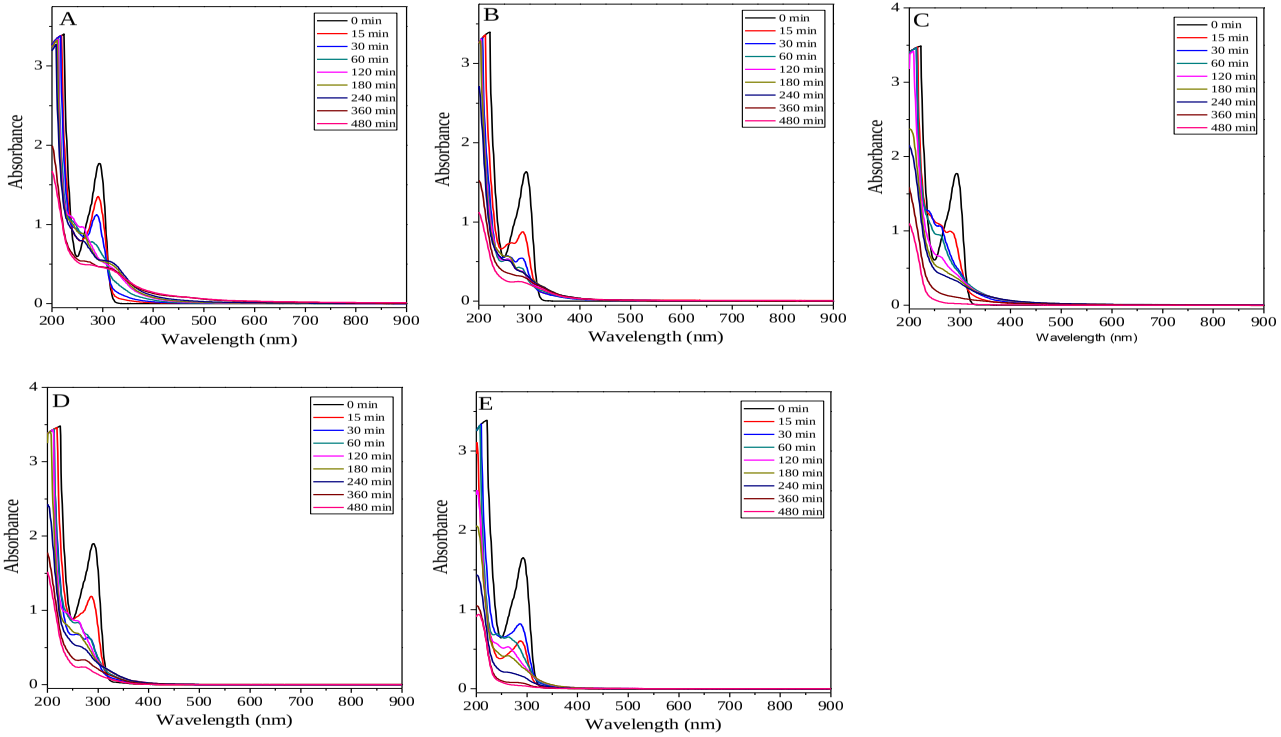

Source: Author's own elaboration.